Supporting Information

Bead Mill-Driven Acceleration in Catalytic Methanolysis Reaction of Poly(ethylene terephthalate) Toward Low-Energy Chemical Recycling of Polymers

Tomoya Kawase, Haruro Ishitani,* and Shū Kobayashi*

Table of Contents

SI-1. General Information

- Nuclear magnetic resonance (NMR) spectra were recorded on a JEOL ECZ-500R spectrometer, operating at 500 MHz for ^{1}H, 125 MHz for ^{13}C NMR in $CDCl_3$, CD_3OD, DMSO-d_6. $CDCl_3$ ($\delta = 7.26$), CD_3OD ($\delta = 3.30$), or DMSO-d_6 ($\delta = 2.49$) was used as the internal standard for ^{1}H NMR. $CDCl_3$ ($\delta = 77.0$), CD_3OD ($\delta = 49.0$), or DMSO-d_6 ($\delta = 39.5$) was used as the internal standard for ^{13}C NMR.

- Gas chromatography (GC) spectra were recorded on a Shimadzu GC-2030AF, 100V spectrometer using SH-Rtx-5 Amine column (30 m, 0.25 mmID, 0.25 μm df) with following conditions: gas pressure: 274.1 kPa; total flow: 204.4 mL/min; column flow: 6.35 mL/min; velocity: 87.1 cm/sec; purge flow: 3.0 mL/min; sprit ratio: 30.7; injector: 280 ˚C, FID: 320 ˚C; column program: starting from 40.0 ˚C for 5 min, then 5 ˚C/min to 150 ℃, then 20 ℃/min to 260 ˚C, 10 min hold).

- Thermogravimetric (TG) analysis was performed with Rigaku Thermo plus EVO2 TG-DTA8122. Samples were heated from room temperature to 1,000 ℃ at a rate of 4 ℃/min in air.

- Gel permeation chromatography (GPC) spectra of the reagent PET (PET A) were measured using a dedicated device equipped with columns of 2x PLgel 5μm MIXED-D and 7.5 x 300 (Agilent Technologies, Inc.), a dual pump (KP-22-13, FLOM, Inc.), an automatic injection device (717plus, Nihon Waters K.K.), and a UV-visible detector (2487, Nihon Waters K.K.) with following conditions: mobile phase: chloroform for HPLC from Wako Pure Chemical Industries, Ltd.; flow rate: 1.0 mL/min; injection volume: 2.5 μL; detection wavelength: 254 nm. This measurement was conducted by Mitsui Chemicals, Inc.

- Gel permeation chromatography (GPC) spectra of the other samples (PET B, C, and D) were measured using a column of Shodex GPC KF-805L (Resonac Corporation), a dual pump (LC-20AT, Shimadzu), an automatic injection device (SIL-20A HT, Shimadzu), a column heater (CTO-10A VP, Shimadzu) and a UV-visible detector (SPD-10A, Shimadzu) with following conditions: mobile phase: chloroform for HPLC from Wako Pure Chemical Industries, Ltd.; flow rate: 1.0 mL/min; column heater: 40 ℃; injection volume: 10 μL; detection wavelength: 254 nm.

- High performance liquid chromatography (HPLC) spectra were measured using a column of Shim-pack GIST C18 (250 mm × 4.6 mm I.D., 5 μm) (Shimadzu, P/N: 227-30017-08), a dual pump (LC-20AB, Shimadzu), an automatic injection device (SIL-20A, Shimadzu), a column heater (CTO-20A, Shimadzu) and a UV-visible detector (SPD-M20A, Shimadzu) with following conditions: mobile phase: H_2O/methanol (3:7); total flow rate: 0.5 mL/min; column heater: 35 ℃; injection volume: 5 μL; detection wavelength: 254 nm.

- Dynamic light scattering (DLS) measurements were carried out on a laser diffraction/scattering type particle size distribution analyzer (MT3300, MicrotracBEL Corp.). This measurement was conducted by AIMEX Co., Ltd.

- Differential scanning calorimetry (DSC) was measured by DSC7000X (Hitachi High-Tech Corporation) with following conditions: sample weight: 10 mg (vacuum dried overnight at 50 °C prior to the measurement); temperature program: cool from 25 °C to -100 °C at 10 °C/min, hold for 5 minutes, then heat from -100 °C to 300 °C at 10 °C/min. This measurement was conducted by Mitsui Chemicals, Inc. For calculation of crystallinity of each PET sample, melting enthalpy was corrected by the actual PET components determined by TG analysis (Figure 6, Table 6).

- Scanning electronic microscopy (SEM) analysis was performed by using JSM-6700F. Energy-dispersive X-ray spectroscopy (EDS) images were obtained using a JEOL JEM-2100F

instrument operated at 200 kV. All EDS specimens were prepared by placing a sample directly on carbon-coated copper grids. These analyses were carried out by Dr. Tei Maki from JEOL Ltd.

- N_2 and H_2O adsorption isotherm were measured by Shimadzu-Micromeritics Automatic Specific Surface Area/Pore Distribution Measurement Device 3Flex. The samples were heated at 60 °C for 4 h under vacuum prior to the measurement. These measurements were carried out by Shimadzu Corp.

- Infrared (IR) spectra were obtained using a Shimadzu IRSpirit spectrometer. Data are represented as frequency of absorption (cm^{-1}).

- Powder X-ray diffraction (PXRD) analysis was performed on a Rigaku MiniFlex 300/600.

- High resolution electrospray ionization mass spectrometry (ESI-MS) was measured by Bruker Daltonics compact system.

- For apparatuses for batch-type bead milling, a demonstration machine of a commercial "Easy Nano RMBII-type" (AIMEX Co., Ltd.) was used. For apparatus for continuous bead milling, a demonstration machine of a commercial "Start Lab RMH-type" (AIMEX Co., Ltd.) was used.

- Preparative thin-layer chromatography (PTLC) was carried out using Wakogel B-5F from Wako Pure Chemical Industries, Ltd.

- Organic solvents used in this study were commercially available solvents, which were distilled appropriately under an argon atmosphere, and were stored over molecular sieves prior to use.

- Poly(ethylene terephthalate) for a standard sample of this study was purchased from Sigma-Aldrich® (P/N: 429252) as a granular form containing glass particles as reinforcer. The amorphous PET pellets (P/N: PBKI) and the crystalline PET pellets (P/N: EFG70) were provided by Bell Polyester Products, Inc. The post-consumer PET bottles used in this study were 2L bottles for natural mineral water supplied by Suntory Holdings Ltd.

- 1,5,7-triazabicyclo[4.4.0]dec-5-ene (TBD) was prepared following the literature.[1] Tetramethylammonium methyl carbonate was prepared following the literature.[2] 1-*n*-butyl-3-methylimidazolium hydroxide ([Bmim]OH) was prepared following the literature.[3] Tetrabutylammonium *tert*-butoxide was prepared from tetrabutylammonium fluoride and potassium *tert*-butoxide in the similar method as tetramethylammonium methoxide (TMAM) in SI-2-2. Other reagents and catalysts were purchased from reagent companies and used directly.

SI-2. Experimental Procedures

SI-2-1. Experimental Procedures for Bead Mill Treatment of PET

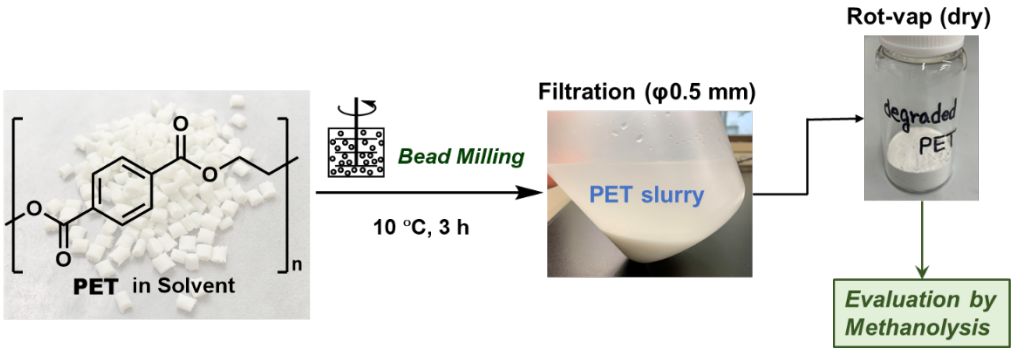

Bead mill treatment of poly(ethylene terephthalate) (PET) was generally performed as follows: PET (5.0 g), toluene (100 mL), and ZrO_2 beads (φ2 mm, 160 mL) were put in a vessel equipped with a mechanical stirrer. The vessel was set to the bead mill apparatus Easy Nano RMBII-type, and the reactor was cooled to 10 ℃ using a cooling system. Then, the mechanical stirring was started at 2,500 rpm for 3 h. The mixture was then filtered by φ0.5 mm mesh filter to remove ZrO_2 beads and large particles of PET. The solvent of the obtained slurry sample was then evaporated, and the remaining solid was dried under vacuum at room temperature. About 4 g of white powder was obtained after loosening the sample using a mortar and pestle. The sample was stored in air and used in methanolysis reactions.

As evident from the subsequent investigations, prolonged bead mill treatment will further lead micronization and molecular weight reduction. Therefore, it is expected that the amount of PET powder obtained at this stage would also increase. However, in this study's initial investigation of methanolysis conditions, the bead mill time was kept constant at 3 hours. While these bead mill conditions may not be optimal from the perspective of PET powder recovery, it is clear from the results shown in Table 3 of the main text that extending the bead mill time has little effect on methanolysis performance.

At the initial stages of the study, to ensure the reproducibility of the two-step conversion process consisting of bead mill treatment and catalytic methanolysis, as well as to accurately evaluate the effect of the bead mill treatment on methanolysis, the conditions for the bead mill treatment were standardized and consistently applied to samples used in methanolysis. For example, under the specific conditions mentioned above, a single bead mill treatment converted 5 g of PET pellets into approximately 4 g of PET powder. However, the yield of this powder varied. To ensure the homogeneity of the PET powder used in methanolysis and to minimize errors, we repeated this procedure 10 times, thoroughly mixing the resulting PET powders to define them as a single batch of PET powder samples. The total yield over these 10 runs was 36.4 g in average.

Due to the nature of the bead mill process, the material of the beads used in the milling inevitably introduces trace amounts of particles of bead material into the processed samples. Such wear implies that the conditions of each bead mill treatment may slightly differ. However, by combining the samples from multiple treatments into a single batch, these variations were averaged out. Additionally, the beads used for milling were replaced with new ones after each set of ten bead mill treatments. This precaution effectively minimized variations between batches.

Furthermore, the contamination of the PET powder by bead materials in each batch, produced under the standardized conditions of ten bead mill treatments, was quantified using methods described later in this section (SI-2-7). This approach ensured the reliability and consistency of the

samples used in subsequent methanolysis experiments.

In the case of bead mill treatment of the used beverage PET flake (PET D), post-consumer bottles were washed, dried and cut into 5 x 5 mm pieces prior to pulverize as shown in **SI-2-4**.

SI-2-2. Preparation of Tetramethylammonium Methoxide (TMAM)

Tetramethylammonium methoxide was prepared by a following method: to a dry methanol solution (10 mL) of tetramethylammonium chloride (25 mmol, 2.74 g) was added methanol solution of KOMe (30 w/w% in methanol, 25 mmol, 7.4 mL). The mixture was stirred under an argon atmosphere at room temperature overnight. A white precipitate of KCl was formed immediately after stirring was started. Then, the solution was filtered under vacuum to remove the precipitate, and washed with cold dry methanol. Collected filtrate was then diluted in a 50 mL measuring flask by adding dry methanol to give 0.5 M methanol solution of tetramethylammonium methoxide. The prepared solution was stored in a fridge in a glovebox, and used directly to reactions. ^{1}H NMR (500 MHz, CD_3OD) δ 5.60 (s, 3H), 3.16 (s, 12H). ^{13}C NMR (125 MHz, CD_3OD) δ 55.9, 49.9. IR (methanol solution) 3027, 2807, 2758, 1491, 1401, 1037, 950 cm^{-1}.

SI-2-3. Experimental Procedures for Methanolysis of PET

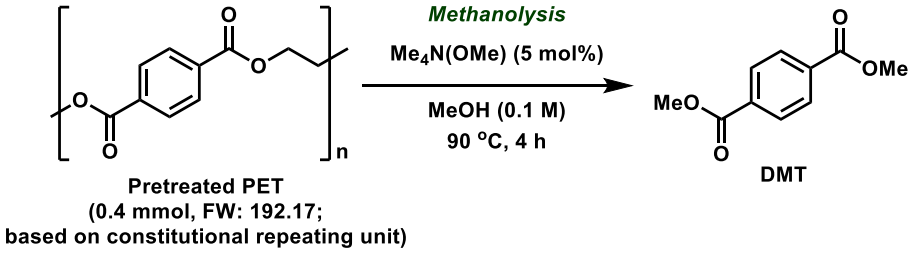

The methanolysis reactions of PET were generally performed as follows: the bead-milled reagent PET (PET A; 145.6 mg, containing 76.9 mg of organic materials which correspond to 0.4 mmol of ethylene terephthalate unit), tetramethylammonium methoxide (5 mol%, 0.02 mmol, 40 μL of 0.5 M stock solution), and dry methanol (4 mL) were put in a sealed tube with an argon flushed. The solution was then stirred and heated at 90 °C using an oil bath. After 4 h, the solution was cooled to room temperature. Then, decane was added as a GC internal standard, followed by adding chloroform (4 mL) and stirring for several minutes. The resulting solution was analyzed by GC. The yield of dimethyl terephthalate was calculated to be 76%, accompanied with 41% yield of ethylene glycol. For isolation of dimethyl terephthalate: after stirring with chloroform, the solution was filtered to remove insoluble species. The filtrate was evaporated and purified by preparative thin-layer chromatography (hexane/EtOAc = 2/1) to give dimethyl terephthalate (59.8 mg, 75% yield) as a white crystal. NMR spectra were consistent with a previous report.[4] ^{1}H NMR (500 MHz, $CDCl_3$) δ 8.06 (s, 4H), 3.91 (s, 6H). ^{13}C NMR (125 MHz, $CDCl_3$) δ 166.1, 133.8, 129.4, 52.3.

SI-2-4. Experimental Procedures for Bead Mill Treatment and Methanolysis of the Used Beverage PET Flake (PET D)

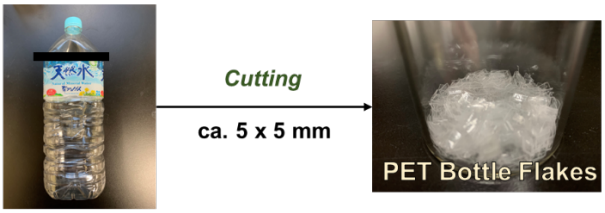

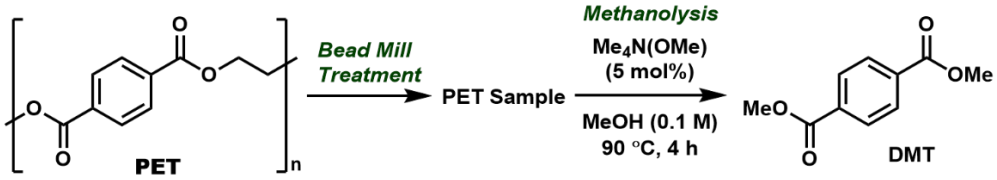

The bead mill treatment and the methanolysis of the used beverage PET flake (PET D) were performed as follows: post-consumer PET bottles for natural mineral water were washed well, dried in air, and cut into ca. 5 x 5 mm pieces. Resulted PET bottle flakes were treated under the bead mill conditions (see procedures in **SI-2-1**). The bead-milled PET sample (PET D, 79.9 mg, containing 76.9 mg of organic materials which correspond to 0.4 mmol of ethylene terephthalate unit), tetramethylammonium methoxide (5 mol%, 0.02 mmol, 40 μL of 0.5 M stock solution), and dry methanol (4 mL) were put in a sealed tube with an argon flushed. The solution was then stirred and heated at 90 °C using an oil bath. After 4 h, the solution was cooled to room temperature. Then, decane was added as a GC internal standard, followed by adding chloroform (4 mL) and stirring for several minutes. The resulting solution was analyzed by GC. The yield of dimethyl terephthalate was calculated to be 82%, accompanied with 85% yield of ethylene glycol. For isolation of dimethyl terephthalate: after stirring with chloroform, the solution was filtered to remove insoluble species. The filtrate was evaporated and purified by preparative thin-layer chromatography (hexane/EtOAc = 2/1) to give dimethyl terephthalate (65.9 mg, 84% yield) as a white crystal.

SI-2-5. Experimental Procedures for Aminolysis of PET

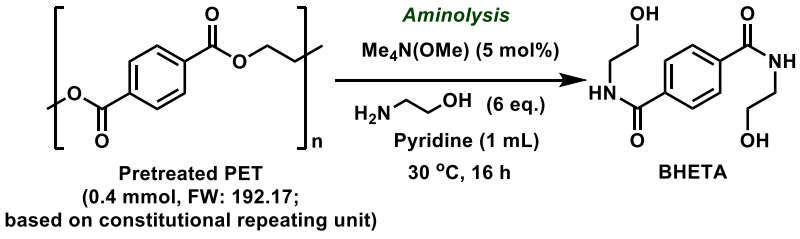

The aminolysis reactions of PET were generally performed as follows: the bead-milled reagent PET sample (PET A; 145.6 mg, containing 76.9 mg of organic materials which correspond to 0.4 mmol of ethylene terephthalate unit), tetramethylammonium methoxide (5 mol%, 0.02 mmol, 40 μL of 0.5 M stock solution), 2-aminoethaol (144 μL; 6 equiv.), and pyridine (1 mL) were put in a 10 mL flask with an argon flushed. The solution was then stirred at 30 °C using an oil bath. After 16 h, the solution was poured into CH_2Cl_2 (50 mL) to form a precipitate of *N*,*N'*-bis(2-hydroxyethyl) terephthalamide (BHETA). Then, the precipitate was collected through vacuum filtration and was washed by CH_2Cl_2 and THF. The resulting precipitate was dried under vacuum overnight. To this dried solid 1,3,5-trimethoxybenzene was added as an NMR internal standard, and also was added DMSO-d_6 to dissolve

all soluble species. Subsequently, the solution was analyzed by ^{1}H NMR. The yield of BHETA was calculated to be 79%. For isolation of BHETA: the precipitate was recrystallized with water, followed by vacuum filtration washed by water and THF. After dry under vacuum at 50 °C overnight, 79.3 mg (79% yield) of BHETA was obtained as a white solid. NMR spectra were consistent with a previous report.[5] ^{1}H NMR (500 MHz, DMSO-d_6) δ 8.55 (t, J = 5.5 Hz, 2H), 7.91 (s, 4H), 4.74 (br, 2H), 3.51 (t, J = 6.0 Hz, 4H), 3.33 (q, J = 6.0 Hz, 4H). ^{13}C NMR (125 MHz, DMSO-d_6) δ 165.7, 136.7, 127.1, 59.7, 42.3.

SI-2-6. Experimental Procedures for Glycolysis of PET

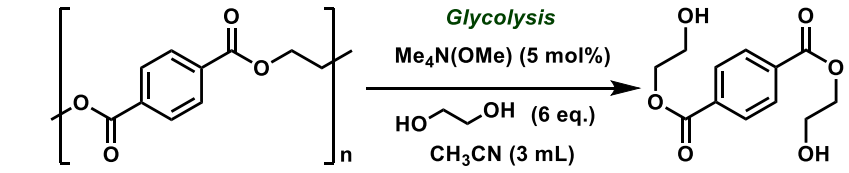

The glycolysis reactions of PET were generally performed as follows: the bead-milled amorphous PET (PET B; 76.9 mg, containing 76.9 mg of organic materials which correspond to 0.4 mmol of ethylene terephthalate unit), tetramethylammonium methoxide (5 mol%, 0.02 mmol, 40 µL of 0.5 M stock solution), ethylene glycol (134 µL, 6 equiv.), and CH_3CN (3 mL) were put in a sealed tube with an argon flushed. The solution was then stirred and heated at 60 °C using an oil bath. After 24 h, the solution was cooled, and CH_3CN was removed by evaporation. To the resulting mixture, anisole was added as a HPLC internal standard, and was also added by DMSO (5 mL) with sonication for 30 min and stirring for 10 min. Subsequently, the solution was analyzed by HPLC. The yield of bis(2-hydroxyethyl) terephthalate (BHET) was calculated to be >99%. For isolation of BHET: the residue was chilled in a freezer (-20°C) overnight, then filtered and washed to remove ethylene glycol with cold water. Subsequently, the residue was recrystallized with water, followed by vacuum filtration washed by cold water. After dry under vacuum at 50 °C overnight, 91.4 mg (90% yield) of BHET was obtained as a white solid. NMR spectra were consistent with a previous report.[6] ^{1}H NMR (500 MHz, DMSO-d_6) δ 8.10 (s, 4H), 4.69 (br, 2H), 4.31 (t, J = 5.0 Hz, 4H), 3.71 (q, J = 4.0 Hz, 4H). ^{13}C NMR (125 MHz, DMSO-d_6) δ 165.2, 133.7, 129.5, 67.0, 59.0.

SI-2-7. Experimental Procedures for the One-pot Bead-Milling/Methanolysis Reaction in Batch System

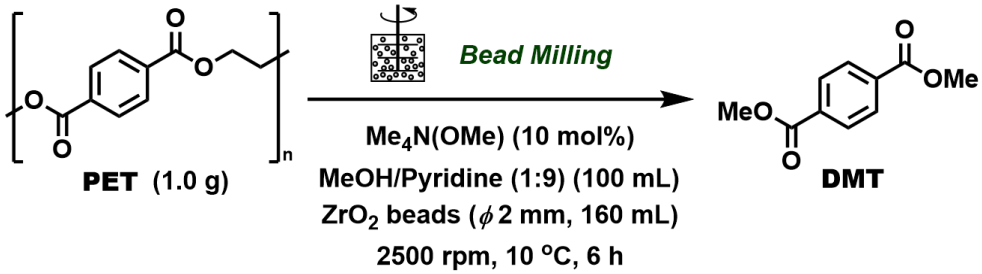

To investigate the one-pot process, the used beverage PET flakes (5 x 5 mm) were processed under the following procedures: the used beverage PET flakes (1.0 g, 5.2 mmol), tetramethylammonium methoxide (10 mol%, 0.52 mmol, 1.04 mL of 0.5 M stock solution), dry methanol (100 mL), and ZrO_2 beads (φ2 mm; 160 mL) were placed in a bead mill vessel of Easy Nano RMBII-type (AIMEX Co.,

Ltd.). Then, the mechanical stirring at 2,500 rpm was carried out at 10 ℃ for 6 h. The mixture was then quenched by acetic acid, and filtered by φ0.5 mm mesh filter to remove ZrO_2 beads, washed with chloroform. After the addition of decane as an internal standard, the resulting solution was analyzed by GC. The yield of dimethyl terephthalate was calculated to be 72%. After that, purification was conducted over silica gel column chromatography (hexane/EtOAc = 2/1) to give dimethyl terephthalate (0.73 g, 72% yield) as a white crystal.

SI-2-8. TG Analysis for Determination of Net PET Content

Because the reagent PET sample (PET A) supplied from Sigma-Aldrich® contained glass particles as reinforcers, TG analysis was carried out to determine an actual amount of organic components (Figure S1). Based on weight-loss in TG analysis, this Sigma-Aldrich® PET sample contained 52.8% of organic components, and the composition was the same after bead milling in case of the standard conditions in SI-2-1. To confirm the credibility of this result, 1.0 g of PET A was calcined in air at 600 ℃for 16 h to burn out all organic components, and remaining solid was weighed to determine an glass particle amount (Figure S2). The amount was 45.2 (±0.2) %, and therefore the amount of organic component can be estimated to be ca. 54.8%. The results of these two experiments were in good agreement to each other. Based on the above results, in the depolymerization reaction using PET powder derived from the reagent PET pellet, the yield was calculated assuming that 52.8% of the weight of the PET sample used was actually depolymerizable PET components (ethylene terephthalate units).

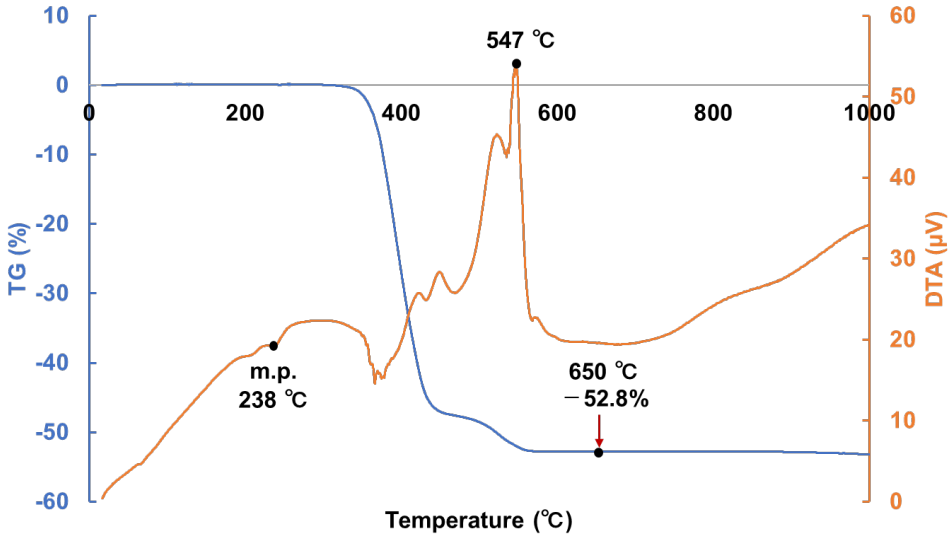

Figure S1. TG Analysis of Poly(ethylene terephthalate) purchased from Sigma-Aldrich®

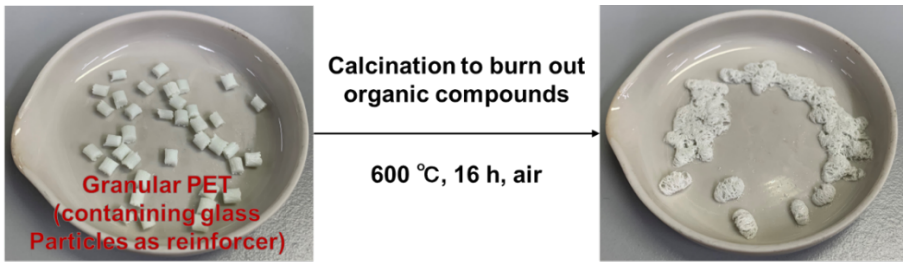

(purchased from Sigma-Aldrich)

Sample weight (g)	After calcination (g)	Impurity ratio (w/w%)
1.0139	0.4595	45.32
1.0345	0.4678	45.22
1.0513	0.4727	44.96
	Average (w/w%)	45.2 (±0.2)

Figure S2. Evaluation of Impurity Amount by Calcination

In addition to the reagent PET containing reinforcer, corrections are also required for the other PET samples (PET B, C, and D). As mentioned above (**SI-2-1**), in the bead mill process, a small amount of bead material may be contaminated due to wear of the beads used. Therefore, according to the above-mentioned method, the pulverized PET powder was subjected to TG analysis to determine the amount of combustible components and the net amount of polymerizable PET contained in the sample. The results are summarized in Table S1. As a result, a maximum of about 4%, which is the case for used beverage PET flake, was suggested as inorganic contamination.

Whether this ZrO_2 contamination is involved in the reaction was confirmed separately. For example, in a control experiment, 10 mol% ZrO_2 powder was added to the reagent PET pellets and stirred with methanol without a catalyst at 90 °C for 4 h, but no DMT was observed in the reaction solution by GC analysis, indicating that ZrO_2 had little effect on the methanolysis.

Table S1. TG Analysis of Combustible Component in the PET Samples

Entry	PET Sample	Bead Milling	Combustible Component (w/w%)[a]
1	Reagent PET (PET A)	Not Done	52.8
2		Done	52.8
3	Amorphous PET (PET B)	Not Done	100.0
4		Done	100.0
5	Crystalline PET (PET C)	Not Done	100.0
6		Done	99.0
7	Used beverage PET flake (PET D)	Not Done	100.0
8		Done	96.2

[a] Determined by TG analysis (Combastible at 600 °C)

SI-3. Additional Information on Analytical Studies of PET Samples

SI-3-1. Particle Size Distribution Analysis

Dynamic light scattering (DLS) measurements of bead-milled PET samples were carried out on an analyzer, Microtrac MT3300 (LOW-WET) (MicrotracBEL Corp.), to determine the particle size distribution. After bead mill treatment, obtained PET slurry was directly analyzed with bead mill solvent. Results of the distribution are shown in Figures S3–S7. In some cases, primary particles were prone to agglomerate during the measurements. We considered that this agglomeration probably originated from electrostatic interaction of fine particles. Since strength of "interparticle" interaction in secondary particles was considered to be significantly inferior to that of "intermolecular" interaction in primary particles, the correlation with the reaction yield was discussed with the primary particle size.

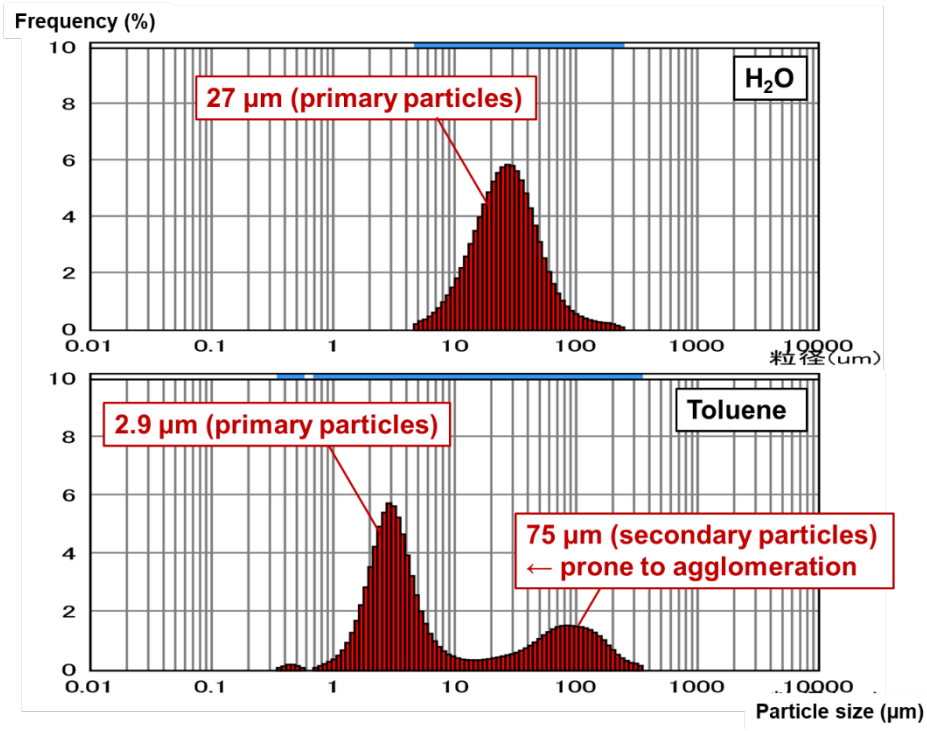

Figure S3. Particle Size Distribution of Bead-Milled reagent PET (PET A) with ZrO_2 Beads in H_2O (Above) or Toluene (Below)

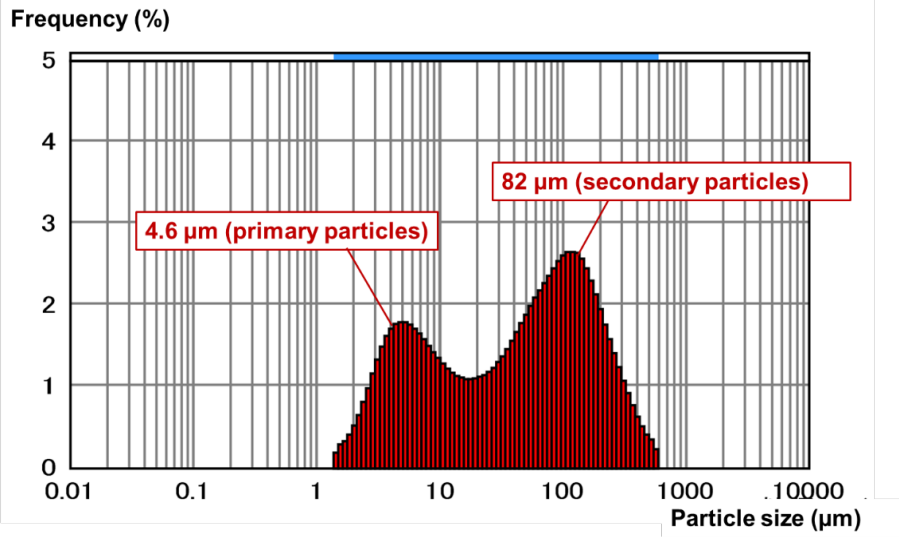

Figure S4. Particle Size Distribution of Bead-Milled Reagent PET (PET A) with Al_2O_3 Beads in Toluene

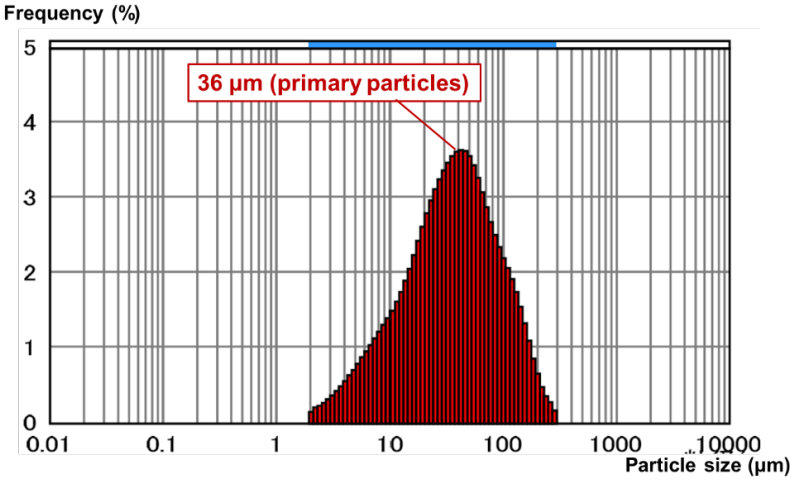

Figure S5. Particle Size Distribution of Bead-Milled Amorphous PET (PET B) with ZrO_2 Beads in Toluene

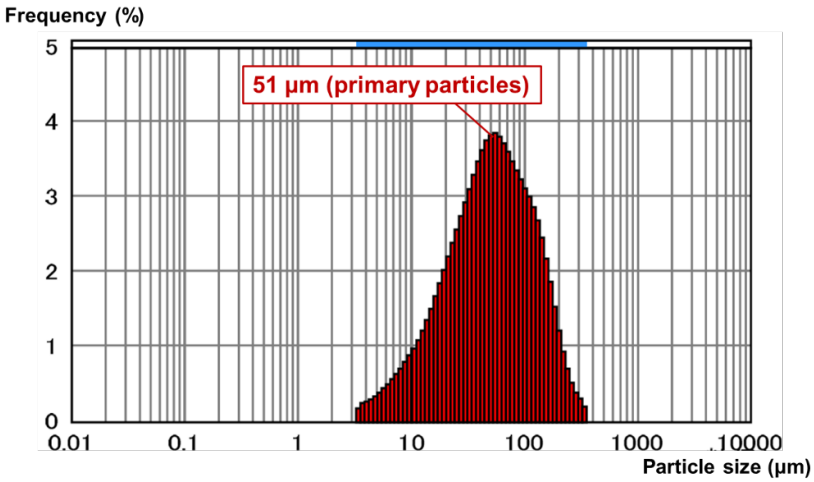

Figure S6. Particle Size Distribution of Bead-Milled Crystalline PET (PET C) with ZrO_2 Beads in Toluene

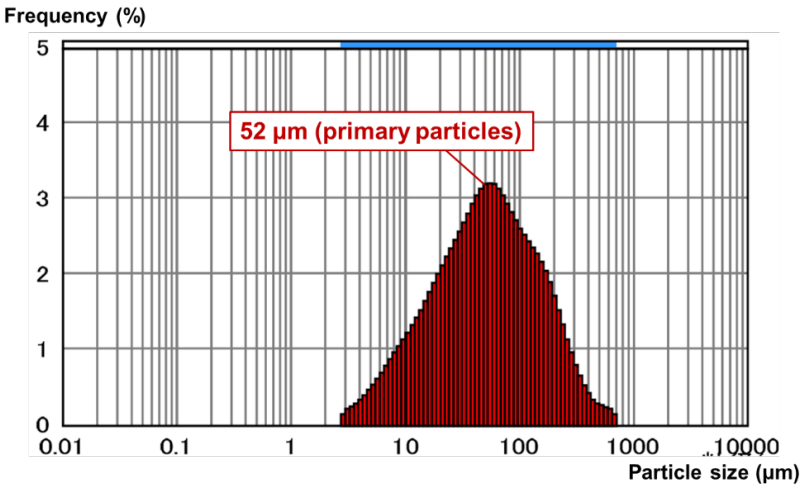

Figure S7. Particle Size Distribution of Bead-Milled beverage PET (PET D) with ZrO_2 Beads in Toluene

SI-3-2. GPC Analysis

To analyze molecular weight distribution of PET samples, GPC was used. For preparation of GPC samples, approximately 3 mg of PET samples were dissolved in HFIP/$CHCl_3$ (1:1) (4 mL) overnight, followed by filtration using a membrane filter (PTFE, φ0.22 μm pore size). The GPC chromatograms of reagent PET samples (PET A) under different bead mill conditions are shown in Figure S8-Figure S9.

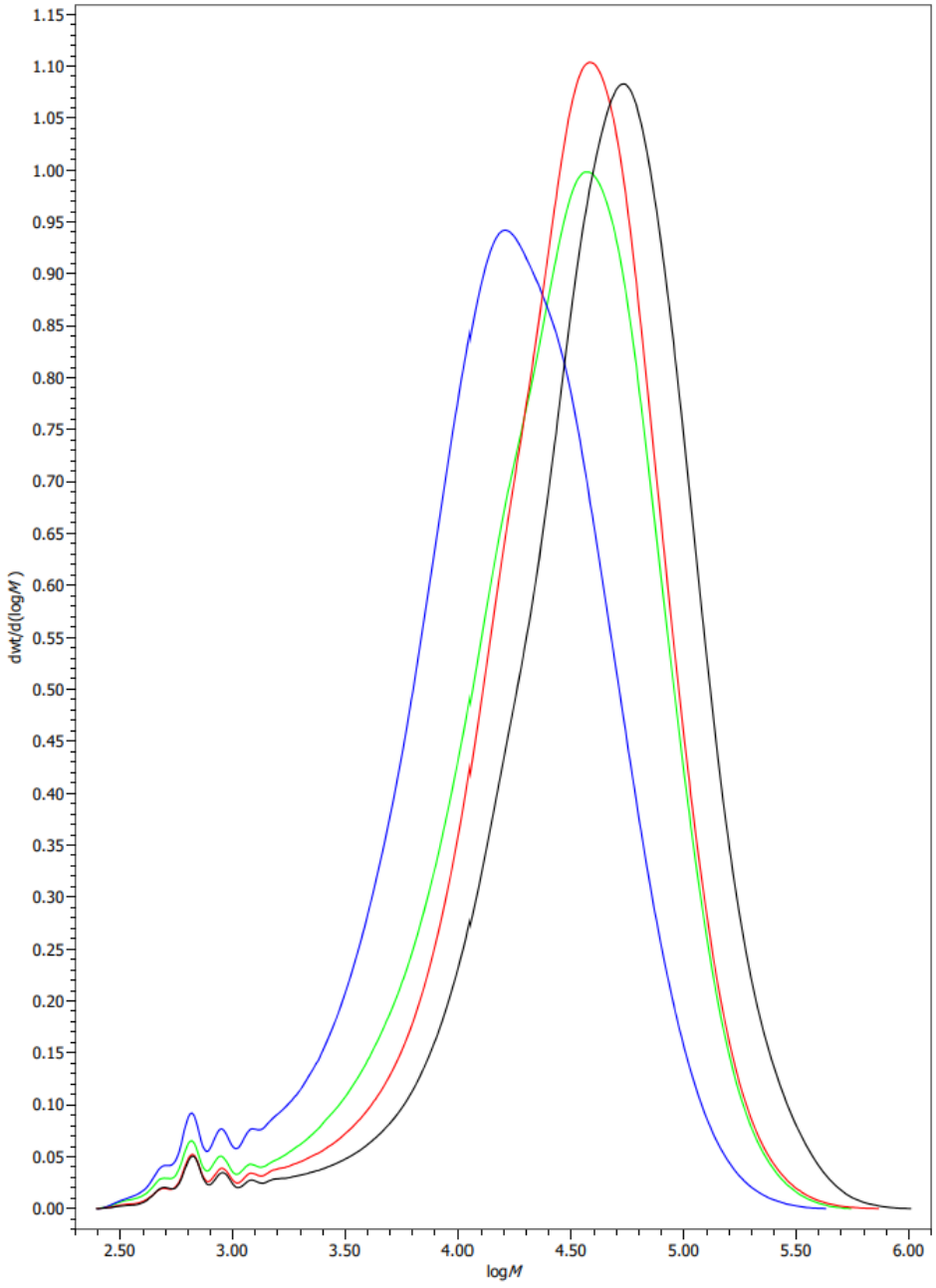

Figure S8. GPC Chromatograms of the Reagent PET Samples (PET A)

Black, as purchased sample before bead milling; Blue, the sample after bead milling under the standard conditions; Green, the sample after bead milling using Al_2O_3 beads; Red, the sample after bead milling using H_2O as a solvent.

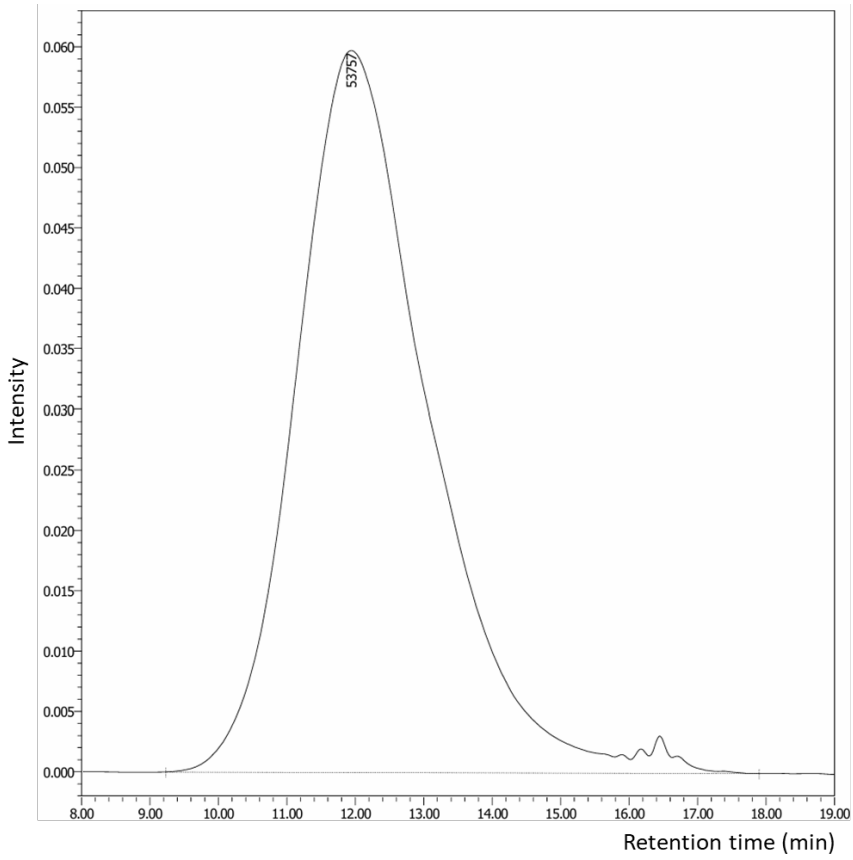

Figure S9. GPC Chromatogram of Bead-Milled Reagent PET (PET A)

with ZrO_2 Beads in $CHCl_3$

Figure 7 in the main text shows the molecular weight change over time during bead mill treatment for the amorphous and the crystalline PET pellets. In addition to this, Figure S10 shows those change in used the beverage PET flakes. After 48 hours of bead mill treatment, the peak top molecular weight (*Mp*) was 1,300, which was consistent with that of the amorphous PET (Figure 7(a) of the main text). As shown in Table 7 of the main text, the molecular weight distribution changed more uniformly and the *Mw*/*Mn* value was lower for the flake sample of used beverage PET compared to the pellet samples. Such a relatively uniform molecular weight change for the used beverage PET may be due to its thin molded structure that allows efficient transfer of mechanical energy. In contrast, for large block samples such as pellets, the agglomerated PET may act as a buffer and hinder efficient transfer of mechanical energy in the early stages of bead mill treatment.

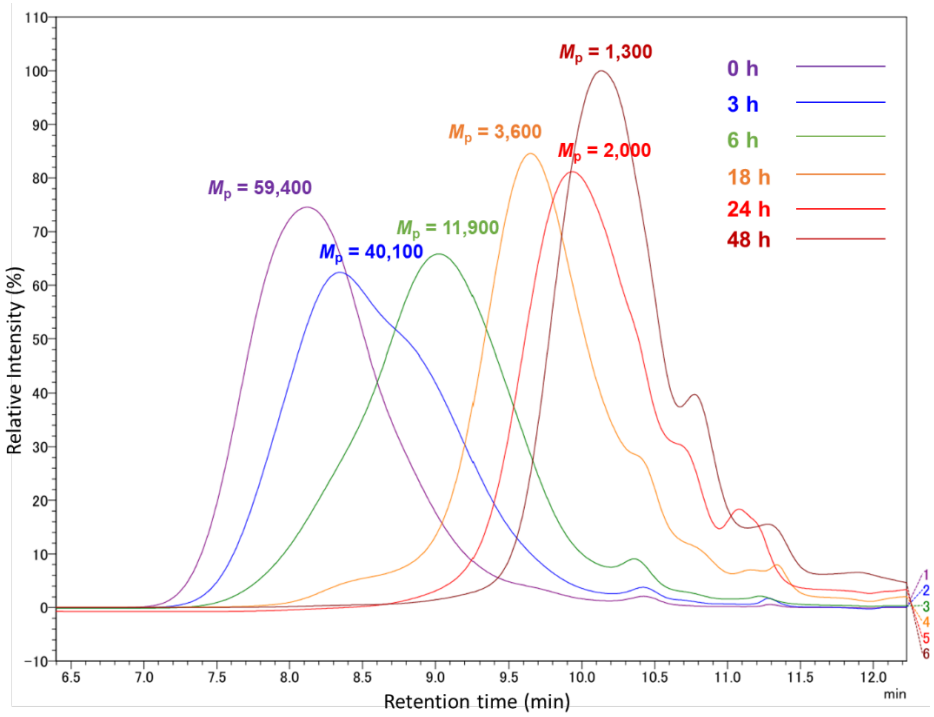

Figure S10. Time on Stream of Molecular Weight Changes During Bead Milling of the Used Beverage PET Flake

To aid the discussion regarding depolymerization, we will provide the following mechanism (Figure S1):

1. Initially, gradual depolymerization of high-molecular-weight PET occurs. As the molecular weight decreases, the reaction rate increases.

2. Subsequently, a PET oligomer with M_p 2,900 is formed. Depolymerization of this oligomer yields soluble PET species.

3. Once the PET dissolves, the homogeneous reaction proceeds rapidly, yielding the monomer DMT.

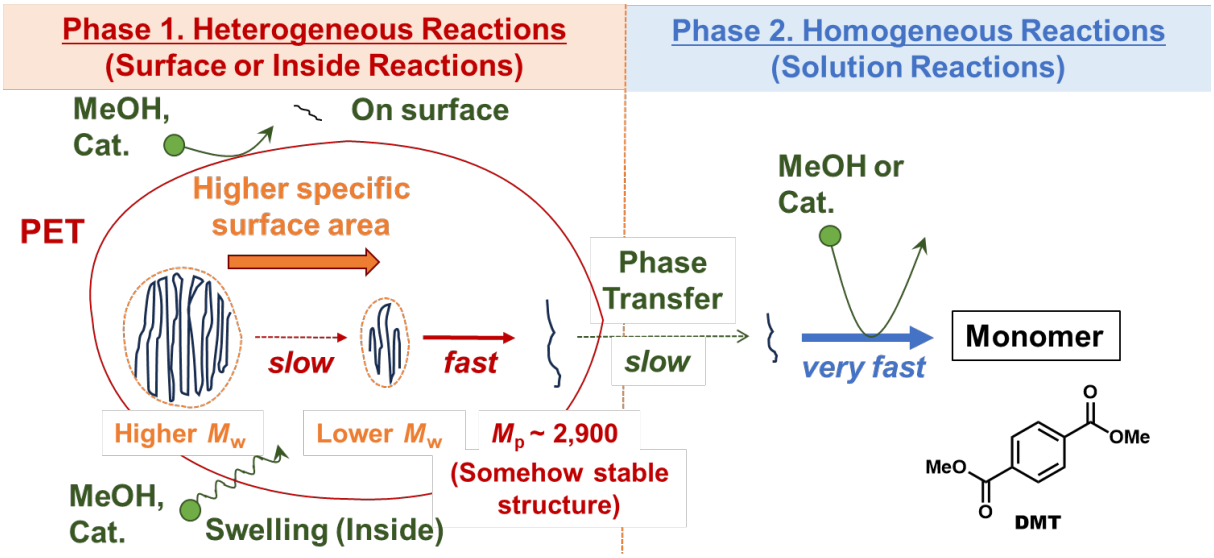

Figure S11. Schematic Proposed Mechanism of the Depolymerization Reactions of PET

SI-3-3. Crystallinity of Bead-Milled PETs

Figure 6 and Table 6 and the surrounding sentences in the main text discuss the correlation between crystallinity and reactivity. First, this section begins with the DSC analysis results of the reagent PET pellets used as standard samples (Figures S12 and S13). As noted in the figures, the crystallinity of the reagent PET samples increased after bead mill treatment. Interestingly, the crystallinity (Xc)[7] of all samples converged to about 35% after bead milling, regardless of the initial crystallinity. This observation is consistent with previous reports on mechanical grinding.[8,9] Here, note that the melting enthalpy in Table 6 in the main text has been corrected by weight.

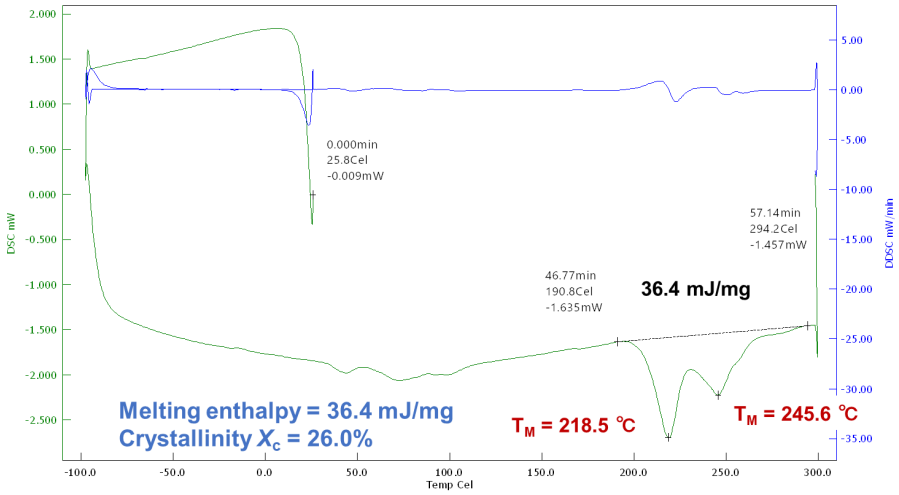

Figure S12. DSC Analysis of the Reagent PET (PET A) Before Bead Milling

(*The melting enthalpy was corrected by the actual PET component of 52.8 w/w%)

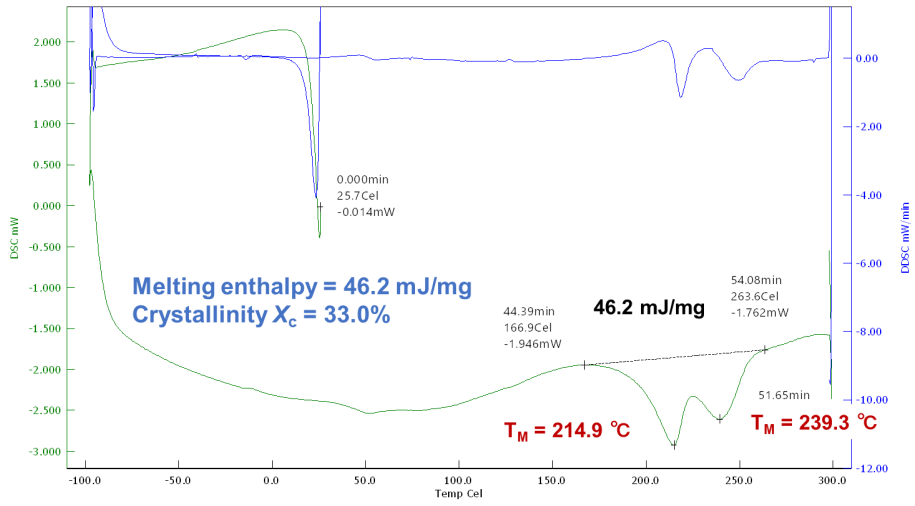

Figure S13. DSC Analysis of the Reagent PET (PET A) After Bead Milling

(*The melting enthalpy was corrected by the actual PET component of 52.8 w/w%)

As additional information on crystallinity, the PXRD profile of a bead milled amorphous PET sample is shown in Figure S14. It is possible to see how the crystalline structure grew.[8]

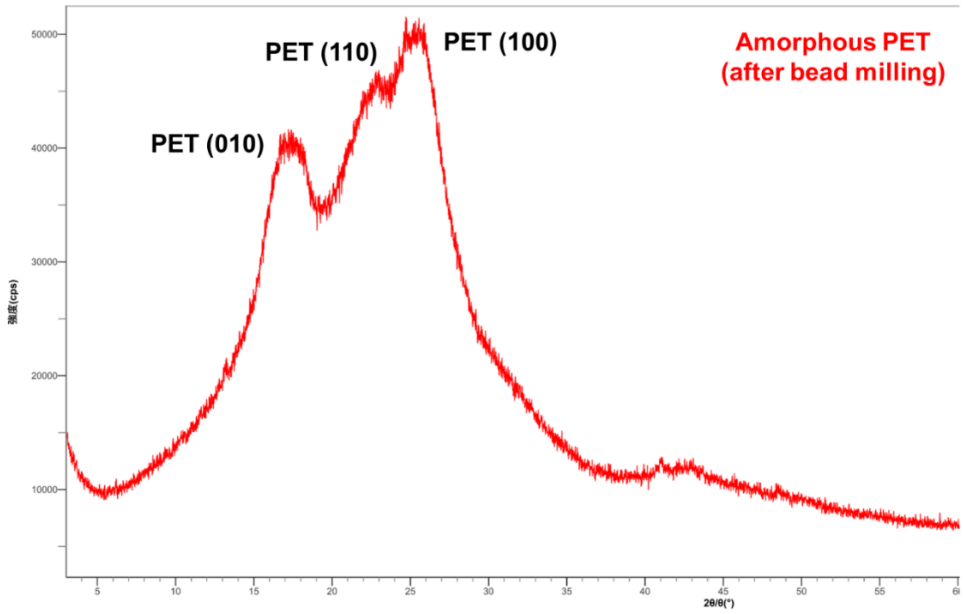

Figure S14. PXRD Analysis of the Amorphous PET Sample After Bead Milling

The increase in crystallinity observed during bead milling of the amorphous PET samples is discussed below, including some considerations not mentioned in the main text. To aid in the explanation, the considerations are shown as images in Figure S15.

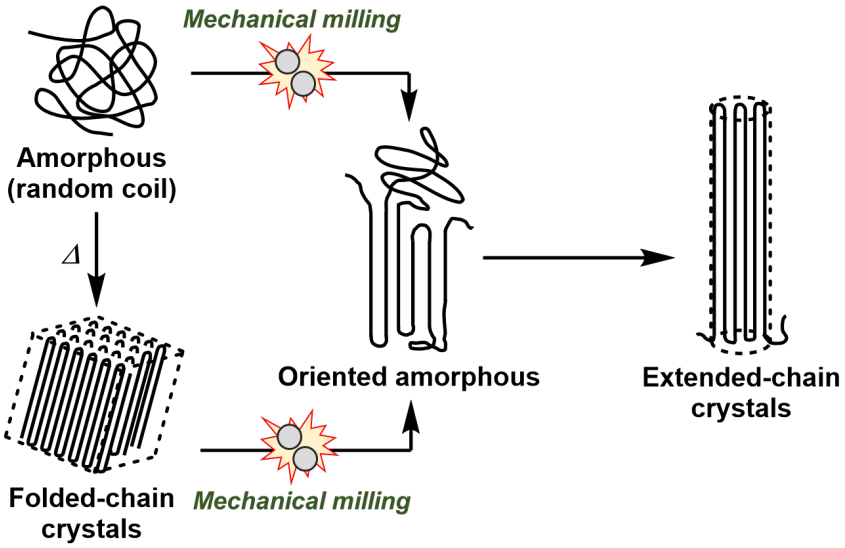

Figure S15. Proposed Morphological Changes of PET During Mechanical Milling[8]

The collision energy between the beads and the PET generates localized heat, raising the temperature above the glass transition temperature (Tg) (Figure S15 upper side). This localized heating leads to the formation of a polymer structure with locally oriented but rotationally disordered molecules.[8] This morphology is called "oriented amorphous".[10.11] When further mechanical energy was applied and this structure was locally heated, extended-chain crystals with an orientation close to the current orientation were formed, rather than folded-chain crystals, which are the most stable crystalline structure.[8] Previous studies have shown that extended-chain crystals tend to form under such stress conditions.[8,12] Under bead mill conditions, the locally heated and oriented polymer structure is rapidly cooled by the surrounding solvent, preventing the reorientation of the polymer chains and causing chain distortion. In this situation, the molecular density of the remaining amorphous regions decreases, making the molecular chains more susceptible to breakage due to strain caused by shrinkage stress. Thus, applying mechanical energy to these distorted chains causes them to break. Finally, the reduction in molecular weight increases the crystallization rate of the polymer, accelerating post-crystallization processes.[13]

The fact that the surface structure of amorphous PET changed due to local heating can also be seen in the SEM images in Figures S16–30. Comparison of the 3,000x scale images in Figure S16 and Figure S17 revealed significantly finer particle sizes in the sample after bead milling. The 30,000x scale image of the bead-milled sample showed evidence of local melting and stretching (Figure S17). Similar morphology was observed in all other bead-milled PET samples (Figures S18–20), indicating that the local temperature of the PET samples during bead milling exceeded their melting points.

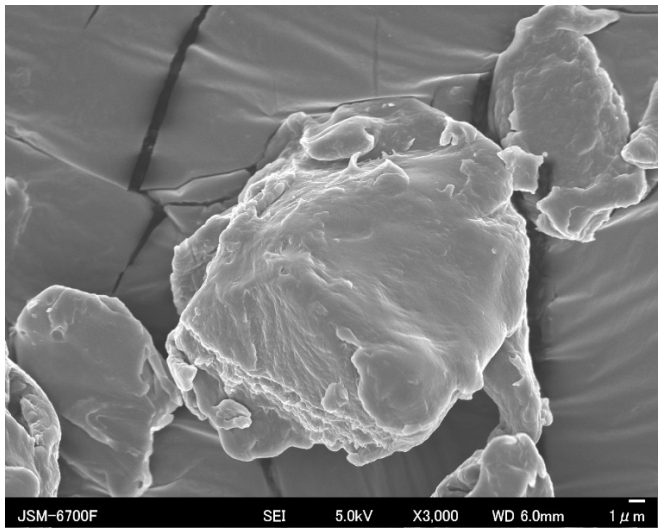

Figure S16. A SEM Image of the Reagent PET Pellets (PET A) (Before Bead Milling)

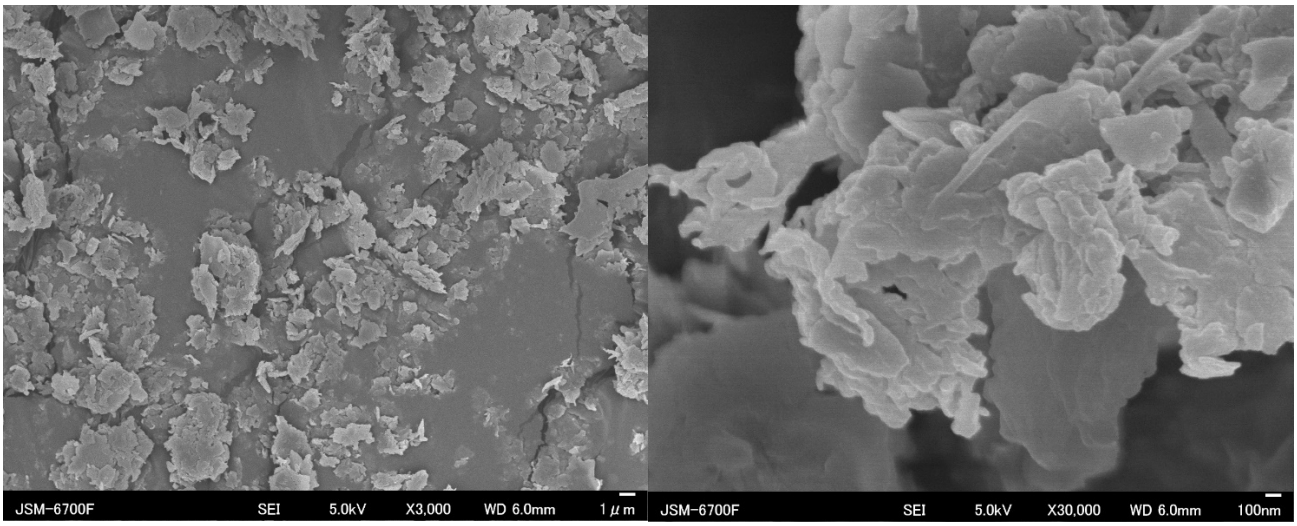

Figure S17. SEM Images of the Reagent PET (PET A) (After Bead Milling)

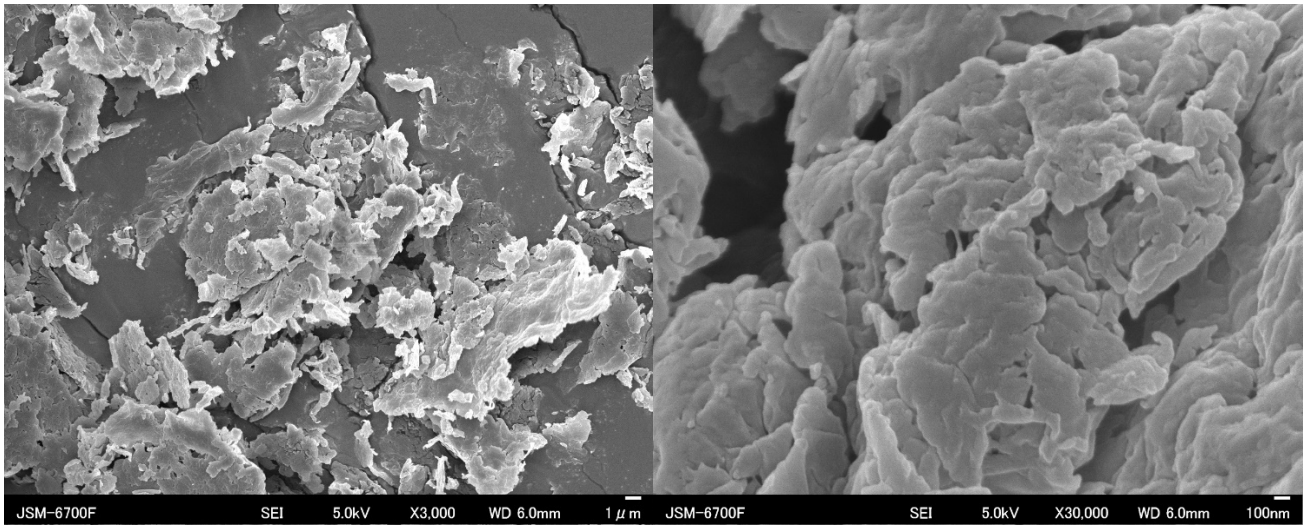

Figure S18. SEM Images of the Amorphous PET (PET B) (After Bead Milling)

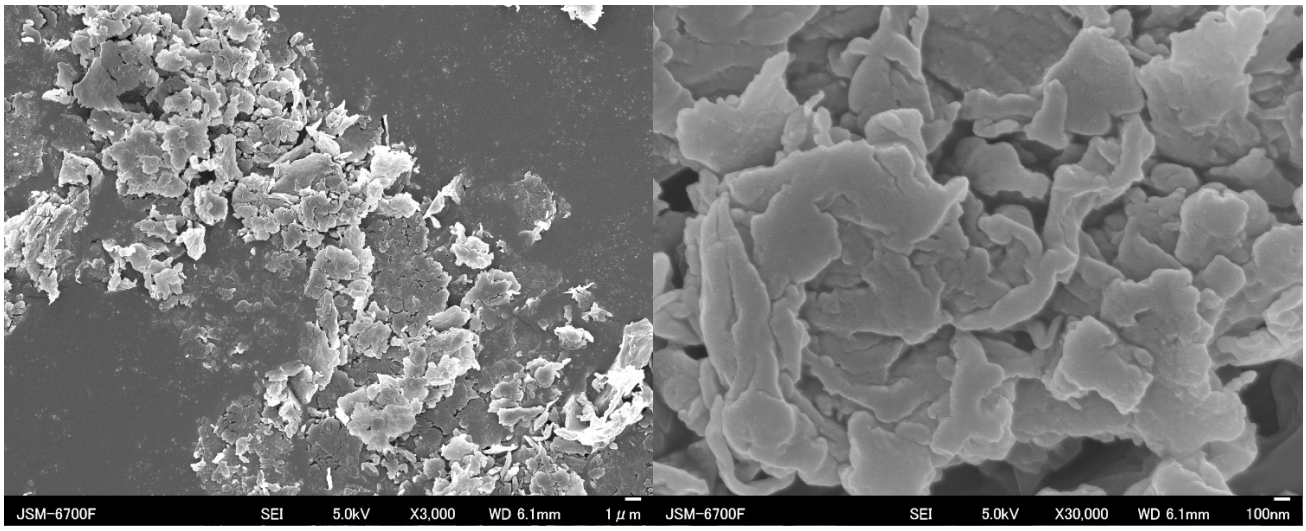

Figure S19. SEM Images of the Crystalline PET (PET C) (After Bead Milling)

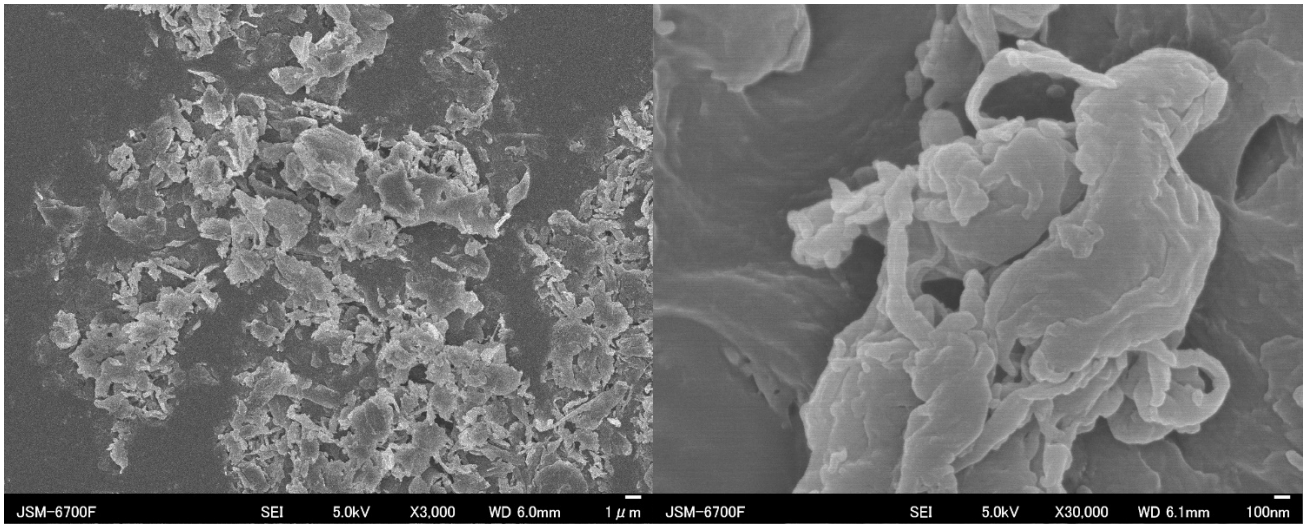

Figure S20. SEM Images of the Used Beverage PET (PET D) (After Bead Milling)

In the case of the crystalline PET sample (Figure S15, bottom side), when the local heat generation exceeded the melting point, it is expected that the polymer chains would also reorient. At this time, the originally highly crystalline structure was destroyed, and an oriented amorphous form was formed, followed by the formation of extended chain crystals.[8]

In this way, it can be considered that the change in orientation due to local heating ultimately led to a similar crystalline state regardless of the initial crystallinity.

SI-3-4. Specific Surface Area of Bead-Milled PETs

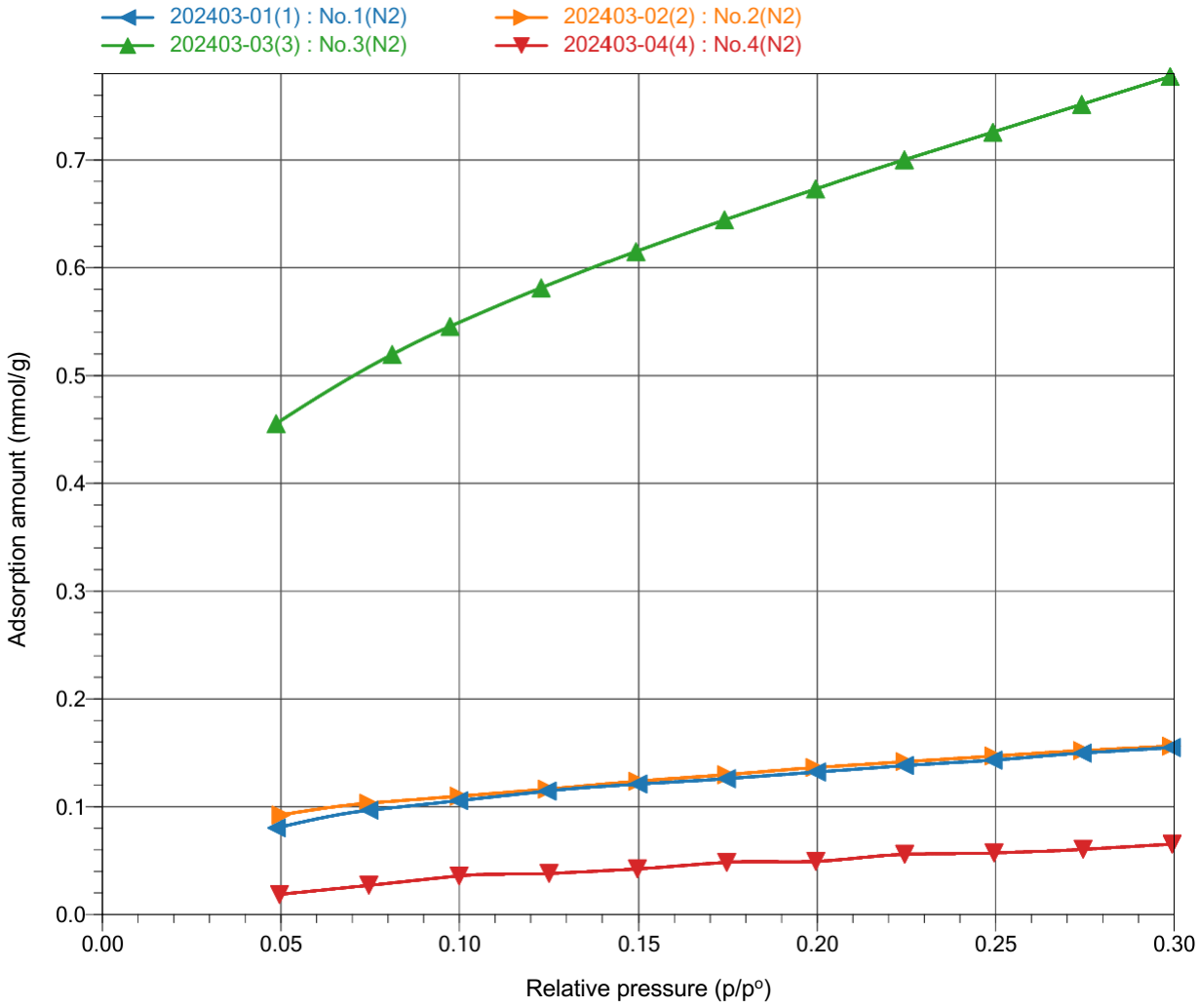

Figure S21. N_2 Adsorption Isotherm of Bead-Milled PET Samples

Blue, the amorphous PET sample after bead milling under the standard conditions; Orange, the crystalline PET sample after bead milling under the standard conditions; Green, the amorphous PET sample after bead milling using water as a solvent; Red, the amorphous PET sample after bead milling using Al_2O_3 beads.

Table S2. BET Specific Surface Area Derived from N_2 Adsorption Isotherm

No.	PET Sample	Bead Mill Coditions	BET Specific Surface Area
1	Amorphous Pellets	Standard Conditions	11.2442 ± 0.0654 m²/g
2	Crystalline Pellets	Standard Conditions	11.2346 ± 0.0835 m²/g
3	Amorphous Pellets	H_2O Solvent was used	55.5741 ± 0.2570 m²/g
4	Amorphous Pellets	Al_2O_3 Beads were used	5.5083 ± 0.1869 m²/g

*Analyzed sample amount was around 100 mg

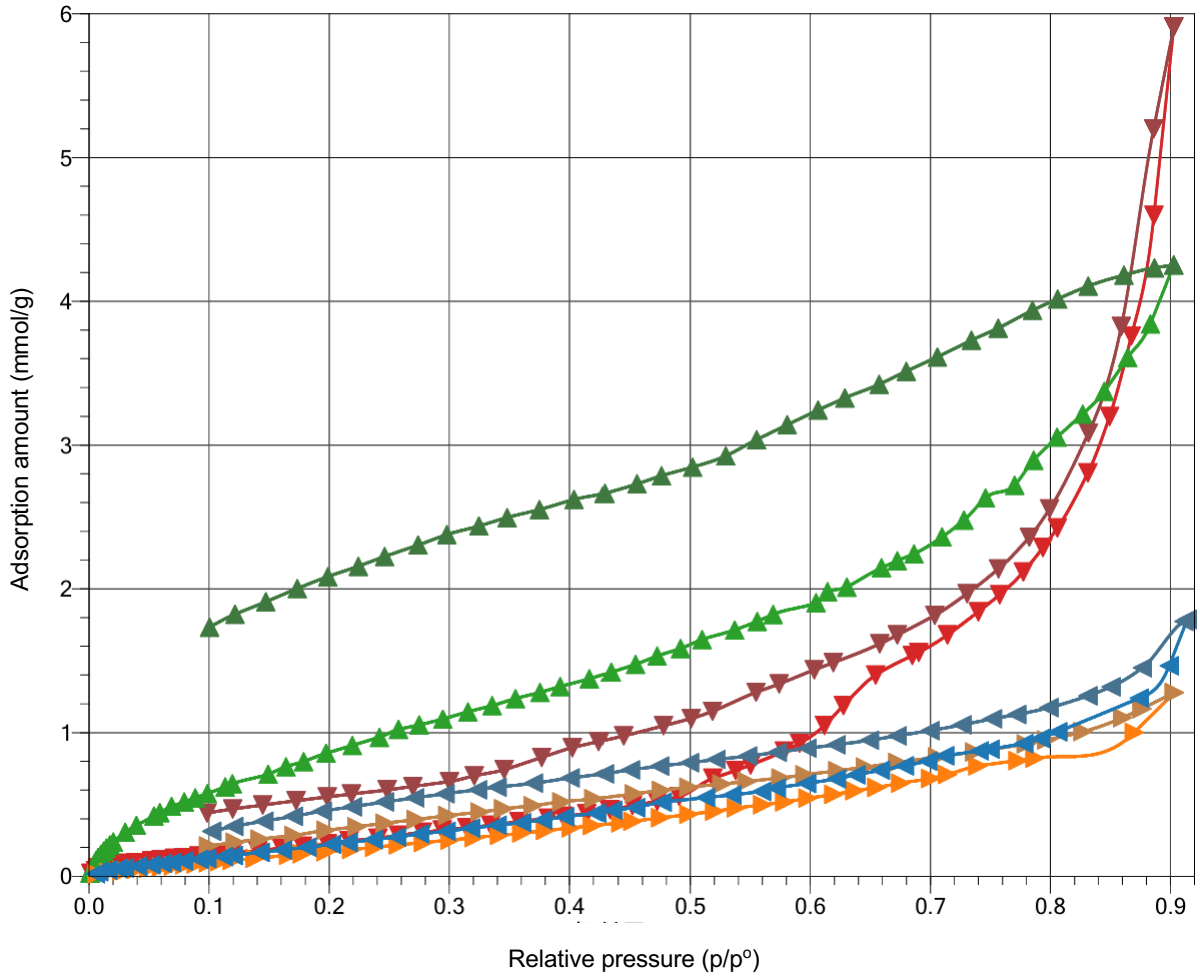

Figure S22. H_2O Adsorption Isotherm of Bead-Milled PET Samples

Blue, the amorphous PET sample after bead milling under the standard conditions; Orange, the crystalline PET sample after bead milling under the standard conditions; Green, the amorphous PET sample after bead milling using water as a solvent; Red, the amorphous PET sample after bead milling using Al_2O_3 beads.

Table S3. H_2O Adsorption Amount Based on the Isotherm

No.	PET Sample	Bead Mill Coditions	H_2O Adsorption Amount	Relative Pressure
1	Amorphous Pellets	Standard Conditions	1.79 mmol/g	0.914
2	Crystalline Pellets	Standard Conditions	1.28 mmol/g	0.903
3	Amorphous Pellets	H_2O Solvent was used	4.25 mmol/g	0.903
4	Amorphous Pellets	Al_2O_3 Beads were used	5.91 mmol/g	0.903

*Analyzed sample amount was around 100 mg

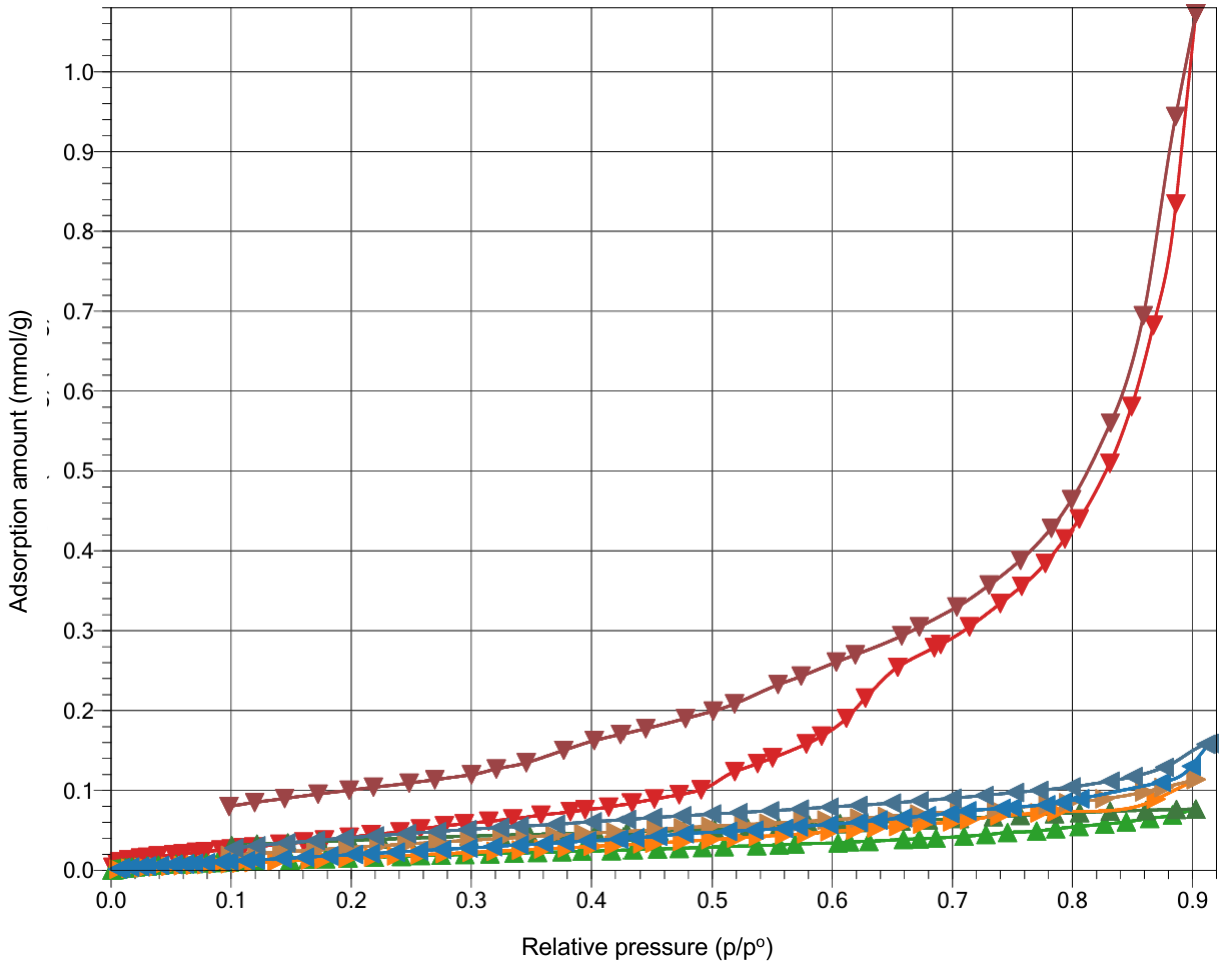

Figure S23. H_2O Adsorption Isotherm per Surface Area of Bead-Milled PET Samples

Blue, the amorphous PET sample after bead milling under the standard conditions; Orange, the crystalline PET sample after bead milling under the standard conditions; Green, the amorphous PET sample after bead milling using water as a solvent; Red, the amorphous PET sample after bead milling using Al_2O_3 beads.

Table S4. Relative H_2O Adsorption Amount to the Surface Area of the Samples

No.	PET Sample	Bead Mill Coditions	H_2O Adsorption per Surface Area	Relative Pressure
1	Amorphous Pellets	Standard Conditions	0.159 mmol/m²	0.914
2	Crystalline Pellets	Standard Conditions	0.114 mmol/m²	0.903
3	Amorphous Pellets	H_2O Solvent was used	0.0765 mmol/m²	0.903
4	Amorphous Pellets	Al_2O_3 Beads were used	1.07 mmol/m²	0.903

*Analyzed sample amount was around 100 mg

SI-4. Hansen's Solubility Parameters and Relative Energy Difference (RED) Values

As discussed on Table 2 in the main text, we assumed that the affinity between PET and solvents should play an important role under bead mill conditions to stabilize the polymer structures,[14,15] and to give finer particles and shorter chains. Especially, treatment with toluene caused the smallest molecular weight, and the peak top molecular weight (M_p) was less than 1/3 after 3 h of the treatment compared to that of the untreated sample (entry 4, Table 2 in the main text). The molecular weight reduction was remarkably faster than a dry milling method:[16] molecular weight was still 95% of the original one after 12 h under dry ball milling, and 70% even after 48 h.

The representative parameter to describe the affinity is a Hansen solubility parameter.[17] This parameter is based on the idea that two substances with similar interaction behavior are likely to dissolve in each other. It consists of the following three parameters in $MPa^{1/2}$ units: the energy derived from dispersion interactions (δ_d), dipolar interactions (δ_p), and hydrogen bonding (δ_h)). As a function of these three parameters, substances whose coordinates are close in three-dimensional space (Hansen space) are considered to have high affinity. If the parameters of substance 1 are (δ_{d1}, δ_{p1}, δ_{h1}) and that of substance 2 are (δ_{d2}, δ_{p2}, δ_{h2}), the distance (R_a) between substances 1 and 2 is expressed as follows:

$$R_a{}^2 = 4(\delta_{d2} - \delta_{d1})^2 + \left(\delta_{p2} - \delta_{p1}\right)^2 + (\delta_{h2} - \delta_{h1})^2$$

When R_0 is determined experimentally as a distance in which substances have boundary affinity, the relative energy difference (RED) can be expressed as follows:

$$RED = \frac{R_a}{R_0}$$

A RED value with less than 1 indicates that these two substances have relatively high affinity. Hansen parameters of PET and solvents are described in TableTable S S5.[17–20] When comparing water, acetonitrile, and toluene, toluene has the lowest RED value (RED = 0.85); in other words, it has the highest affinity to PET among them. Therefore, there seemed to be a certain correlation between such an affinity and effects of micronization and molecular weight reduction.

Table S6 shows a summary of the correlation between the reaction acceleration effect depending on bead mill solvents and the RED values.[17–20] In poor solvents with a RED of more than 1, lower RED values contributed to a higher effect on the reaction acceleration, probably due to the higher milling efficiency caused by solvation, as mentioned above. On the other hand, when the RED value was lower than toluene, the acceleration effect was deteriorated in chloroform, which could dissolve PET. These results indicated that the ideal solvent for bead milling was one that had good affinity for PET but does not dissolve it, and toluene was such an example.

Table S5. Hansen Solubility Parameters of PET and Several Solvents[17–20]

Material	Hansen Parameters[a] ($MPa^{1/2}$)			R_a[b]	RED[c] (= R_a/R_0)
	δ_d	δ_p	δ_h		
PET	18.2	6.4	6.6	-	-
MeOH	14.7	12.3	22.3	18.2	2.27
Ethylene glycol	17.0	11.0	26.0	20.1	2.51
$NH_2(CH_2)_2OH$	17.0	15.5	21.2	17.4	2.17
H_2O	15.5	16.0	42.3	37.4	4.67
CH_3CN	15.3	18.0	6.1	13.0	1.62
Toluene	18.0	1.4	2.0	6.8	0.85
$CHCl_3$	17.8	3.1	5.7	3.5	0.44
Pyridine	19.0	8.8	5.9	3.0	0.37
CH_2Cl_2	18.2	6.3	6.1	0.5	0.06

[a] δ_d, the energy from dispersion forces; δ_p, dipolar intermolecular forces; δ_h, hydrogen bonds.

[b] $R_a^2 = 4*(\delta_d - \delta_d(PET))^2+(\delta_p - \delta_p(PET))^2+(\delta_h - \delta_h(PET))^2$. [c] Relative enrgy difference, RED = R_a/R_0, R_0 = 8.0.

Orange column, parameters for PET; Blue column, parameters for depolymerization solvents; Yellow column, parameters for bead mill solvents; Gray column, parameters for cosolvents in depolymerization)

Table S6. Effect of Bead Mill Solvents Correlated with the RED Values[17–20]

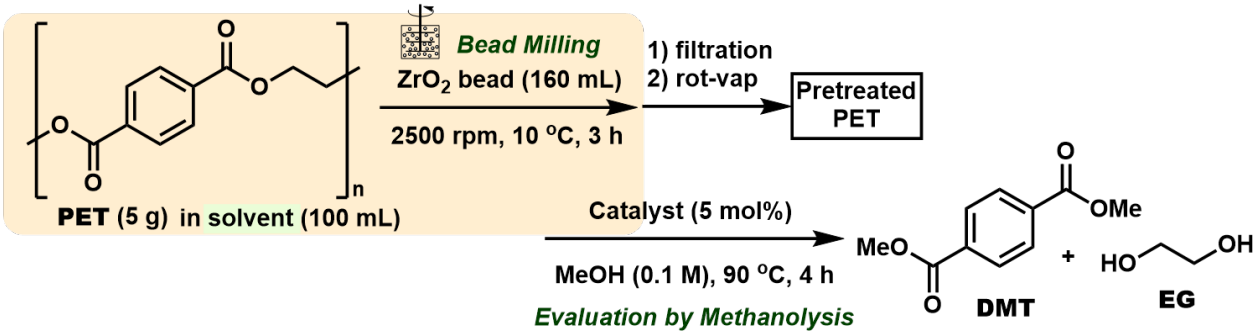

Entry	Bead Mill Solvent	Catalyst	Yield (%)[a]		RED[b]
			DMT	EG	
1	H_2O	no catalyst	9	6	4.67
2		$^n Bu_4NOH$	39	28	
3	MeOH	no catalyst	11	7	2.27
4		$^n Bu_4NOH$	38	26	
5	CH_3CN	no catalyst	14	10	1.62
6		$^n Bu_4NOH$	53	36	
7	Benzene	no catalyst	28	20	0.99
8		$^n Bu_4NOH$	59	39	
9	Toluene	no catalyst	31	13	0.85
10		$^n Bu_4NOH$	69	36	
11	$CHCl_3$	no catalyst	23	18	0.44
12		$^n Bu_4NOH$	58	37	

[a] Determined by GC analysis; [b] Relative energy difference to PET, based on Hansen solubility parameters

SI-5. Additional Experimental Results for Bead Mill Treatment and Methanolysis

SI-5-1. Catalyst Screening for Methanolysis of PET

In addition to the results in the main text (Table 5), a wide variety of catalysts were screened in methanolysis to find the optimal catalyst. At initial investigations, reported catalysts were tested (Table S7). In the case of the reagent PET (PET A) as a starting material, the reaction somehow proceeded after the bead mill treatment even without a catalyst, giving 31% yield of DMT. Using a reported $La(acac)_3$ catalyst[21] slightly accelerated the reaction to give 38% yield of DMT (entry 2). Other lanthanum salts were also tried such as La_2O_3 and $La(OTf)_3$, which were reported as catalysts for transesterification.[22,23] Although $La(OH)_3$, La_2O_3, and $La(OTf)_3$ revealed no catalytic effect (entries 3-5), a combination of $La(OTf)_3$ and NaOMe catalysts improved the yield to 41% (entry 6). About this combination, Brown *et al*. proposed that *in situ* formation of a methoxy-bridged La(III) dimer complex was a key to efficiently catalyze a transesterification process through Lewis acid-Lewis base dual activation of esters.[24] The commonly used $Zn(OAc)_2$ catalyst[25–34] somehow diminished the yield (entry 7). 1,5,7-Triazabicyclo[4.4.0]dec-5-ene (TBD) reported as a good catalyst[35,36] did not show catalytic effect under the reaction conditions. On the other hand, inorganic bases such as KOMe, NaOMe, and K_2CO_3[35–37] showed good catalytic activities, affording over 60% yield of DMT (entries 9-11). Among the reported catalysts, KOMe was found to be the best to afford 69% yield of DMT.

Table S7. Investigation of Reported Catalysts

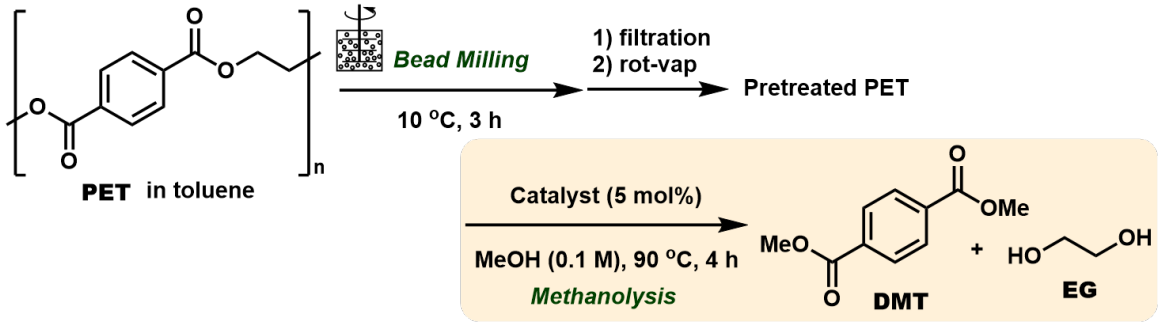

Entry	Catalyst	Yield (%)[a]		Entry	Catalyst	Yield (%)[a]	
		DMT	EG			DMT	EG
1	no catalyst	31	13	7	$Zn(OAc)_2$	14	N.D.
2	$La(acac)_3$	38	17	8	TBD	29	17
3	$La(OH)_3$	30	27	9	KOMe	69	44
4	La_2O_3	33	17	10	NaOMe	63	33
5	$La(OTf)_3$	29	21	11	K_2CO_3	62	43
6	$La(OTf)_3$ + NaOMe	41	22				

[a] Determined by GC analysis; N.D. Not Detected

Although these approaches using metal complexes or metal oxides as catalysts are effective ways in accelerating methanolysis reactions, the presence of residual metal components in the products can sometimes cause toxicity and discoloration issues.[25,38] Therefore, developing non-expensive and easy-to-remove organocatalysts to replace metal catalysts could lead to more sustainable processes. We hypothesized that an ionic liquid would be one of the most promising candidates as an organocatalyst to promote the methanolysis of PET. This was because ionic liquids have the following attractive

properties:

1. **High affinity for PET:** Ionic liquids have a high affinity for PET and can increase its solubility, which could loosen the molecular chains of insoluble PET, making it easier for catalysts and methanol to access.[39]

2. **Dual activation:** Since ionic liquids form ion pairs, a countercation activates a carbonyl group, and simultaneously a counteranion activates an alcohol, resulting in an efficient transesterification process.[6,38–42]

3. **Easy separation:** While many ionic liquids are soluble in water, the product DMT is insoluble, making it easy to separate the catalysts by washing with water.[41]

For example, McKeown *et al*. developed a methanolysis process of PET using tetramethylammonium methyl carbonate (TMC) as a catalyst, and were able to obtain DMT in 72% yield under mild conditions of 100 °C, although a long reaction time of 16 hours was required.[38]

We then started investigation of quaternary ammonium salts (Table S8). Fortunately, initial trials clarified that tetrabutylammonium hydroxide (TBAOH) showed good catalytic activity, affording DMT in an average yield of 69% over two experiments (entry 2). This catalytic activity was comparable to that of KOMe, which showed the best activity among the reported catalysts (entry 9). Changing the counter anion to acetate or iodide led to lower catalytic activity (entries 3-4). The order of the basicity of counter anions, $^{-}OH > {}^{-}OAc > I^{-}$, correlated with catalytic activity, indicating that the basicity of the ammonium salts was important for catalysis. Next, the effect of the counter cation was investigated. Tetrabutylphosphonium hydroxide, $^{n}Bu_4POH$, showed lower catalytic activity than TBAOH, affording 41% yield of DMT (entry 5). Other quaternary ammonium hydroxides with different alkyl chains were also investigated (entries 6-12). Although tetramethylammonium hydroxide (TMAOH) showed comparable activity to TBAOH (entry 6), simple ammonium hydroxide (ammonia aqueous solution) exhibited no catalytic activity (entry 7). We also investigated other quaternary ammonium salts with the structure of RMe_3NOH (entries 8-12**,** R = benzyl, phenyl, adamantyl, hexadecyl, hydroxyethyl), and found that $PhMe_3NOH$ especially showed high catalytic activity, and 76% yield of DMT was obtained (entry 9).

On the other hand, when the counter anion was changed to methoxide to increase the basicity, improvement of the yield was observed (entry 13). Tetramethylammonium methoxide (TMAM) efficiently catalyzed the reaction to give 76% yield of DMT. In addition, increasing the catalyst amount to 10 mol% further promoted the reaction, and 81% yield of isolated DMT was obtained (entry 14). It was proposed that the reported tetramethylammonium methyl carbonate (TMC) catalyst underwent decarboxylation upon heating, *in situ* producing TMAM as the active species.[2,38] The methanolysis reaction was tried using TMC prepared according to the literature,[2] but the catalytic activity was insufficient, giving DMT in 49% yield (entry 15). Because the reaction required a long time of 16 h to proceed at 100 °C in the original paper,[38] the reaction progress was considered to have been suppressed under the lower temperature of 90 °C and the shorter reaction time of 4 h. Therefore, TMAM should be a promising catalyst that can exhibit high catalytic activity even at low temperatures. Here, the proposed mechanism of the TMAM-catalyzed methanolysis is shown in Figure S24, based on the previous reports.[2,38,43]

On the other hand, when the basicity of the counter anion was further increased, tetrabutylammonium *tert*-butoxide, $^{n}Bu_4N(O^{t}Bu)$, showed slightly deteriorated reactivity, affording 60% yield of DMT (Table S8, entry 16). The stability of $^{n}Bu_4N(O^{t}Bu)$ was insufficient, as ^{1}H NMR analysis revealed that it readily decomposed even with mild heating at 40-60 °C to form $^{n}Bu_3N$. This was likely due to Hoffmann elimination caused by the counteranion ($^{-}O^{t}Bu$) abstracting the β-hydrogen of the tetrabutylammonium cation.[2,44] Therefore, from the viewpoint of thermal stability, the optimal

countercation was determined to be tetramethylammonium (Me_4N^+), which does not undergo Hoffmann elimination.[2] Another type of quaternary ammonium salt, butylmethylimidazolium hydroxide, [Bmim]OH,[3] was also tested, but the catalytic activity was inferior (entry 17). Taking all of the above into consideration, TMAM was determined to be the optimal catalyst for effectively promoting the methanolysis of PET under mild conditions at 90 °C.

Table S8. Investigation of Quaternary Ammonium Salt Catalysts

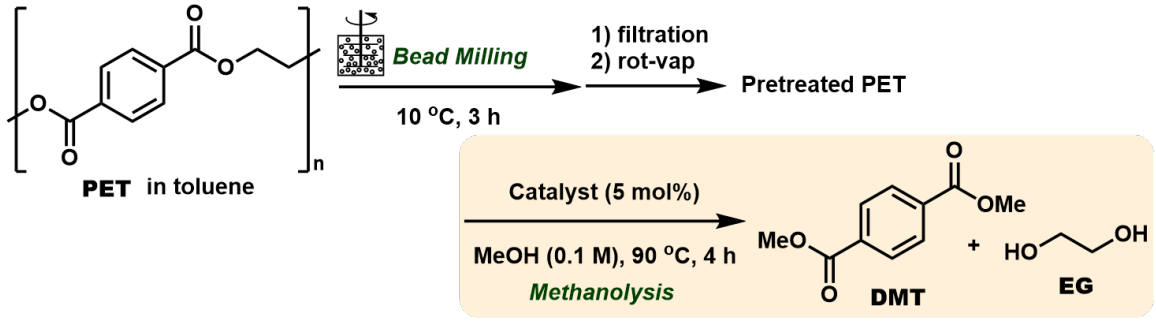

Entry	Catalyst	Yield (%)[a]	
		DMT	EG
1	no catalyst	31	13
2	^{n}Bu$_4$NOH	69	36
3	^{n}Bu$_4$NOAc	42	19
4	^{n}Bu$_4$NI	36	16
5	^{n}Bu$_4$POH	41	22
6	NH$_4$OH (NH$_3$ aq.)	28	19
7	Me$_4$NOH	67	32
8	BnMe$_3$NOH	62	28
9	PhMe$_3$NOH	76	38
10	AdMe$_3$NOH	47	22
11	(C$_{16}$H$_{33}$)Me$_3$NOH	29	21
12	Choline	67	37
13	Me$_4$N(OMe)	76 (75)[b]	41
14[c]	Me$_4$N(OMe)	81[b]	37
15	Me$_4$N(OCO$_2$Me)	49	26
16	^{n}Bu$_4$N(O^tBu)	60	36
17	[Bmim]OH	40	20

[a] Determined by GC analysis; [b] Isolated yield; [c] Cat. (10 mol%)

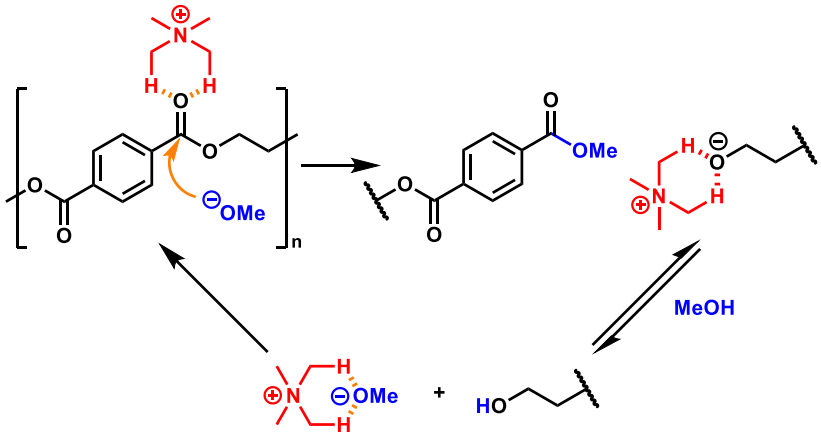

Figure S24. Proposed Mechanism of the TMAM-Catalyzed Methanolysis of PET[2,38,43]

As a trial to find an optimal reaction conditions for methanolysis, higher concentration of 0.4 M was tried instead of 0.1 M for the standard concentration (Table S9). Simply decreasing the amount of solvent caused a stirring issue due to insufficient solvent volume (entry 2). However, scaling up the system solved this issue and afforded a comparable yield to that obtained with 0.1 M (entry 3), indicating that higher concentrations would be achievable.

Table S9. Trials of Higher Concentrations

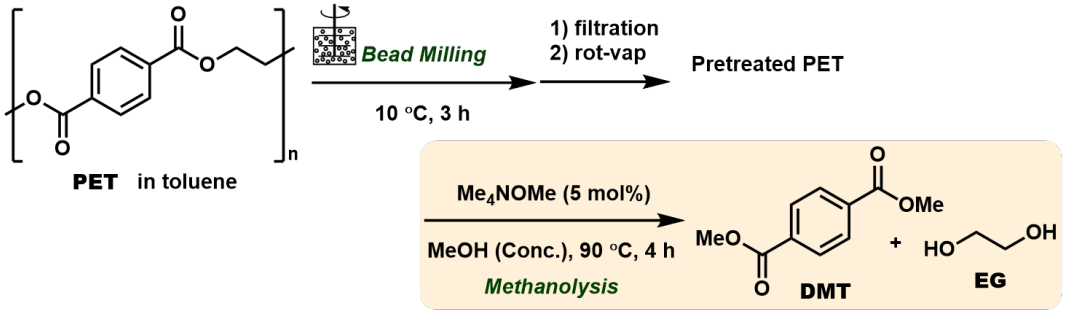

Entry	Reaction scale	Concentration	Yield (%)[a]	
			DMT	EG
1	0.4 mmol	0.1 M	76	41
2	0.4 mmol	0.4 M	65	41
3	1.6 mmol	0.4 M	70	43

[a] Determined by GC analysis

SI-5-2. Application to Several PET Samples

In this section, we present the details of the results visually depicted in Figure 4 of the main text which displayed using amorphous pellets (PET B), crystalline pellets (PET C), and beverage PET bottle flakes (PET D) provided by a PET supplier (Table S10) as the PET substrate. We have examined the above four types of PET samples, including the reagent PET (PET A), under given four conditions: with or without bead mill treatment, and with or without the addition of catalyst TMAM. Not surprisingly, the reaction does not proceed without milling or the use of a catalyst. Strikingly, in the three newly tested samples, the reaction barely proceeds without either bead milling or the use of TMAM. This fact can be said to reveal the effect of bead mill treatment and TMAM found as a result of our investigation.

In addition, as described in the text, there are differences in methanolysis performance depending on the properties of PET. This data motivates us to examine the details.

Table S10. Applicability of the Developed Bead Mill Method to Several PET Samples

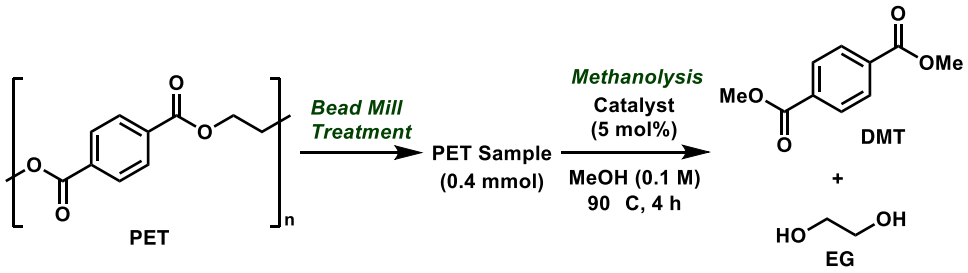

Entry	PET Sample	Bead Milling	Catalyst	Yield (%)[a]	
				DMT	EG
1	Reagent PET (PET A)	Not Done	none	0	N.D.
2			TMAM	14	N.D.
3		Done	none	31	13
4			TMAM	69	36
5	Amorphous PET (PET B)	Not Done	none	N.D.	N.D.
6			TMAM	1	2
7		Done	none	N.D.	N.D.
8			TMAM	84	79
9	Crystalline PET (PET C)	Not Done	none	N.D.	N.D.
10			TMAM	1	2
11		Done	none	N.D.	N.D.
12			TMAM	64	58
13	Used beverage PET flake (PET D)	Not Done	none	0	N.D.
14			TMAM	1	N.D.
15		Done	none	1	<2
16			TMAM	82 (84)[b]	82

[a] Determined by GC analysis; N.D., Not Detected. [b] Isolated yield.

SI-5-3. Details of Reaction Profiles for Methanolysis Reactions

Figure 3 in the main text shows the reaction profile of methanolysis performed using the PET powder derived from the reagent PET pellets with 5 mol% TMAM (red circles), with comparing to the methanolysis performed using the PET powder without catalyst addition (blue circles), and methanolysis performed using the reagent PET pellets without bead milling, with (black squares) and without (white squares) the catalyst TMAM, respectively. The yield at each plot for this figure is shown in Table S11 below.

Table S11. Reaction Profile of the Methanolysis of the Reagent PET Over 24 h

Entry	Bead Mill Treatment	Catalyst	Reaction time (h)							
			0.5	1	2	3	4	6	10	24
1	no	no catalyst	0	0	0	0	0	8	9	16
2		$Me_4N(OMe)$	1	3	6	10	18	27	47	74
3	yes	no catalyst	6	20	28	32	31	37	48	59
4		$Me_4N(OMe)$	59	70	70	73	76	78	79	78

[a] Determined by GC analysis

Similarly, reaction profiles for other PET samples, namely, amorphous PET pellets, crystalline PET pellets, and used beverage PET flakes, were also investigated and are shown in this section (Figures 25–27, Tables S12–14). The data presented in the previous section, i.e., details of Figure 4 in the main text, is an excerpt of the DMT yield at the 4-hour time point for the data introduced below.

As mentioned in the text, the reaction proceeds only when both bead milling and a methanolysis catalyst are used in amorphous PET samples, crystalline PET samples, and beverage PET samples. Also, for non-crystalline PET samples, including reagent PET samples, it can be seen that the DMT yield in the methanolysis reaction almost reaches a plateau-like state within 1 hour after the start of the reaction. Only crystalline PET proceeds somewhat slowly, and the reaction is not yet complete at the 4-hour time point.

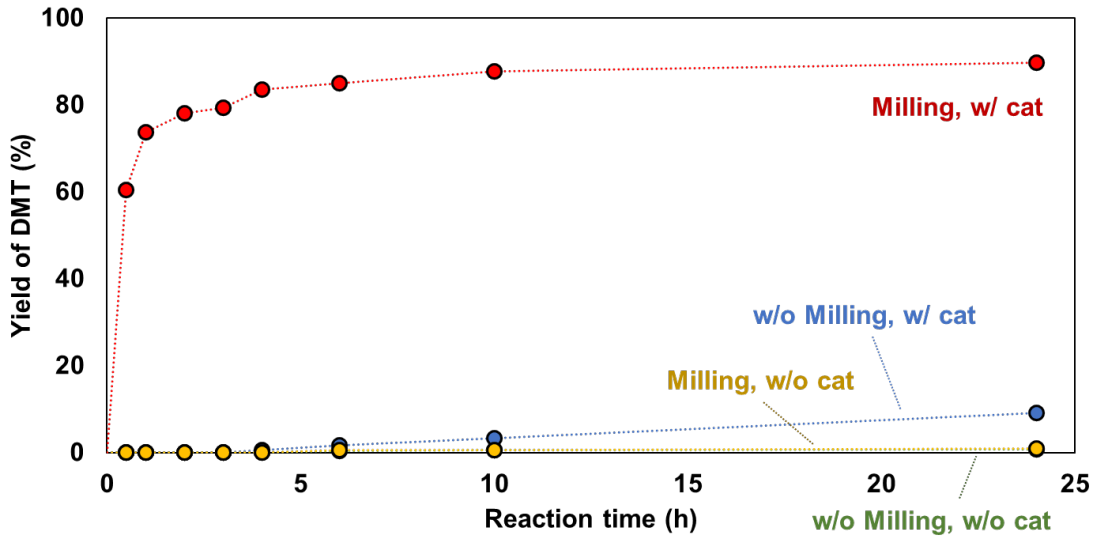

Figure S25. Reaction Profile of the Methanolysis of the Amorphous PET Sample Over 24 h

Red circles, with bead mill treatment and with TMAM catalyst; Yellow circles, with bead mill treatment and w/o the catalyst; Blue circles, w/o bead mill treatment and with TMAM catalyst; Green circles (hidden by the yellow circles), w/o bead mill treatment and w/o a catalyst.

Table S12. Reaction Profile of the Methanolysis of the Amorphous PET Sample (PET B) Over 24 h

Entry	Bead Mill Treatment	Catalyst	Reaction time (h)							
			0.5	1	2	3	4	6	10	24
1	no	no catalyst	0	0	0	0	0	0	1	1
2		$Me_4N(OMe)$	0	0	0	0	1	2	3	9
3	yes	no catalyst	0	0	0	0	0	0	1	1
4		$Me_4N(OMe)$	61	74	78	79	84	85	88	90

[a] Determined by GC analysis

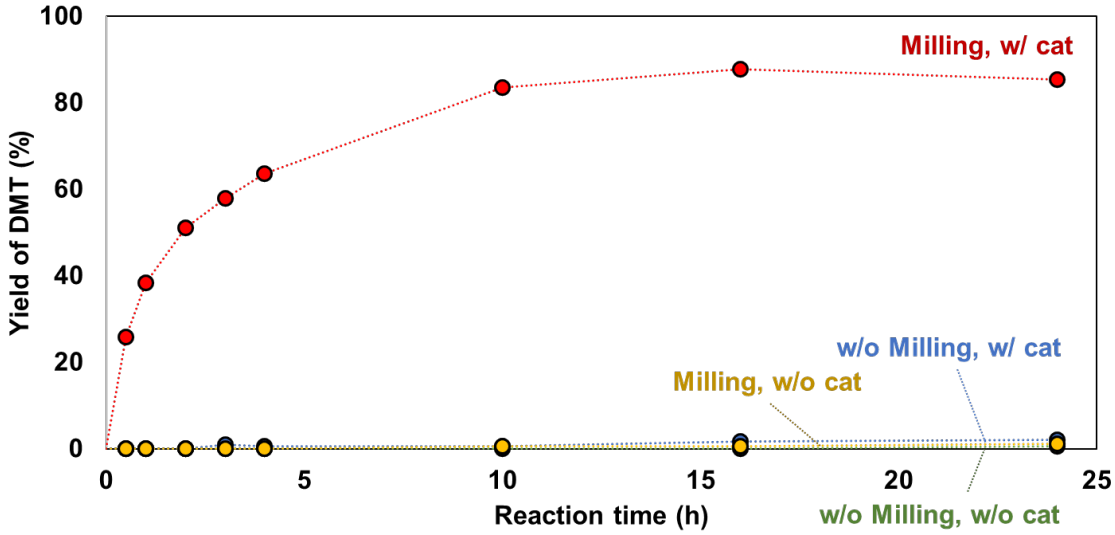

Figure S26. Reaction Profile of the Methanolysis of the Crystalline PET Sample Over 24 h

Red circles, with bead mill treatment and with TMAM catalyst; Yellow circles, with bead mill treatment and w/o the catalyst; Blue circles (almost hidden by the yellow circles), w/o bead mill treatment and with TMAM catalyst; Green circles (hidden by the yellow circles), w/o bead mill treatment and w/o a catalyst.

Table S13. Reaction Profile of the Methanolysis of the Crystalline PET Sample (PET C) Over 24 h

Entry	Bead Mill Treatment	Catalyst	Reaction time (h)							
			0.5	1	2	3	4	10	16	24
1	no	no catalyst	0	0	0	0	0	0	0	1
2		$Me_4N(OMe)$	0	0	0	1	1	1	2	2
3	yes	no catalyst	0	0	0	0	0	1	1	1
4		$Me_4N(OMe)$	26	38	51	58	64	83	88	85

[a] Determined by GC analysis

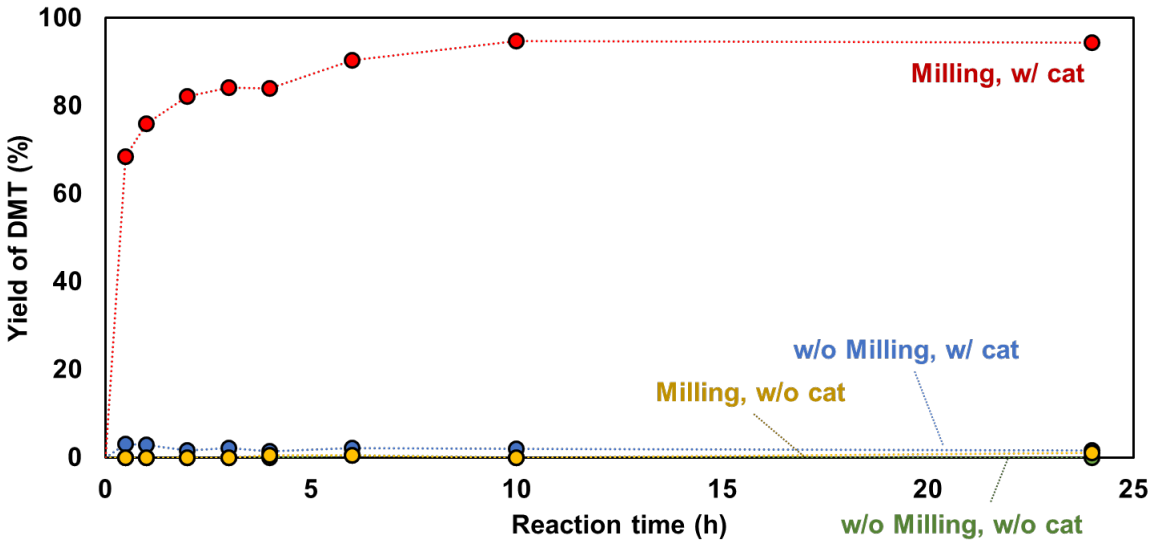

Figure S27. Reaction Profile of the Methanolysis of the Used Beverage PET Sample Over 24 h

Red circles, with bead mill treatment and with TMAM catalyst; Yellow circles, with bead mill treatment and w/o the catalyst; Blue circles, w/o bead mill treatment and with TMAM catalyst; Green circles (hidden by the yellow circles), w/o bead mill treatment and w/o a catalyst.

Table S14. Reaction Profile of the Methanolysis of the Used Beverage PET Sample (PET D) Over 24 h

Entry	Bead Mill Treatment	Catalyst	Reaction time (h)							
			0.5	1	2	3	4	6	10	24
1	no	no catalyst	0	0	0	0	0	0	0	0
2		$Me_4N(OMe)$	3	3	2	2	1	2	2	2
3	yes	no catalyst	0	0	0	0	1	0	0	1
4		$Me_4N(OMe)$	68	76	82	84	84[b]	90	95	94

[a] Determined by GC analysis; [b] Isolated yield

It is possible to identify the characteristic that it reaches nearly 90% after 16 to 24 hours have elapsed.

The reaction profiles shown in this section were obtained by performing individual batch reactions for a predetermined time, and then plotting the results obtained after usual work-up procedures on a time axis. The absence of unnatural deviations in the plots, which would significantly impair the linearity of the data, can be regarded as evidence that the methanolysis in this study exhibits good reproducibility.

SI-5-4. Effect of Co-solvents on the Room Temperature Methanolysis

Table 4 in the main text shows that the methanolysis reaction proceeds at 60 °C by using a bead mill in combination with a catalyst. The study shown in Table 4 in the main text was conducted before catalyst optimization, but by using the optimized catalyst TMAM, 43% of DMT can be obtained in 4 hours and 50% in 24 hours (Table S15). On the other hand, even when 20 mol% of TMAM was used, there was no dramatic improvement in yield, leaving issues with progress below 60 °C.

Table S15. Initial Trials of the Methanolysis at 60 °C

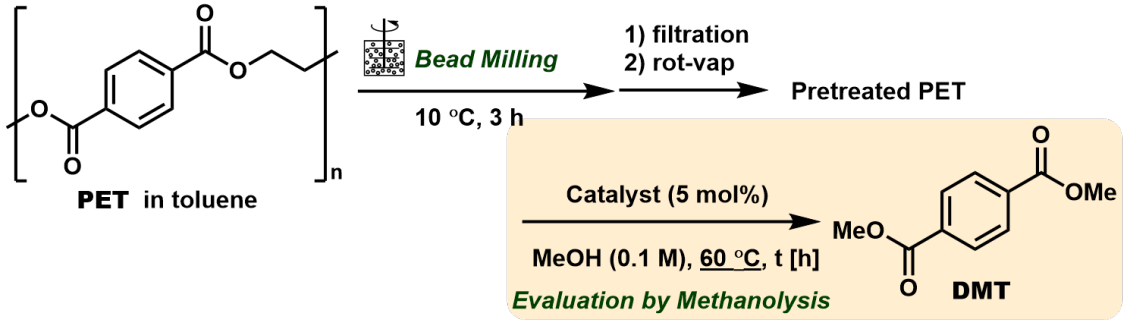

Entry	Bead Mill Treatment	Catalyst	Yield (%)[a]	
			4 h	24 h
1	no	no catalyst	0	-
2		$^{n}Bu_4NOH$	1	-
3	yes	no catalyst	6	19
4		$^{n}Bu_4NOH$	37	-
5		$Me_4N(OMe)$	43	50, 63[b]

[a] Determined by GC analysis; [b] 20 mol% of $Me_4N(OMe)$ was used

Previous studies have examined the reaction below 60 °C using co-solvent conditions. [35,37,38,45–48] In this study, the effect of co-solvents was also examined (Tables S16 and S17). All of them were 1:1 co-solvents with methanol, and PET powder derived from the standard reagent PET was utilized as a substrate.

The yield was improved when several types of solvents were used (Table S9). In particular, THF (entry 4), pyridine (entry 9), and DMF (entry 11) were notable. Therefore, in Table S17, ether solvents were examined in detail. Among them, when 1,4-dioxane was used, DMT was obtained in 67% yield. In Table S16, DMF also effectively promoted the reaction, but because of its high boiling point and the complicated purification process after the reaction, it was not further examined.

Table S16. Effect of Cosolvents on the Methanolysis at 60 °C

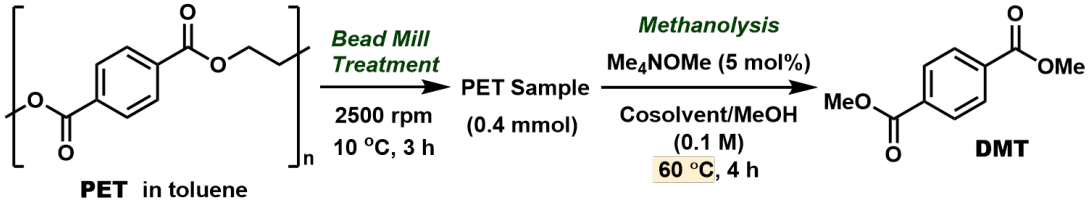

Entry	Cosolvent[a]	Yield (%)[b]	Entry	Cosolvent[a]	Yield (%)[b]
1	MeOH only	43	7	CH_3CN	52
2	toluene	57	8	acetone	56
3	cyclohexane	52	9	pyridine	70
4	THF	61	10	Et_3N	49
5	EtOAc	19	11	DMF	62
6	MeOAc	38	12	CH_2Cl_2	56

[a] Cosolvent/MeOH (1:1) (total 4 mL); [b] Determined by GC analysis

Table S17. Effect of Ethers as a Cosolvent

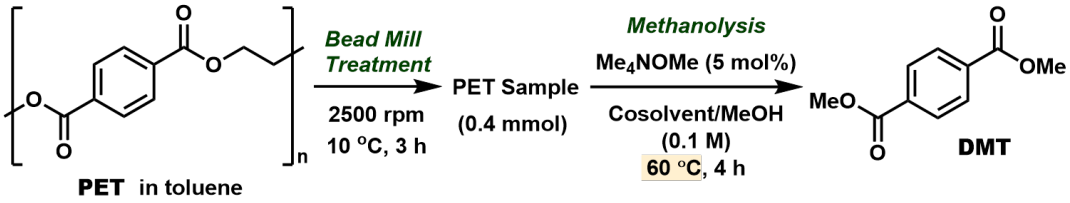

Entry	Cosolvent[a]	Yield (%)[b]
1	THF	61
2	2-MeTHF	60
3	4-MeTHP	56
4	CPME	59
5	diisopropyl ether	55
6	DME	49
7	diglyme	52
8	1,4-dioxane	67

[a] Cosolvent/MeOH (1:1) (total 4 mL); [b] Determined by GC analysis

In addition, pyridine analogues were examined in Table S18. When these solvents were used, the yield of DMT was about 65-70% in all cases (entries 1-5).[49,50] On the other hand, when 5 mol% of the highly nucleophilic 4-dimethylaminopyridine (DMAP) was added, the reaction promotion effect was almost nonexistent (entry 6). In addition, when a catalyst was not added to the pyridine/MeOH mixed solvent system, the reaction did not proceed at all (entry 10). When the solvent ratio of pyridine to MeOH was optimized (entries 2, 7-9), it was revealed that the yield of DMT was the highest at 75% in the pyridine/MeOH (1:3) mixed solvent system.

Table S18. Effect of Pyridines as a Cosolvent

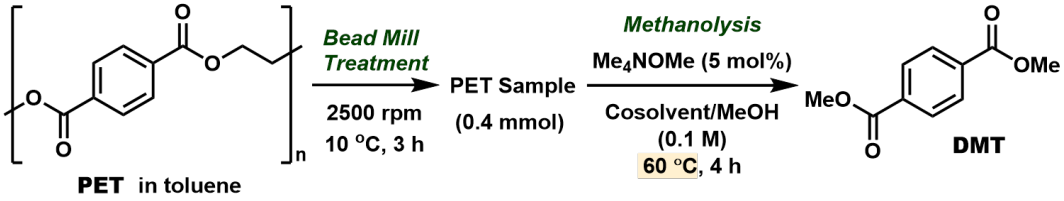

Entry	Cosolvent[a]	Cosolvent / MeOH	Yield (%)[b]
1	MeOH only	-	43
2	pyridine	1 / 1	70
3	2-methylpyridine	1 / 1	67
4	4-methylpyridine	1 / 1	65
5	2,6-lutidine	1 / 1	66
6	DMAP (5 mol% as additive)	-	47
7	pyridine	3 / 1	75
8	pyridine	1 / 3	57
9	pyridine	0.5 / 3.5	52
10	pyridine (w/o catalyst)	1 / 1	<1

[a] Cosolvent/MeOH (total 4 mL); [b] Determined by GC analysis

Finally, this condition was determined to be optimal, and methanolysis at 30 °C was attempted. The results are shown in the main text Scheme 2. Table S19 shows the results of applying the 30°C condition to PET B–C. Although the use of pyridine as a co-solvent deviates from our original concept, it is noteworthy that a 90% yield was obtained in the case of used beverage-grade PET.

Table S19. Summary of the Methanolysis of Several PET Samples at 30 °C

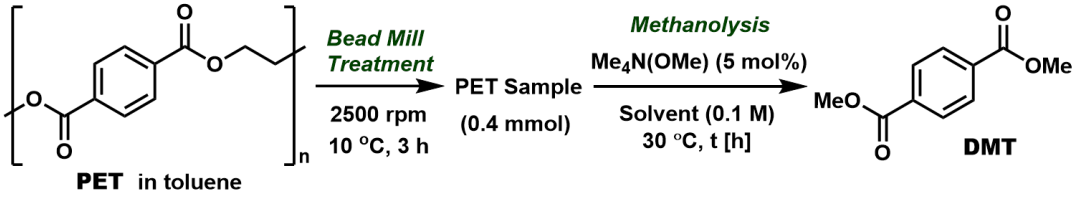

Entry	PET sample	Solvent	Reaction time (h)	Yield (%)[a]
1	Reagent (Sigma-Aldrich)	MeOH	24	35
2		MeOH/pyridine(1:3)	4	58
3			24	70
4	Post-consumer bottle	MeOH	24	28
5		MeOH/pyridine(1:3)	4	90
6	Amorphous PET	MeOH	24	39
7		MeOH/pyridine(1:3)	4	85
8	Crystalline PET	MeOH	24	4
9		MeOH/pyridine(1:3)	4	28

[a] Determined by GC analysis

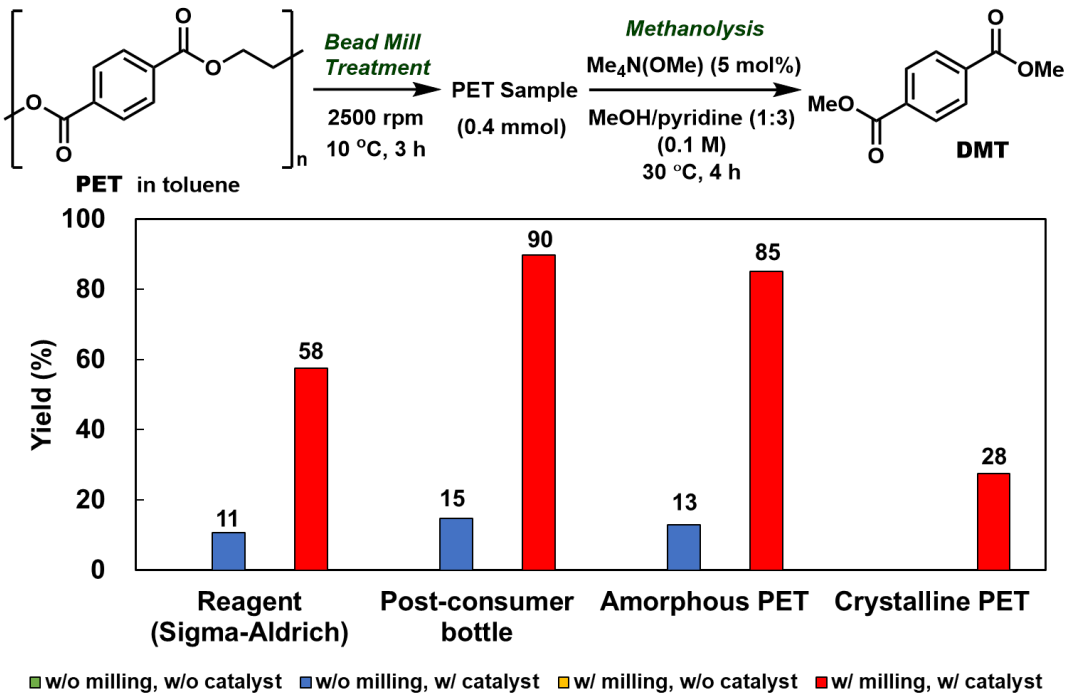

Figure S28. Methanolysis of Several PET Samples and Effect of Bead Mill Treatment and the Catalyst

Table S20. The Methanolysis Reactions of PET Samples at 30 °C Without Cosolvents

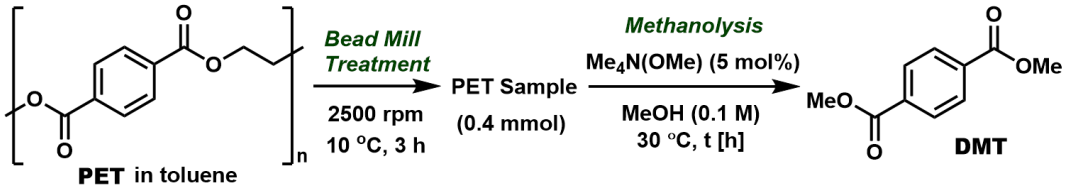

Entry	PET	Reaction time (h)	Yield (%)[a]
1	Sigma-Aldrich	4	16
2		24	35
3		72	47
4	Amorphous PET	24	39
5		72	51
6	Post-consumer bottle	24	28
7		72	50

[a] Determined by GC analysis

SI-5-5. Investigation of Ionic Liquids as Co-solvents

As discussed in the previous section and in literatures, the use of co-solvents promotes the low-temperature depolymerization of PET. However, as is the purpose of this study, the use of extra organic solvents imposes new environmental burdens. As one way to utilize the function of co-solvents, we focused on the potential of ionic liquids, which have attracted attention as green solvents due to their stability and ease of separation and recovery. [51,52]

Various ionic liquids were first investigated under the evaluation condition of methanolysis at 30 °C (Table S21). When a representative ionic liquid, 1-butyl-3-methylimidazolium chloride ([bmim]Cl) or 1-butyl-3-methylimidazolium bis(trifluoromethanesulfonyl)imide ([bmim]NTf_2)[53], was used as a co-solvent, the reaction was accelerated compared to when methanol was used alone. On the other hand, ammonium and pyridinium ionic liquids ended up with low yields.[54–56] Ionic liquids are generally soluble in water, so they can be separated from the product DMT by extraction into a water. [bmim]NTf is separable from water and diethyl ether (Et_2O) phases, so DMT could be extracted from the mixture into Et_2O phase.

Table S21. The Effect of Ionic Liquids as a Cosolvent (1)

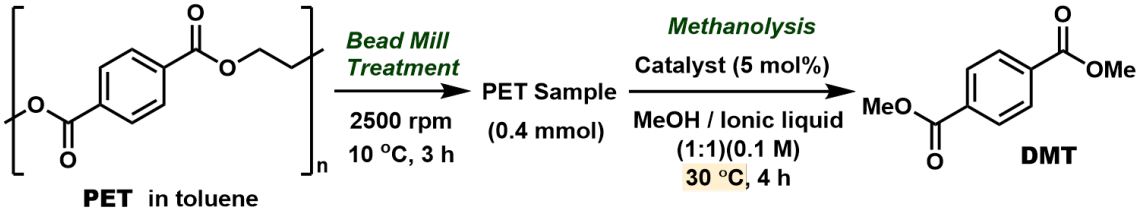

Entry	Ionic liquid	Catalyst	Yield (%)[a]	Entry	Ionic liquid	Catalyst	Yield (%)[a]
1	none	Me_4NOMe	16[b]	6	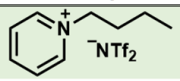	Me_4NOMe	26
2	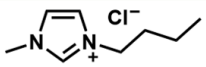 [c]	KO^{t}Bu	4	7	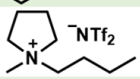	Me_4NOMe	23
3		Me_4NOMe	48				
4	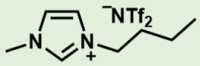	Me_4NOMe	45	8	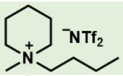	Me_4NOMe	27
5	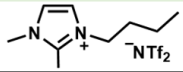	Me_4NOMe	23	9	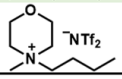	Me_4NOMe	30

[a] Isolated yield; [b] Determined by GC analysis; [c] Solid state at rt (2 g was used)

Table S22 demonstrated further investigation in [Bmim]-series ionic liquids with different counter anions or side chain functionalities, but all studies except [bmim]OH showed negative results. On the other hand, the effect of [bmin]OH was significant, with a DMT yield of 63% (entry 12). The OH anion could deprotonate $[bmim]^+$ to produce NHC.[57,58] However, this ionic liquid is unstable even at room temperature, and we concluded that its use as a co-solvent is an obstacle.

Table S22. The Effect of Ionic Liquids as a Cosolvent (2)

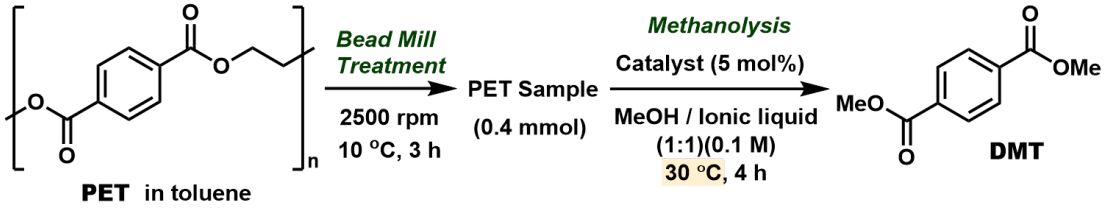

Entry	Ionic liquid	Catalyst	Yield (%)[a]	Entry	Ionic liquid	Catalyst	Yield (%)[a]
10	$^{n}Bu_4PBr$[b]	Me_4NOMe	trace	14	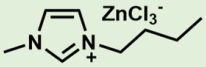	Me_4NOMe	7
11	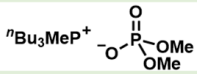	Me_4NOMe	15	15	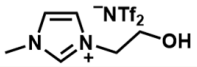	Me_4NOMe	11
12	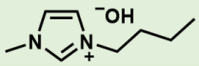	Me_4NOMe	63	16	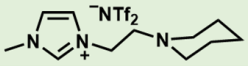	Me_4NOMe	14
13	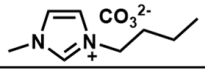	Me_4NOMe	26	17	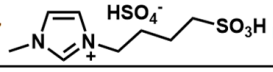	no catalyst	3

[a] Isolated yield; [b] Solid state at rt (2 g was used)

Based on the above investigation of ionic liquids, [bmim]NTf_2 was identified as the most promising, and its mixture ratio with methanol was then optimized (Table S23). However, this study did not improve the yield. Also, there was no improvement in yield even when the reaction time was extended to 24 h, and the highest yield in this system was 49%.

Table S23. Investigation of the ratio of MeOH/Ionic Liquid

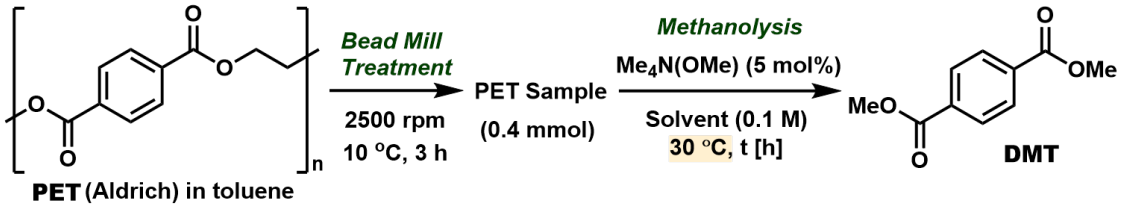

Entry	Solvent	Reaction time (h)	Yield (%)[a]
1	MeOH	4	16
2	MeOH	24	35
3	MeOH/[Bmim]NTf_2(1:1)	4	45
4	MeOH/[Bmim]NTf_2(1:3)	4	35
5	MeOH/[Bmim]NTf_2(3:1)	4	23
6	MeOH/[Bmim]BF_4(1:1)	4	8
7	MeOH/[Bmim]PF_6(1:1)	4	36
8	MeOH/[Bmim]NTf_2(1:1)	24	49

[a] Determined by GC analysis (entries 1-2), isolated yield (entries 3-8)

In Table S24, PET powder derived from the amorphous PET pellets was used. In this case, DMT was obtained in a maximum yield of 75%.

Table S24. Investigation of Reaction Conditions of MeOH/[Bmim]NTf_2 Mixed Solvent System

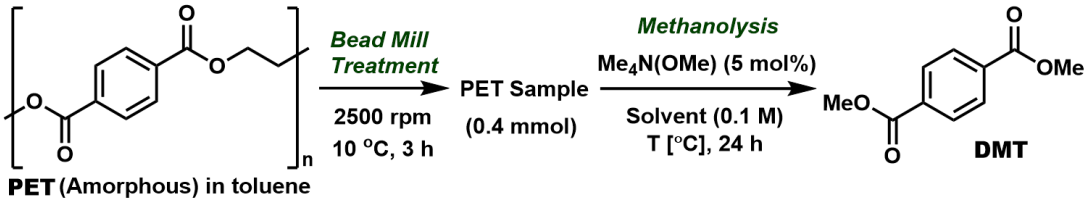

Entry	Solvent	Temperature (°C)	Yield (%)[a]
1	MeOH	30	39
2	MeOH/[Bmim]NTf_2(1:1)		61
3[b]	MeOH	30	49
4[b]	MeOH/[Bmim]NTf_2(1:1)		75
5	MeOH	60	69
6	MeOH/[Bmim]NTf_2(1:1)		77
7	MeOH	45	53
8	MeOH/[Bmim]NTf_2(1:1)		73
9[c]	MeOH/[Bmim]NTf_2(1:1)		74
10	MeOH/[Bdmim]NTf_2(1:1)		61

[a] Determined by GC analysis (entries 1,3,5,7), isolated yield (entry 2,4,6,8-10)

[b] 20 mol% of cat. was used; [c] Reaction time was 72 h

(*In this table, the amorphous PET sample was used as a starting material.)

In summary, [bmim]NTf_2 certainly accelerates the reaction, but its effectiveness as a substitute for pyridine, which shows superior reaction-accelerating properties, is unclear.

SI-6. Additional Information for Aminolysis Reaction

In this chapter, we briefly introduce the results of optimization studies leading to the best result of the depolymerization reaction with 2-aminoethanol shown in Scheme 3 of the main text. Here, we refer to this reaction as aminolysis.

First, we investigated the reactivity of the aminolysis of the PET powder derived from the reagent PET (PET A) using 5 mol% TMAM catalyst according to the conditions used for methanolysis (Table S25). The reaction of the bead milled sample gave the desired BHETA in 84% yield. Since the aminolysis yield was comparable even without a catalyst, we carried out studies at 30 °C, where the effects of bead mill treatment and catalyst are most pronounced, and decided to improve the yield at this temperature.

Table S25. Effect of Reaction Temperatures on the Aminolysis of PET

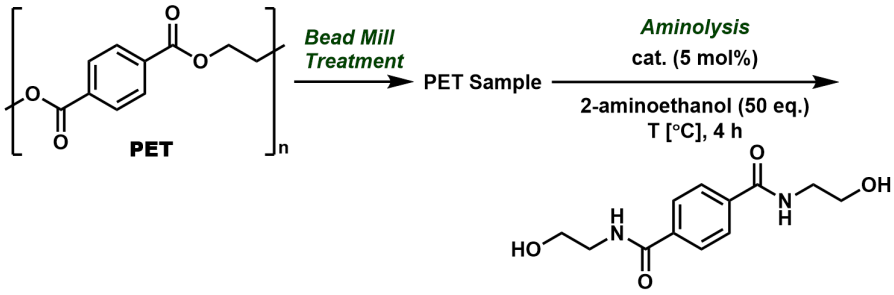

Entry	Bead Mill Treatment	Catalyst	Yield (%)[a]		
			30 °C	60 °C	90 °C
1	no	no catalyst	-	<1	48
2		$Me_4N(OMe)$	-	2	62, 85[b]
3	yes	no catalyst	20	59	76
4		$Me_4N(OMe)$	46	80	84, 84[b]

[a] Determined by NMR analysis; [b] Reaction time was 24 h

Table S26 examines the reaction time and catalyst amount. When the reaction time was extended to 24 h, the difference in the yield of BHETA with and without a catalyst was reduced. Therefore, we increased the amount of catalyst and found that the difference became apparent when it was 20 mol%.

Table S26. Effect of the Reaction Time and the Catalyst Amount

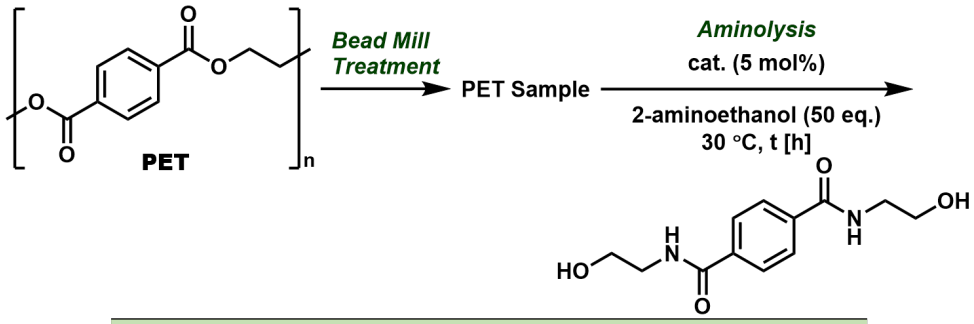

Entry	Catalyst	mol%	Reaction time (h)	Yield (%)
1	no catalyst	-	4	20
2	$Me_4N(OMe)$	5	4	46
3	no catalyst	-	24	45
4	$Me_4N(OMe)$	5	24	57
5	$Me_4N(OMe)$	10	24	78
6	$Me_4N(OMe)$	20	24	84

[a] Determined by NMR analysis

Table S27 shows the results of investigations aimed at shortening the reaction time and reducing the amount of catalyst used. Several base catalyst candidates that were also effective in methanolysis gave comparable yields, but without significant improvement, compared to the 46% yield of TMAM.

Table S27. Catalyst Screening for the Aminolysis of PET

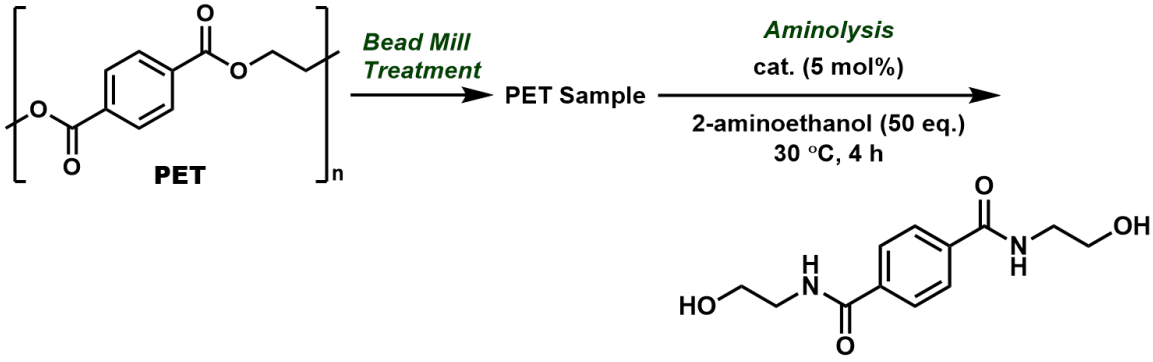

Entry	Conditions	Yield (%)[a]	Entry	Conditions	Yield (%)[a]
1	no additive	20	8	Bu_2SnO (5 mol%)	4
2	$Me_4N(OMe)$ (5 mol%)	46	9	TBD (5 mol%)	26
3	$PhMe_3NOH$ (5 mol%)	47	10	$La(OTf)_3$ (5 mol%)	22
4	$^n Bu_4NOH$ (5 mol%)	46	11	CaI_2 (5 mol%)	23
5	KOMe (5 mol%)	48	12	1,2,4-triazole (5 mol%), DBU (5 mol%)	11
6	Na(OAc) (5 mol%)	19			
7	$Zn(OAc)_2$ (5 mol%)	18	13	TFE (20 mol%), K_3PO_4 (1 eq.)	71

[a] Determined by ^{1}H NMR analysis

Based on these considerations, we chose to use the co-solvent system, as in methanolysis at 30 °C.[54] Again, various co-solvents were tested, including DMSO, DMF, pyridine, acetonitrile, 1,4-dioxane, MeOH, and H_2O (Table S28, entries 3-7, 9, 11). With the exception of H_2O, almost all co-solvents promoted the reaction faster than the sole-solvent system. DMF gave the highest BHETA yield at a reaction time of 4 h (68%, entry 7), but extending the reaction time had no effect. On the other hand, the yield improved to 75% when pyridine was used, and the reaction time was extended to 16 h. In the previous studies, 50 equiv. of 2-aminoethanol were used because it was used as a sole-solvent or in a co-solvent system, but even when the amount was reduced to 6 equiv., the yield remained at 79% (entry 12).

Table S28. Effect of Cosolvents on the Aminolysis of PET

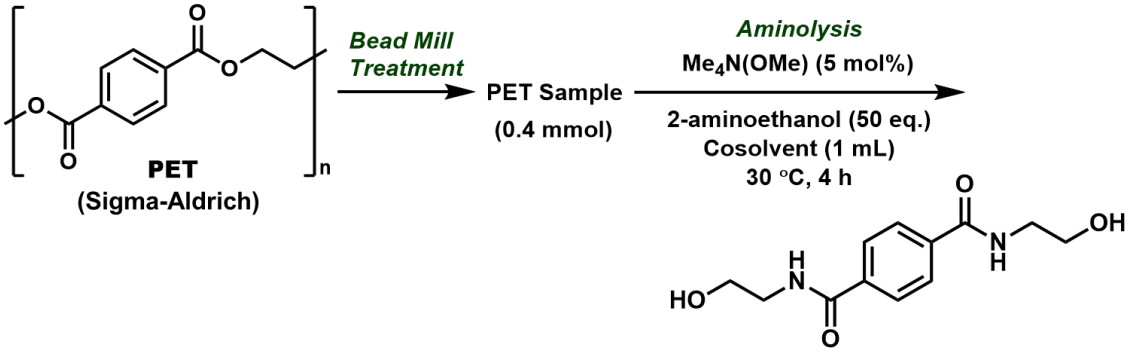

Entry	Cosolvent	Yield (%)[a]	Entry	Cosolvent	Yield (%)[a]
1[b]	-	20	7	DMF	68
2	-	46	8[c]	DMF	68
3	DMSO	61	9	Pyridine	62
4	H_2O	8	10[c]	Pyridine	75
5	MeOH	38	11	1,4-dioxane	54
6	CH_3CN	28	12[cd]	Pyridine	79

[a] Determined by ^{1}H NMR analysis; [b] w/o catalysts; [c] Reaction time was 16 h; [d] Ethanolamine (6 equiv.)

Scheme 3 in the main text shows the results when the above conditions were applied to the PET powder derived from used beverage PET flake (PET D) instead of the reagent PET.

Table S29 shows the results observed over time under the same conditions. The reaction proceeded very smoothly, reaching a yield of 83% after 30 min and converting to BHETA with a yield of 96% after 1 h. These results indicate that the developed aminolysis reaction is significantly faster under milder conditions than previously reported methods.[5,25–30,32,59–61]

Table S29. The Aminolysis of the Used Beverage PET and Time on Stream of the Yield

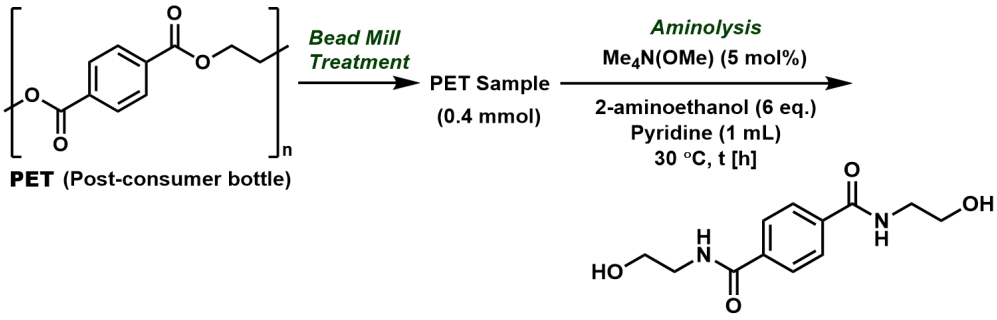

Reaction time (h)	0.5	1	2	3	4	16
Yield of BHETA (%)[a]	83	96	>99	91	93	91

[a] Determined by ^{1}H NMR analysis

SI-7. Additional Information for the Glycolysis Reactions

In this chapter, we will show the details of the glycolysis reaction shown in Scheme 3 in the main text. Based on the methanolysis investigations, PET powder derived from the amorphous PET pellet was reacted with 50 equiv. (1.1 mL) of ethylene glycol (EG) at 90 °C for 4 h using 5 mol% TMAM catalyst, and 22% of the desired bis-hydroxyethyl terephthalate (BHET) was obtained (entry 1, Table S30). Since this result was not as expected, we decided to use a co-solvent based on the results of the previous chapter (entries 2-8).[14,39,62–64] Pyridine, toluene, dichloromethane (DCM), acetonitrile, DMF, DMSO, and [bmim]NTf_2 were tried, and we found that when acetonitrile was used, the BHET yield was reached to 81% (entry 5).

Table S30. Initial Trials of the Glycolysis of PET and the Effect of Cosolvents

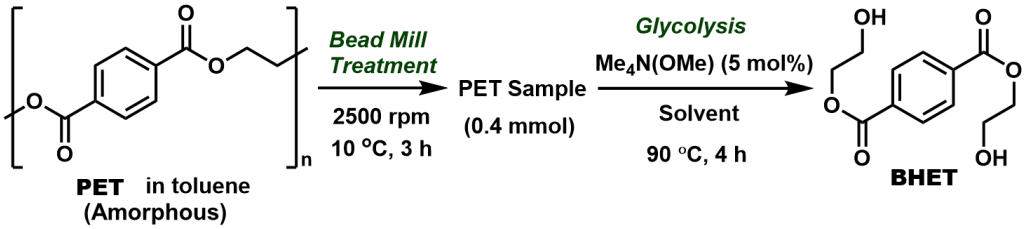

Entry	Solvent[a]	Yield (%)[b]
1	EG (50 eq.)	22
2	EG/Pyridine (1:3)	73
3	EG/Toluene (1:3)	43
4	EG/CH_2Cl_2 (1:3)	69
5	EG/CH_3CN (1:3)	81
6	EG/DMF (1:3)	49
7	EG/DMSO (1:3)	50
8	EG/[bmim]NTf_2 (1:3)	49

[a] EG (50 eq.) was used; [b] Determined by HPLC analysis

In order to achieve more efficient depolymerization conditions, we continued to study the direction of reducing the amount of EG under 60 °C conditions (Table S31), and found that the reaction was steadfastly proceeded to give the target BHET in quantitative yield within 24 h (entry 2). It was further revealed that the same level of the yield was attained with using 6 equiv. of EG (entry 4).

Table S31. Investigation of the Glycolysis at 60 °C

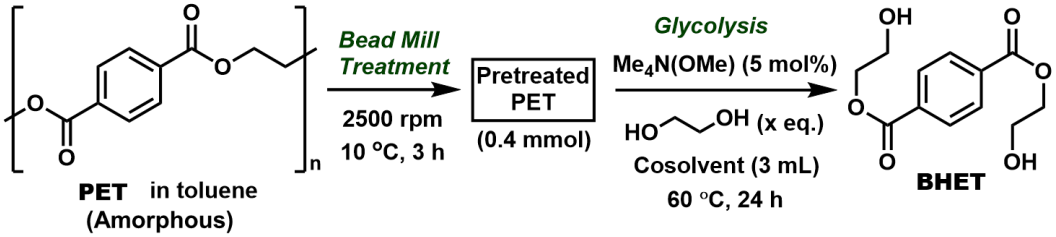

Entry	x (eq.)	Cosolvent	Yield (%)[a]
1	50 eq.	Pyridine	83
2	50 eq.	CH_3CN	>99
3	10 eq.	CH_3CN	>99
4	6 eq.	CH_3CN	>99
5	4 eq.	CH_3CN	76
6	2 eq.	CH_3CN	44

[a] Determined by HPLC analysis

Furthermore, when the reaction temperature was lowered to 30 °C (Table S32), the conversion in the acetonitrile system was significantly reduced, and the yield of BHET was only 35% (entry 2). On the other hand, pyridine was more effective as a co-solvent at this temperature, with a yield of 64% when 50 eq. of EG was used and 51% when 10 eq. was used (entries 1 and 4). In addition, by increasing the substrate concentration with reducing the amount of pyridine used, the highest yield at 30 °C of 73% was obtained (entry 5).

The reaction did proceed sufficiently even at 30 °C, but in terms of yield, it can be said that the 60 °C condition was optimal, as shown in Scheme 3 in the main text.

Table S32. Investigation of the Glycolysis at 30 °C

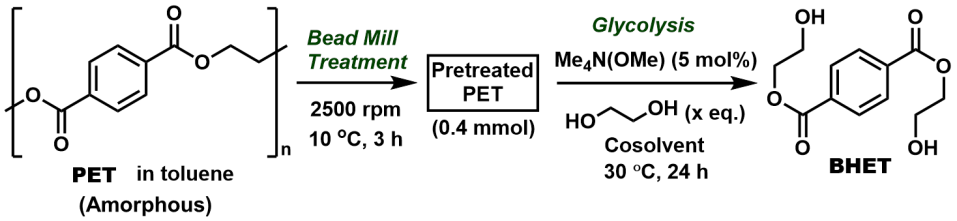

Entry	x (eq.)	Cosolvent	Cosolvent volume (mL)	Yield (%)[a]
1	50 eq.	Pyridine	3	64
2	50 eq.	CH_3CN	3	35
3	50 eq.	Pyridine/CH_3CN(1:1)	2	68
4	10 eq.	Pyridine	3	51
5	10 eq.	Pyridine	0.4	73

[a] Determined by HPLC analysis

SI-8. Recovery and Reuse of the Bead Mill Solvent

This study aims to achieve chemical recycling of plastics with lower energy input by reducing the depolymerization reaction temperature. Although the operation of the bead mill requires energy for motor rotation, it is anticipated that energy can be recycled by transferring the heat generated during operation. Instead, since the bead mill process involves the use of solvents, it is necessary to separate pulverized PET from the slurry. In this study, the separation of pulverized PET from the slurry was performed via evaporation. However, the energy required for solvent recovery by evaporation presents a greater challenge than the bead mill operation itself. The solvent used in the bead mill process is not directly involved in the process for the production of the final products, such as DMT and EG, and thus must be recovered and reused. Since PET is largely insoluble in toluene, it is fundamentally possible to reuse the recovered solvent, but experimental validation is critical. This chapter presents the results of these recovery and reuse experiments.

While the main body of this study focuses on the results of the bead mill process, depolymerization, and the structural changes of polymers during these processes, this topic, recovery and reuse, is equally important. The solvent recovery experiment is shown in Figure S29. As mentioned earlier, this study primarily adopts evaporation for separating toluene and powdered PET. However, the objective of the recovery and reuse experiments is to minimize energy consumption, and thus separation via filtration using smaller pore size filters was attempted.

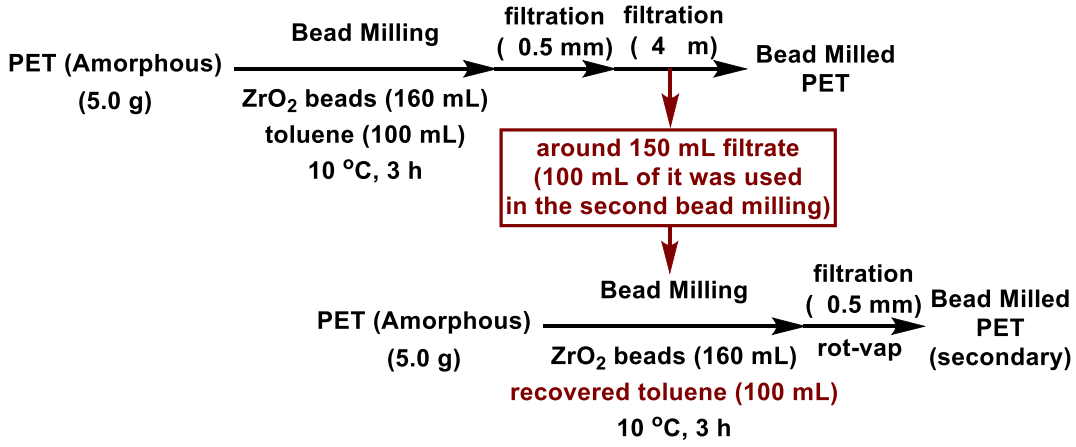

Figure S29. Experimental Procedures for Recovery and Reuse of the Bead Mill Solvent

After processing 5.0 g of the amorphous PET pellets under the standard bead mill conditions, the slurry was first filtered through a 0.5 mm mesh filter. This step was necessary to recover the ZrO_2 beads and to separate PET components that could not be milled sufficiently within the 3 h processing time. The slurry obtained was subsequently filtered through a filter paper with 4 μm pores in the second filtration step. The resulting filtrate was a clear, colorless toluene phase. After each of the first and second filtrations, the residue was washed with a total of 50 mL of toluene. Therefore, the total amount of recovered toluene phase was 150 mL. Of this, 100 mL was used and reused in the next bead mill

process.

The second bead mill treatment was also conducted under the standard conditions by using the above recovered toluene. For comparison, the powdered PET obtained through evaporation after the first filtration was used for the methanolysis under the standard conditions. Even in this methanolysis experiment, DMT was obtained in an 85% yield, demonstrating that toluene recovered through filtration alone is reusable (Figure S30).

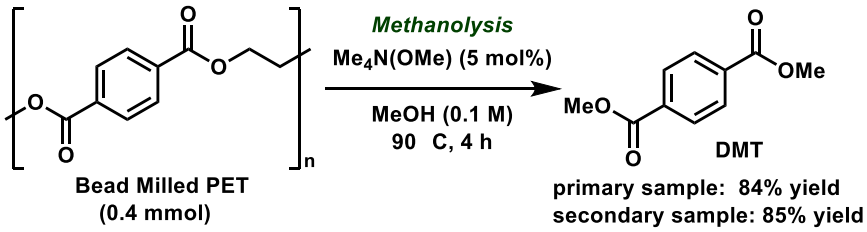

Figure S30. Evaluation of the Reactivity of the Secondary PET Sample in the Methanolysis Reaction

In a separate experiment, the recovered toluene phase obtained through two filtration steps was diluted to 200 mL, and 20 mL of the diluted sample was then concentrated. It was found that the residual solids amounted to 2.2 mg, indicating that 22 mg of PET components, which could not be separated through the second filtration step, were present in the recovered toluene phase. As demonstrated above, the recovered toluene can be reused as a solvent in the bead mill process. However, since the residual PET components would accumulate with repeated reuse, they are expected to eventually impact its reusability. While separation by evaporation (distillation) could prevent this accumulation, the use of appropriate adsorbents may also enable the removal of ultrafine PET particles.

Various techniques are available for the adsorption and removal of microplastics.[65–67] In our study, polystyrene-based adsorbents and activated carbon were tested, and it was found that activated carbon effectively removed ultrafine PET particles. This verification experiment was conducted as follows (Figure S31):

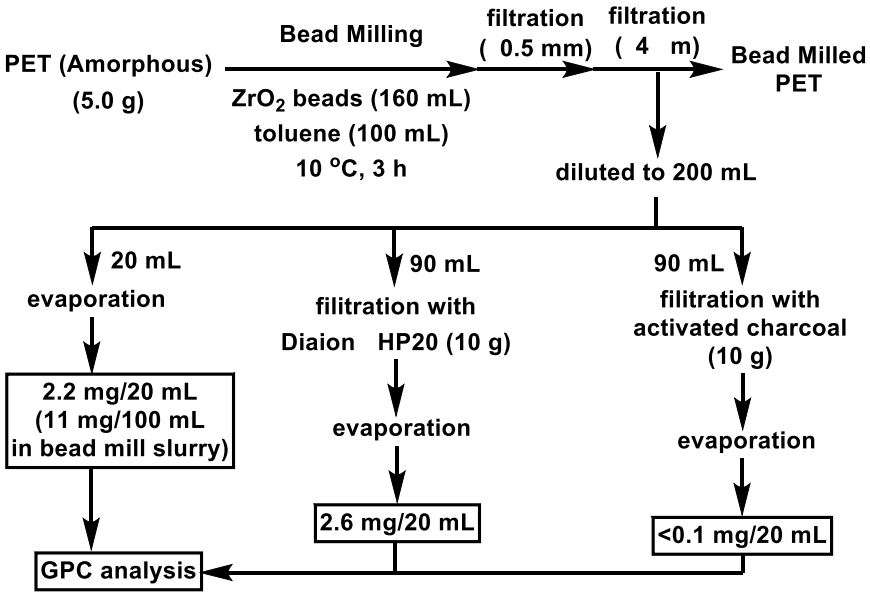

Figure S31. Experimental Procedures for Purification of the Bead Mill Solvent

First, a bead mill treatment was conducted using 100 mL of toluene, followed by two filtration steps to get a recovered toluene phase. The recovered toluene was then diluted to 200 mL. As mentioned earlier, 20 mL of this solution was analyzed by evaporating the toluene, resulting in 2.2 mg of white solid. Meanwhile, half of the remaining the diluted toluene phase was passed through an adsorption column composed of a Hirsch funnel containing 10 g of a polystyrene-divinylbenzene-based synthetic adsorbent (Diaion® HP20, Mitsubishi Chemical Corporation). The other half was passed through an adsorption column containing neutral activated carbon instead of the polystyrene-based adsorbent.

The treated toluene from both adsorption processes was analyzed by evaporating 20 mL of each sample. For the toluene passed through the polystyrene-based adsorbent, 2.6 mg of white solid was obtained. In contrast, for the toluene passed through the activated carbon column, almost no residue remained (<0.1 mg), indicating a large part of PET component in the recovered toluene phase could be removed by activated carbon.

The residual components in the untreated recovered toluene, those obtained after passing through the polystyrene-based adsorbent, and the trace residue from the activated carbon-treated toluene were dissolved in 4 mL of HFIP/$CHCl_3$ (1:1) and analyzed by GPC (Figure S32). The chromatogram of the residue from untreated toluene phase (shown in red line) revealed a peak with a peak-top molecular weight distribution (*Mp*) of 710, corresponding to soluble PET species. Similarly, the chromatogram of the residue from the polystyrene-based adsorbent (shown in blue line) exhibited a similar peak, indicating that soluble PET species could not be removed by the polystyrene-based adsorbent. This adsorbent is suitable for the adsorption of peptides, proteins, and polyphenols with molecular weights exceeding 1,000, but it showed low selectivity for PET oligomers with an *Mp* of 710. On the other hand, the chromatogram of the residue from the activated carbon-treated toluene showed almost no peaks (shown in green line), demonstrating that soluble PET species were effectively removed by

activated carbon.

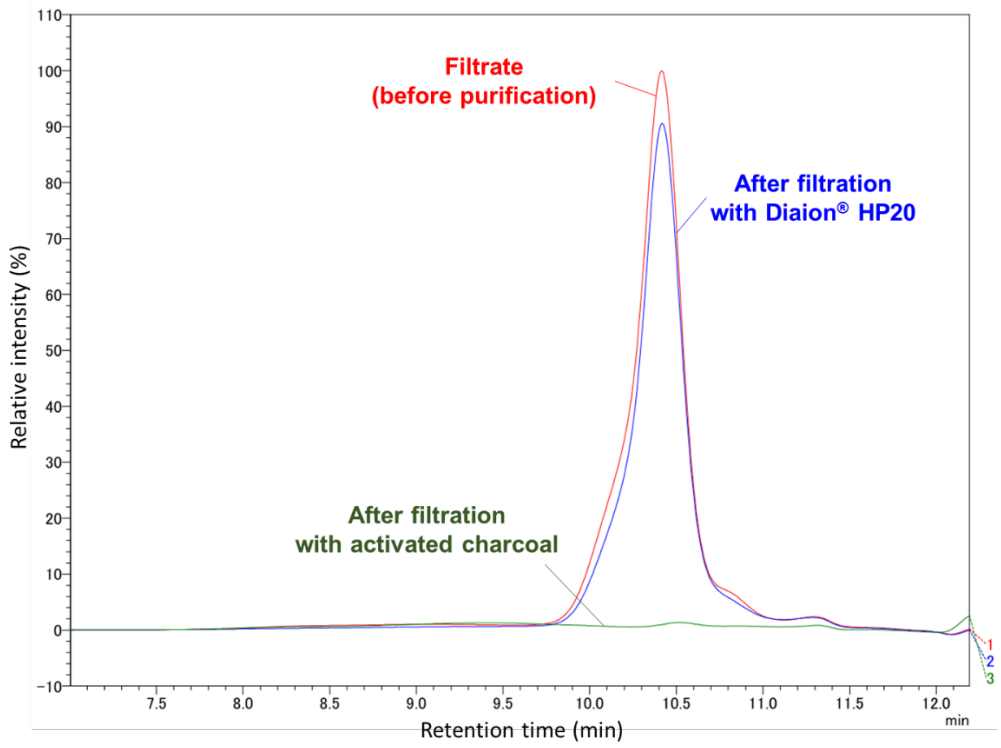

Figure S32. GPC Chromatograms of the Residues

Red, residue form the recovered untreated toluene; *blue*, residue form HP20 treatment; *green,* residue from activated carbon treatment)

Thus, it was demonstrated that the toluene used in the bead mill process can be recovered with minimal energy consumption and reused effectively.

SI-9. ESI-MS Analysis of the Bead-milled PET

To gain further mechanistic insight into the chemical bond cleavages occurring during bead milling, ESI-MS analysis was conducted. After 18 h of bead mill treatment, relatively small molecules with a peak molecular weight (M_p) of 2,700 were observed (Figure 7(a) in the main text). This sample contained sufficiently small molecules for detection by ESI-MS analysis (Figure S33). While no signals were observed in the positive ESI-MS mode, fragmentation peaks corresponding to PET oligomers were detected in the negative mode. Specifically, the oligomer (designated as "oligomer ***A***") had a carboxylate group at one end and an ethylene glycol group at the other. This result suggests that C-O bond cleavage of the ester groups in PET occurred. The carboxylic acid functional group of oligomer ***A*** could potentially quench the base catalysts in the depolymerization reactions. This may explain why prolonged bead mill treatment resulted in a lower monomer yield, due to the generation of a larger amount of carboxylic acid terminals (Table 3, entries 6,7). Furthermore, ESI-MS analysis of the sample after 24 h of bead mill treatment in MeOH revealed the presence of not only oligomer ***A***, but also another oligomer (designated as "oligomer ***B***") with m/z 30 lower than that of oligomer ***A*** (Figure S34). Oligomer ***B*** likely had a carboxylate group at one end and a methyl ester group at the other. This suggests that methanolysis of PET occurred at the chain ends via the following mechanism: C–O bond cleavage of PET during bead milling, followed by quenching by MeOH, resulting in the formation of the methanolysis products.

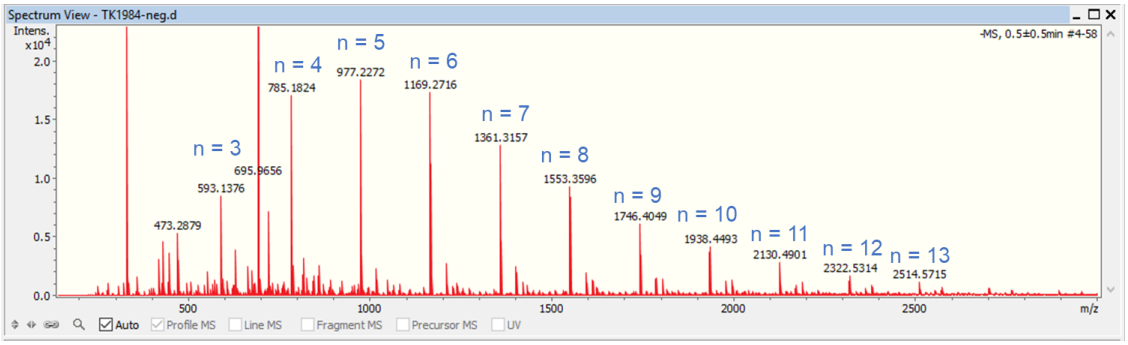

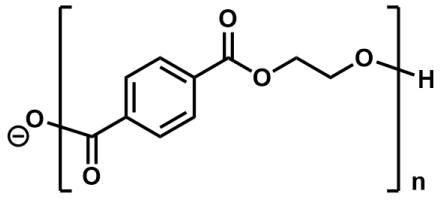

➢ **Plausible structures based on ESI-MS (Neg)**

n	m/z (calculated)	m/z (found)
3	593.13	593.14
4	785.17	785.18
5	977.21	977.23
6	1169.26	1169.27
7	1361.30	1361.32
8	1553.34	1553.36
9	1745.38	1746.40
	(*D isotope: 1746.39)	
10	1938.43	1938.45
11	2130.47	2130.49
12	2322.51	2322.53
13	2514.57	2514.57

Figure S33. ESI-MS Analysis of the Bead-Milled PET in Toluene

(*The amorphous PET sample after bead milling for 18 h)

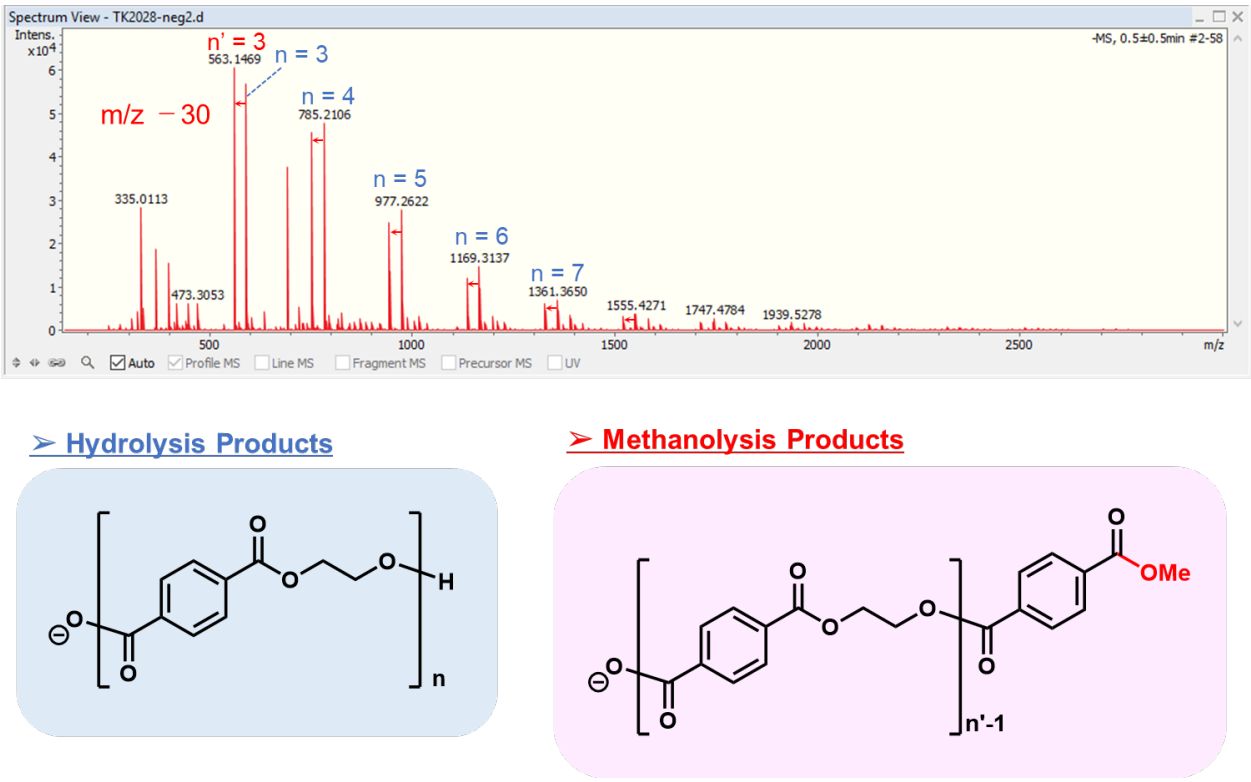

Figure S34. ESI-MS Analysis of the Bead-Milled PET in MeOH

(*The amorphous PET sample after bead milling in MeOH for 24 h)

SI-10. Solvent Effect on the One-pot Bead-Milling/Methanolysis Reaction in Batch System

To investigate the one-pot process, 1.0 g of the used beverage PET (PET D), 10 mol% of TMAM, 100 mL of methanol, and 160 mL of ZrO_2 beads (φ2 mm) were placed in a batch-type bead mill container and reacted for 6 h at 10 °C with a rotation speed of 2,500 rpm (Table S33, entry 1). This initial experiment yielded only 2% DMT. Based on the findings in SI-5-4, where the addition of a cosolvent was found to accelerate the methanolysis reaction, pyridine and DCM were then introduced (Table S33, entries 2, 7). The addition of pyridine resulted in a slight increase in reaction rate, with a DMT yield of 18%. Optimization of the MeOH/pyridine ratio revealed that a ratio of 1:9 yielded the highest DMT yield of 72% (Table S33, entries 2-5). Interestingly, using toluene, which was previously shown to be an effective bead mill solvent, as a co-solvent also produced a similar reaction acceleration effect (Table S33, entry 6).

Table S33. Solvent Effect on the One-pot Bead-Milling/Methanolysis Reaction in Batch System

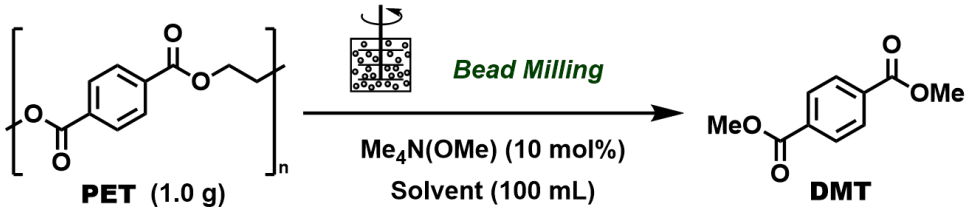

Entry	Solvent	Yield (%)[a]
1	MeOH	2
2	MeOH/pyridine (1:1)	18
3	MeOH/pyridine (1:3)	57
4	MeOH/pyridine (1:9)	72
5	MeOH/pyridine (1:99)	66
6	MeOH/toluene (1:9)	70
7	MeOH/DCM (1:1)	3

[a] Determied by GC analysis

SI-11. Continuous Bead Mill Treatment

SI-11-1. Experimental Procedures for 20 g-Scale Processing

20 g scale PET treatment using the continuous bead mill apparatus (Figure S35) was carried out by the following procedures: ZrO_2 beads (φ2 mm; 245 g, filling rate of 70% (65 mL) relative to the vessel) were placed in the vessel, and bead mill processing was performed with a disk (φ450 mm) rotation speed of 3,500 rpm while supplying toluene at approximately 100 mL/min. The total amount of toluene in the circulation system was 1.0 L. Then, the used beverage PET flakes (5 x 5 mm, 5.0 g) were supplied to the vessel from the inlet. During this bead mill treatment under circulation, the vessel was cooled with cooling water at 10 °C, as in the batch process. The temperature of the slurry was monitored on the receiver and was approximately 30–35 °C at steady state. After 4 h of the circulation operation, the treated slurry in a storage tank was collected, and simultaneously a new PET sample (5.0 g) was fed to the vessel from the inlet. After repeating this process four times, the collected slurry was combined and evaporated to remove the solvent, yielding 17.4 g of PET powder (87 w/w% recovery). GPC Analysis of this sample revealed that the peak top position of the molecular weight distribution was 44,700, which was similar to the PET sample treated by the batch-type bead milling for 3 h (M_p: 40,100) (Figure S36). When the methanolysis reaction was conducted using the treated PET sample, the depolymerization proceeded smoothly to afford 91% yield of DMT accompanied by 95% yield of EG.

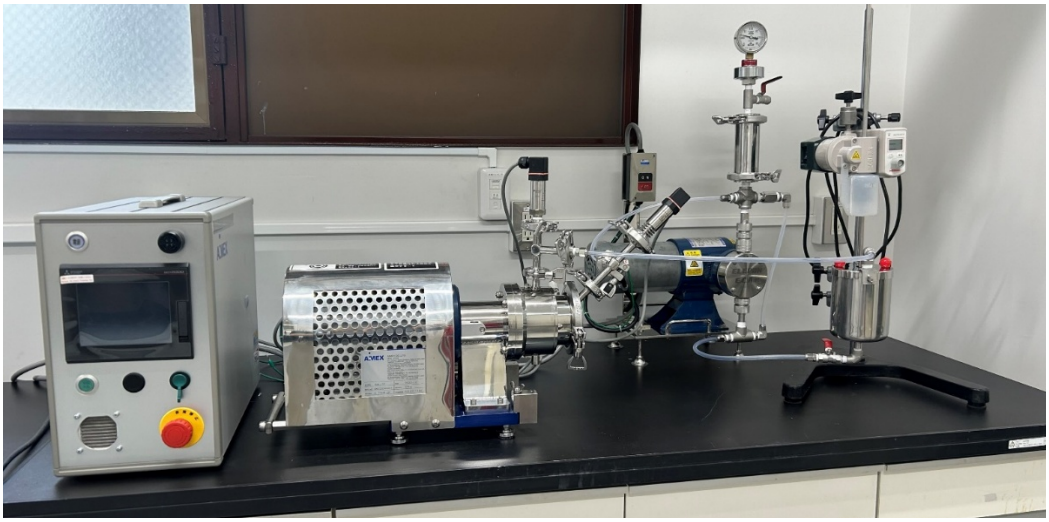

Figure S35. A Photo of the Continuous Bead Mill Apparatus

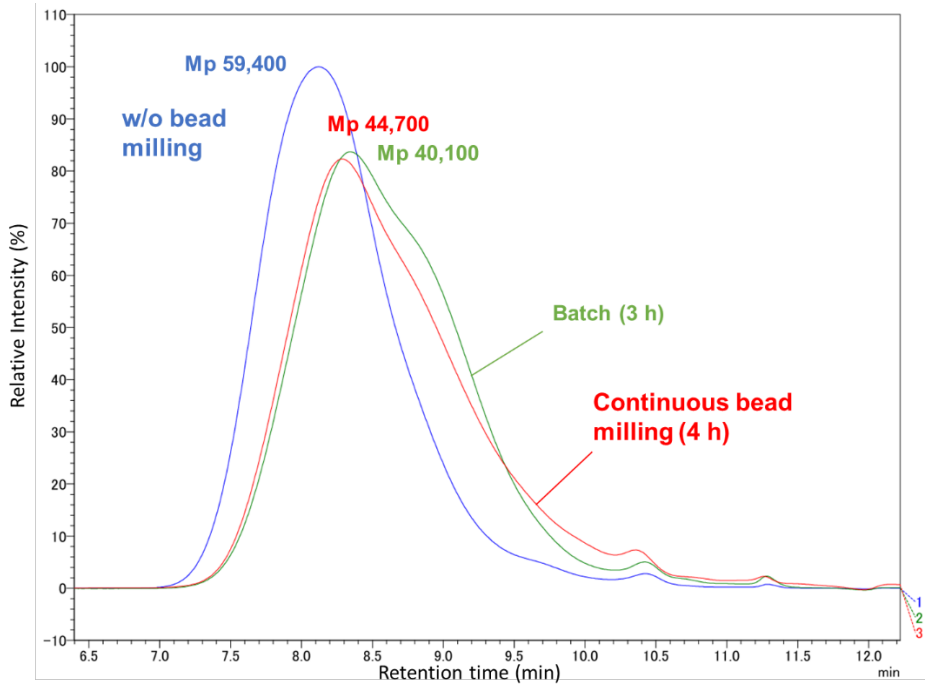

Figure S36. Comparison of Molecular Weight of PETs Using Continuous- and Batch-type Bead Mill

Blue, w/o milling (used beverage PET flakes); Green, PET bead-milled for 3 h by the batch-type apparatus; Red, PET bead-milled for 4 h by the continuous-type apparatus.

SI-11-2. **Experimental Procedures for the One-pot Bead-Milling/Methanolysis Reaction in Continuous System**

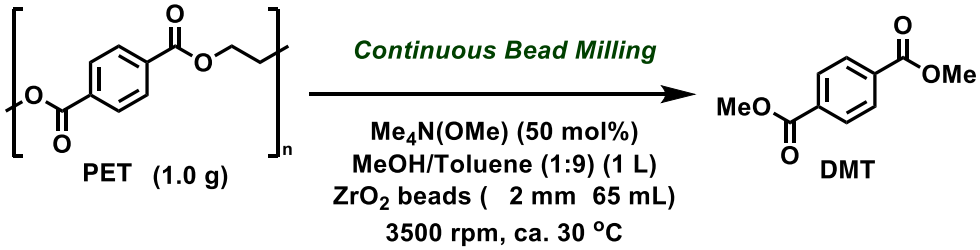

The used beverage PET flakes (1.0 g, 5.2 mmol) and ZrO_2 beads (φ2 mm; 245 g, filling rate of 70% (65 mL) relative to the vessel) were placed in the vessel, and bead mill processing was performed with a rotation speed of 3,500 rpm while supplying MeOH/toluene (1:9) solution of TMAM catalyst at approximately 100 mL/min. The total amount of MeOH/toluene (1:9) solvent in the circulation system was 1.0 L containing 50 mol% (2.6 mmol, 5.2 mL of 0.5 M stock solution) of TMAM. During this bead milling under the circulation, the temperature of the slurry was monitored, which was approximately 30 °C at the steady state. From the start of operation until 24 h had elapsed, 20 mL of the PET slurry in the storage tank was sampled at designated time, and the sample was quenched with acetic acid to determine the yield. Then the crude material was analyzed by GC using decane as an internal standard. For product isolation, for example, the 20 mL sample taken after 3 h of circulation was stirred with chloroform to extract soluble materials, and then the crude material was purified by preparative thin-layer chromatography (hexane/ethyl acetate = 2/1) to obtain dimethyl terephthalate (19.1 mg, 95% yield).

SI-12. Studies on Tamibarotene Synthesis

SI-12-1. Preparation of Starting Materials

Preparation of 2,5-Dichloro-2,5-dimethylhexane

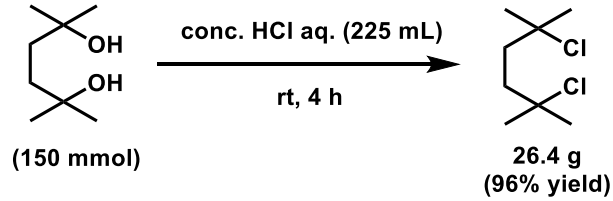

The preparation method was following the literature:[68] concentrated HCl aq. (35-37 wt%; 225 mL) was added dropwise to 2,5-dimethyl-2,5-hexanediol (150 mmol, 21.96 g) in 500 mL flask at room temperature. After stirring for 4 h, the resulting white suspension was filtered to separate insoluble material, and the obtained solid was washed with H_2O. Then the white solid was dissolved in dichloromethane (50 mL), washed with H_2O, brine, and then dried over Na_2SO_4. After filtration and evaporation of dichloromethane, 26.44 g (96% yield) of 2,5-dichloro-2,5-dimethylhexane was obtained as a white solid. NMR spectra were consistent with the literature.[68]

^{1}H NMR (500 MHz, $CDCl_3$) δ 1.94 (s, 4H), 1.59 (s, 12H). ^{13}C NMR (125 MHz, $CDCl_3$) δ 70.3, 41.1, 32.5.

Preparation of 1,2,3,4-Tetrahydro-1,1,4,4-tetramethyl-6-acetaminonaphthalene

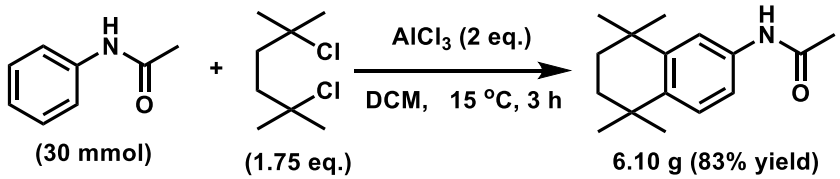

The preparation method was following the literature:[68] acetanilide (30 mmol, 4.06 g) was suspended in dichloromethane (20 mL) in 100 mL three-neck flask. While stirring the suspension at -15 °C, $AlCl_3$ (2 eq., 8.00 g) was added portionwise. After stirring for 10 min, 20 mL dichloromethane solution of 2,5-dichloro-2,5-dimethylhexane (1.75 eq., 9.61 g) was added dropwise, and continued to stir for 2 h with monitoring by TLC. After confirming the reaction has stopped, the resulting solution was poured into iced water (150 mL), followed by extraction with dichloromethane for 3 times. The organic phase was collected and washed by H_2O, brine, and the dried over Na_2SO_4. Subsequently, the solvent was evaporated, and the residue was purified by silica gel column chromatography (hexane/EtOAc = 3/1 to 1/1). After evaporation and dry under vacuum overnight, 6.10 g (83% yield) of 1,2,3,4-tetrahydro-1,1,4,4-tetramethyl-6-acetaminonaphthalene was obtained as a white solid. NMR spectra were consistent with the literature.[68]

^{1}H NMR (500 MHz, $CDCl_3$) δ 7.34 (d, J = 2.5 Hz, 1H), 7.31 (dd, J = 2.0, 8.5 Hz, 1H), 7.24 (d, J = 9.0 Hz, 1H), 2.15 (s, 3H), 1.67 (s, 4H), 1.26 (s, 6H), 1.25 (s, 6H). ^{13}C NMR (125 MHz, $CDCl_3$) δ 168.2, 145.6, 141.1, 135.2, 127.1, 118.0, 117.9, 35.01, 34.98, 34.3, 33.9, 31.80, 31.75, 24.5.

Preparation of 5,6,7,8-Tetrahydro-5,5,8,8-tetramethyl-2-naphthalenamine

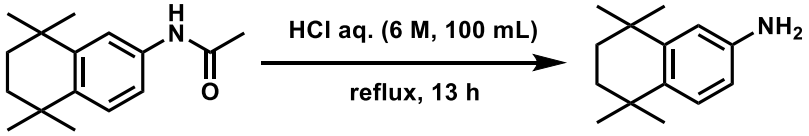

(25 mmol) 3.78 g (75% yield)

The preparation method was following the literature:[69] 1,2,3,4-tetrahydro-1,1,4,4-tetramethyl-6-acetaminonaphthalene (25 mmol, 6.10 g) was suspended in HCl aq. (6 M, 100 mL), and stirred at 100 ℃ for 13 h. TLC of the reaction solution suggested complete consumption of the starting material, and a new spot was observed. The mixture was basified (pH ~9) by NaOH aq. (6 M, ca. 100 mL). The solution was then extracted by diethyl ether (50 mL x 3) and dried over Na_2SO_4. Subsequently, the solvent was evaporated, and the residue was purified by silica gel column chromatography (hexane/EtOAc = 5/1 to 1/1). After evaporation and dry under vacuum for overnight, 3.78 g (75% yield) of 5,6,7,8-tetrahydro-5,5,8,8-tetramethyl-2-naphthalenamine was obtained as an orange solid. NMR spectra were consistent with the literature.[69]

^{1}H NMR (500 MHz, $CDCl_3$) δ 7.10 (d, *J* = 8.0 Hz, 1H), 6.64 (d, *J* = 2.5 Hz, 1H), 6.52 (dd, *J* = 2.5, 8.5 Hz, 1H), 1.65 (s, 4H), 1.25 (s, 6H), 1.24 (s, 6H). ^{13}C NMR (125 MHz, $CDCl_3$) δ 145.8, 143.7, 135.3, 127.4, 113.6, 112.8, 35.2, 34.2, 33.5, 32.0, 31.8.

SI-12-2. Experimental Procedures for Amidation Reaction

General Procedures for the Reaction of DMT with Amine 1

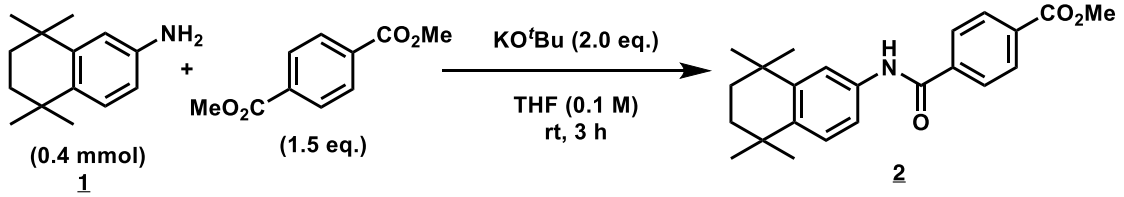

(0.4 mmol) **1** (1.5 eq.) **2**

5,6,7,8-Tetrahydro-5,5,8,8-tetramethyl-2-naphthalenamine (**1**: 0.4 mmol, 78.6 mg), dimethyl terephthalate (0.6 mmol, 116.6 mg), KO^{t}Bu (ca. 1 M THF solution; 0.8 mmol, 0.8 mL), and THF (3.2 mL) were put in 10 mL flask equipped with an argon balloon. After stirring for 3 h, the reaction mixture was quenched by acetic acid (0.8 mmol, 46 μL), and evaporated to remove the solvent. Chloroform and water were added to the residue, and the organic phase was washed with water twice. The resulting organic phase was evaporated, and the resulting residue was analyzed by ^{1}H NMR using tetrachloroethane as an internal standard. Complete conversion of the amine **1** was observed, and the yield methyl 4-[(5,6,7,8-tetrahydro-5,5,8,8-tetramethyl-2-naphthalenyl)caramoyl]benzoate (**2**) was calculated to be 99%. Then, the obtained residue was purified by preparative thin-layer chromatography (hexane/DCM/MeOH = 10/10/1) to give the amide **2** (141.7 mg, >99% yield) as a white crystal. NMR spectra were consistent with a previous report.[70]

^{1}H NMR (500 MHz, $CDCl_3$) δ 8.07 (d, J = 8.5 Hz, 2H), 7.89 (d, J = 8.5 Hz, 2H), 7.53 (s, 1H), 7.44 (d, *J* = 8.5 Hz, 1H), 7.28 (d, *J* = 8.5 Hz, 1H), 3.93 (s, 3H), 1.67 (s, 4H), 1.27 (s, 6H), 1.26 (s, 6H). ^{13}C NMR (125 MHz, $CDCl_3$) δ 166.2, 164.8, 145.8, 141.7, 139.1, 135.0, 132.7, 129.9, 127.2, 127.1, 118.3, 118.2, 52.4, 35.0, 34.9, 34.4, 34.0, 31.8, 31.7.

Experimental Procedures for the Continuous-Flow Amidation with Sonication

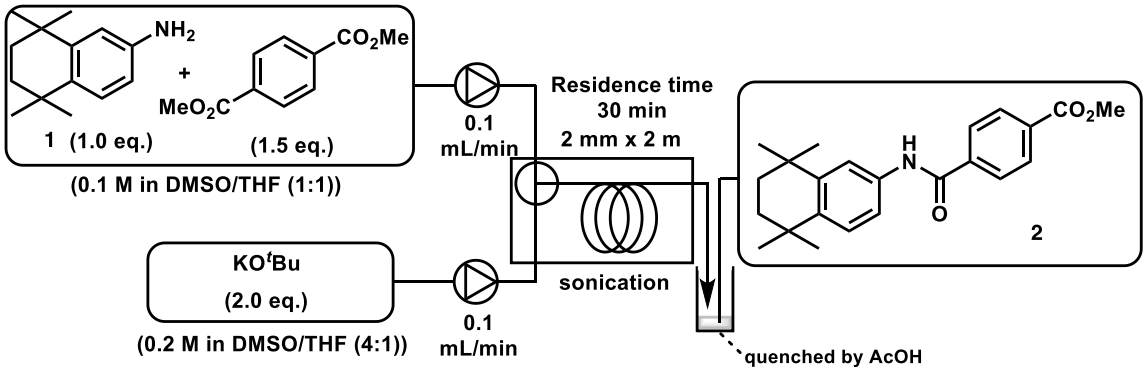

5,6,7,8-Tetrahydro-5,5,8,8-tetramethyl-2-naphthalenamine (**1**: 2.5 mmol, 508.7 mg) and dimethyl terephthalate (3.75 mmol, 728.4 mg) were dissolved in DMSO/THF (1:1) (25 mL) to prepare substrate solution **A**. On the other hand, KO^{t}Bu (ca. 1 M THF solution; 5.0 mmol, 5.0 mL) was mixed with DMSO (20 mL) to prepare substrate solution **B**. The solution **A** and **B** were each delivered separately using plunger pumps (FLOM, dual plunger pump, KP-22 and Al-12) at a flow rate of 0.1 mL/min, and were merged at a Y-shaped connector. The length of the tube from the connector was 195 cm, which had an inner diameter of φ2 mm, and a total volume was 6 mL. By placing the Y-shaped connector and the tube reactor inside a sonication device, clogging in the tube suppressed, ensuring a smooth flow (the photo of reaction set up is shown in Figure S37). The reaction mixture was quenched with 1 mL of acetic acid in a vial. Sampling started 30 min after the solutions passed through the connector, and the sample vial was replaced with a new one every 30 min. Hexane/EtOAc (4:1) and water were added to the sampled solution, and it was mixed thoroughly. After collecting the organic phase, the aqueous solution was extracted with hexane/EtOAc (4:1) for additional four times. The combined organic layer was then washed with water, brine, and dried over Na_2SO_4. After filtration of Na_2SO_4, the solution was evaporated and analyzed by ^{1}H NMR using tetrachloroethane as an internal standard (for detailed profiles of the yields, see Figure 11(b) in the main text) to determine the yield of the product. For example, when a sample taken between 3.5 and 4 h after the start was analyzed by ^{1}H NMR, the yield of the amide **3** was 99%. Subsequently, purification by preparative thin-layer chromatography (hexane/DCM/MeOH = 10/10/1) afforded the amide **2** (108.1 mg, 99% yield) as a white crystal.

Figure S37. Photo of the Reaction Setup with Sonication

Experimental Procedures for the Direct Conversion to Tamibarotene

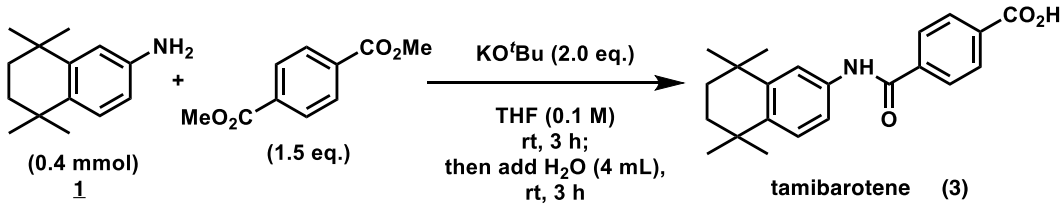

5,6,7,8-Tetrahydro-5,5,8,8-tetramethyl-2-naphthalenamine (**1**: 0.4 mmol, 81.6 mg), dimethyl terephthalate (0.6 mmol, 117.7 mg), KO^{t}Bu (ca. 1 M THF solution; 0.8 mmol, 0.8 mL), and THF (3.2 mL) were put in 10 mL flask equipped with an argon balloon. After stirring for 3 h, water was added to the solution and continued to stir for another 3 h. The solution was then quenched by HCl aq. (1 M; 2 mmol, 2 mL), and extracted by EtOAc for 3 times. The combined organic phase was evaporated and analyzed by ^{1}H NMR using tetrachloroethane as an internal standard. Complete conversion of the amine **1** was observed, and the yield of tamibarotene was calculated to be >99%, accompanied with 47% yield of terephthalic acid. Then, the obtained residue was purified by preparative thin-layer chromatography (MeOH/CH_2Cl_2=1/2) to give tamibarotene (140.1 mg, >99% yield) as a white solid. NMR spectra were consistent with a previous report.[70]

^{1}H NMR (500 MHz, DMSO-d_6) δ 10.2 (s, 1H), 8.09 (d, J = 7.5 Hz, 2H), 7.94 (d, J = 8.0 Hz, 2H), 7.70 (s, 1H), 7.60 (d, J = 7.0 Hz, 1H), 7.24 (d, J = 9.0 Hz, 1H), 1.62 (s, 4H), 1.22 (s, 6H), 1.21 (s, 6H). ^{13}C NMR (125 MHz, DMSO-d_6) δ 170.1, 165.2, 144.5, 140.9, 139.7, 136.7, 136.0, 129.1, 126.9, 126.4, 118.4, 118.2, 34.7, 34.6, 34.0, 33.5, 31.7, 31.7.

SI-12-3. Additional Information for the Synthesis of Tamibarotene

Investigation of Mixed Solvent Systems for the Direct Amidation

In the initial investigation of the continuous flow experiment, the formation of precipitates was observed as the reaction proceeded, necessitating careful selection of the solvent. THF was used as the main solvent in Table 9 of the main text. In this section, mixed solvent systems with THF were investigated. The addition of DMSO, DMF, or NMP as co-solvents resulted in the complete conversion of amine 1 to amide 2 (Table S34, entries 2–4). Although the homogeneity of the reaction mixture was improved when these solvents were used as co-solvents, they did not result in a completely clear solution. This motivated us to adopt sonication for the continuous-flow system.

Table S24. Investigation of Cosolvents to Dissolve the Precipitate

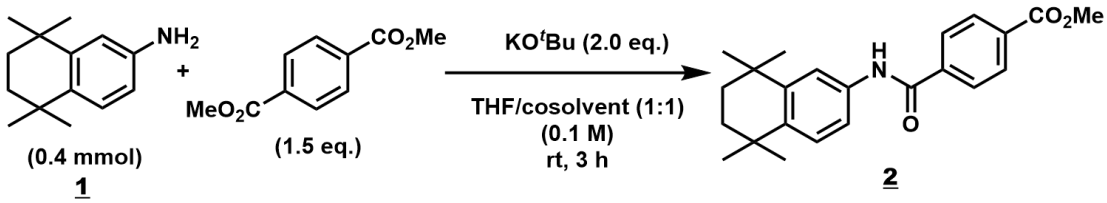

Entry	Cosolvent	Appearance	Conv. (%)[a]	Yield (%)[a]
1	none	white precipitate	full	99 (99)[b]
2	DMSO	clear suspension	full	>99
3	DMF	suspension	full	99
4	NMP	suspension	full	>99[c]
5	^{t}BuOH	white precipitate	21	23

[a] Determined by ^{1}H NMR analysis; [b] Isolated yield; [c] NMP was contaminated

SI-12-4. Mechanistic Insight of the Direct Amidation

While sonication proved effective in preventing clogging from an engineering perspective, we sought to elucidate the reaction mechanism by identifying the structure of the precipitate. To this end, we collected and analyzed the precipitate formed during the reaction (Figures S38–40). To prevent hydrolysis of the precipitate by atmospheric moisture, the reaction and filtration procedures were conducted under an argon atmosphere in a glove box (Figure S38). Upon completion of the amidation reaction, a white precipitate was observed. This precipitate was collected by filtration, washed with THF, and dried, yielding 46.5 mg of a white solid (designated as "precipitate A"). Some precipitate with small particle sizes passed through the filter paper during filtration. Precipitate A was soluble in DMSO-d_6, forming a yellow solution, but insoluble in D_2O. ^{1}H NMR analysis of precipitate A in DMSO-d_6 revealed a peak corresponding to amide **2** (Figure S39). However, the peak positions were shifted compared to those of the neutral amide **2**, particularly the aromatic ring bonded to the nitrogen atom, which was shifted upfield. This observation suggested that amide **2** was deprotonated at the amide nitrogen to form an anionic species. Electrospray ionization mass spectrometry (ESI-MS) analysis of precipitate A in CH_3CN showed a main peak corresponding to the molecular weight of the deprotonated amide **2** [M-H]$^-$ = 364.19) (Figure S40). A peak corresponding to the deprotonated form of tamibarotene **3** ([M-H]$^-$ = 350.18), a potential decomposition product of amide **2**, was also observed.

Based on these NMR and ESI-MS analyses, we assumed that precipitate A was the potassium salt of the deprotonated amide **2**.

In a separate experiment, after filtration (Figure S38), the filtrate ("solution A") was collected and centrifuged outside the glove box to collect the solid precipitate (designated as "precipitate B"). Precipitate B exhibited different properties from precipitate A; it was soluble in D_2O, forming a colorless solution, but insoluble in DMSO-d_6 or CD_3OD. ^1H NMR analysis of precipitate B showed almost no identifiable peaks. Furthermore, no discernible peaks were observed in the ESI-MS analysis. Based on these results, we concluded that precipitate B was likely an inorganic material, such as potassium hydroxide (KOH) formed by hydrolysis of precipitate A upon exposure to air. Quantitative ^1H NMR analysis of solution B (recovered after centrifugation; Figure S38) revealed an 82% yield of amide **2**. Considering the presence of tetrahydrofuran (THF) and methanol (MeOH) in the ^1H NMR spectra (Figure S39), we calculated that the 46.5 mg of precipitate A contained approximately 25% yield of K^+[amide **2**]$^-$ (relative to amine **1**). Combining the yields from precipitate A and solution B accounted for approximately 100% of the amide **2** equivalent.

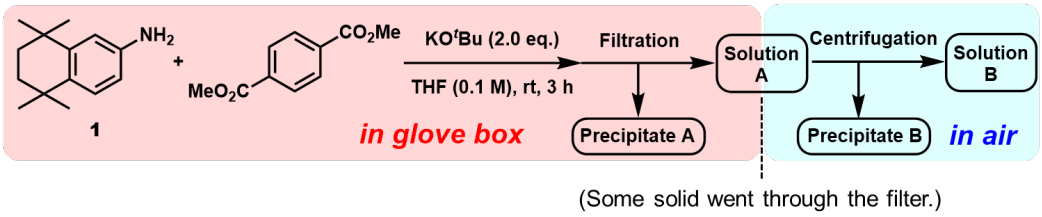

➢ **Precipitate A**: Soluble in DMSO-d_6 (yellow soln.). Insoluble in D_2O (white solid).
→ NMR analysis and ESI-MS analysis suggested the formation of K^+[amide **2** anion]$^-$ salt

➢ **Precipitate B**: Soluble in D_2O (colorless soln.). Insoluble in DMSO-d_6 or CD_3OD (white solid).
→ Almost no identical peak was observed.

➢ **Solution B**: 82% yield of the amide **2**

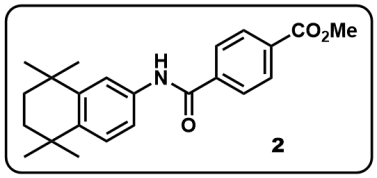

Figure S38. Identifying Chemical Structure of the Precipitate

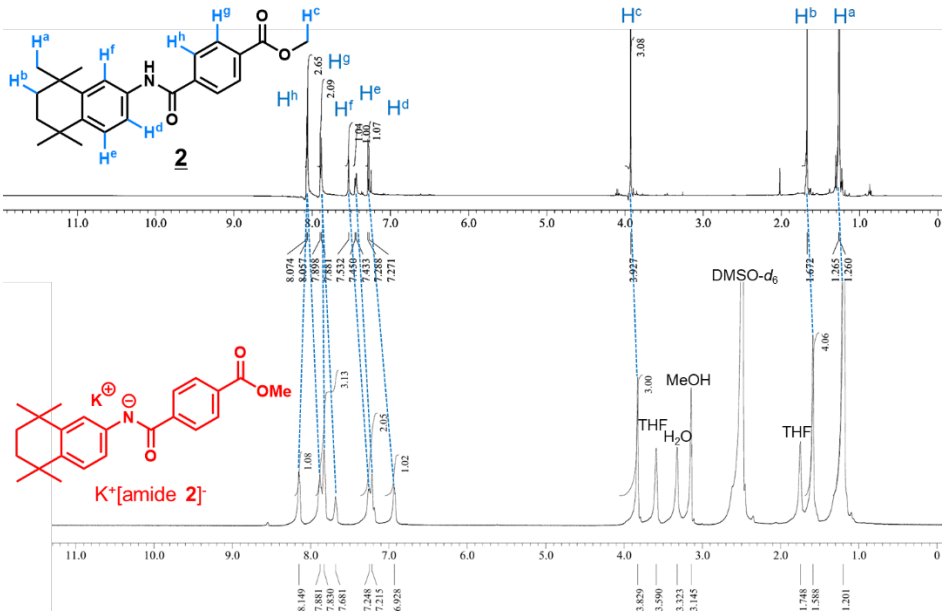

Figure S39. ^{1}H NMR Analysis of the Precipitate Compared with the Amide **2**

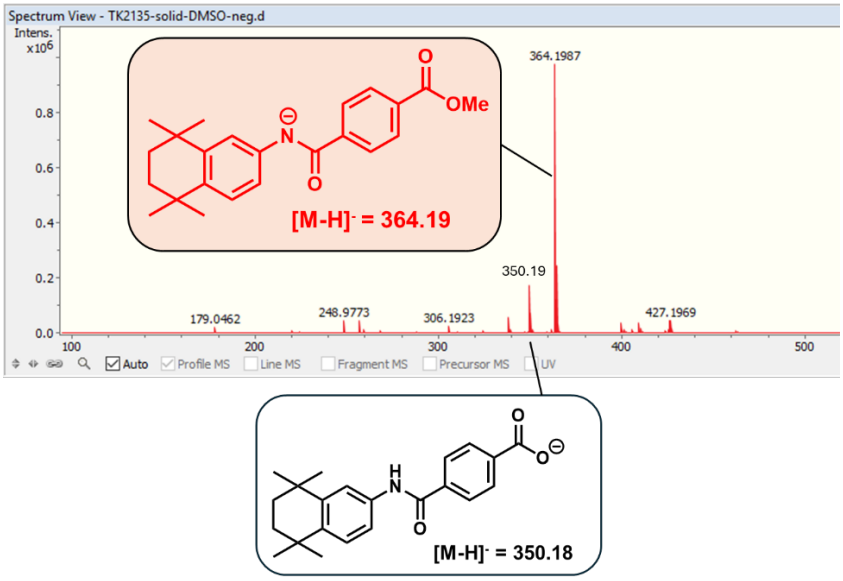

Figure S40. ESI-MS Analysis of the Residue

Based on the aforementioned investigations, we propose the following mechanism for the direct amidation reaction (Figure S41): First, KO^{t}Bu acts as a base to deprotonate amine **1**. This deprotonation is thermodynamically favorable, as the p*K*a of ^{t}BuOH in DMSO is 32.2,[58] while the p*K*a of aniline in DMSO is 30.6.[71,72] The deprotonated amine then undergoes nucleophilic addition to dimethyl terephthalate (DMT) to form amide **2**. A previous report suggests that a radical pathway may also be involved.[73] The byproduct, KOMe, subsequently deprotonates amide **2** to generate the potassium salt K$^+$[amide **2**]$^-$. This deprotonation is also thermodynamically favorable, as the p*K*a of MeOH in DMSO is 29.0,[58] and the p*K*a of *N*-phenylbenzamide in DMSO is 18.8.[74] The resulting anionic amide **2** is electron-rich and less susceptible to further nucleophilic attack, thereby suppressing the formation of a diamide byproduct.

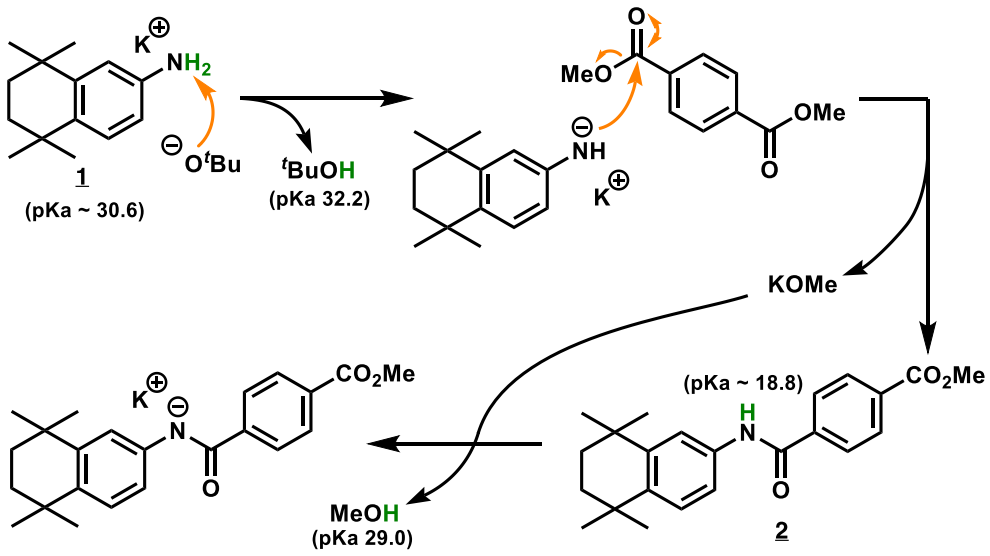

Figure S41. Possible Reaction Mechanism of the Direct Amidation Reaction

SI-12-5. Flow Reaction in the Presence of 18-Crown 6-Ether

Figure 11 in the main text presents the optimal conditions for the continuous synthesis of a tamibarotene precursor **2** using DMT as a starting material. This flow reaction was achieved by suppressing precipitate formation through the use of a sonicator. However, an alternative method is introduced in Figure S42. In this approach, a crown ether was used in combination with a base to solubilize the potassium salts. Smooth flow was achieved without clogging, and the desired product was obtained consistently with a yield exceeding 80% at steady state.

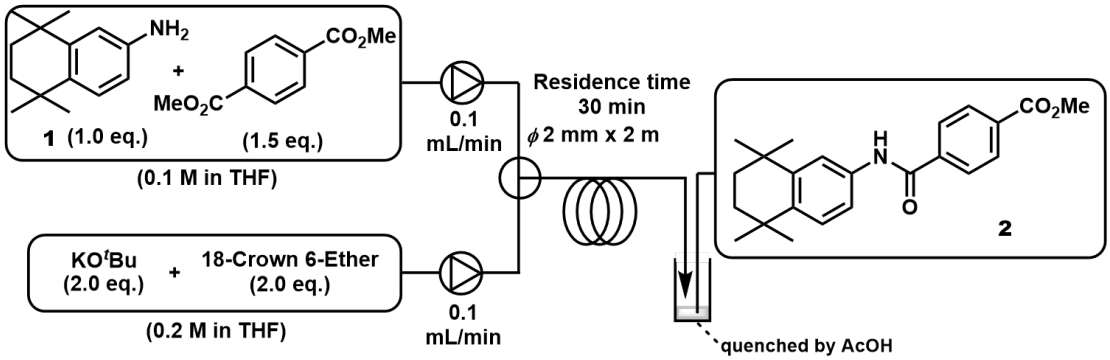

Sampling time[a]	Recovery of **1** (%)[b]	Yield of **3** (%)[b]
0.5 h - 1 h	0	74
1 h - 1.5 h	0	86 (85)[c]
1.5 h - 2 h	0	84
2 h - 2.5 h	0	84
2.5 h - 3 h	0	82 (83)[c]

[a] The time was set to 0 h when substrates solution reached the confluence.

[b] Determined by ^{1}H NMR; [c] Isolated yield

Figure S42. Continuous-flow Direct Amidation Reaction in the presence of 16-Crown 6-Ether

SI-13. ^{1}H and ^{13}C NMR Spectra

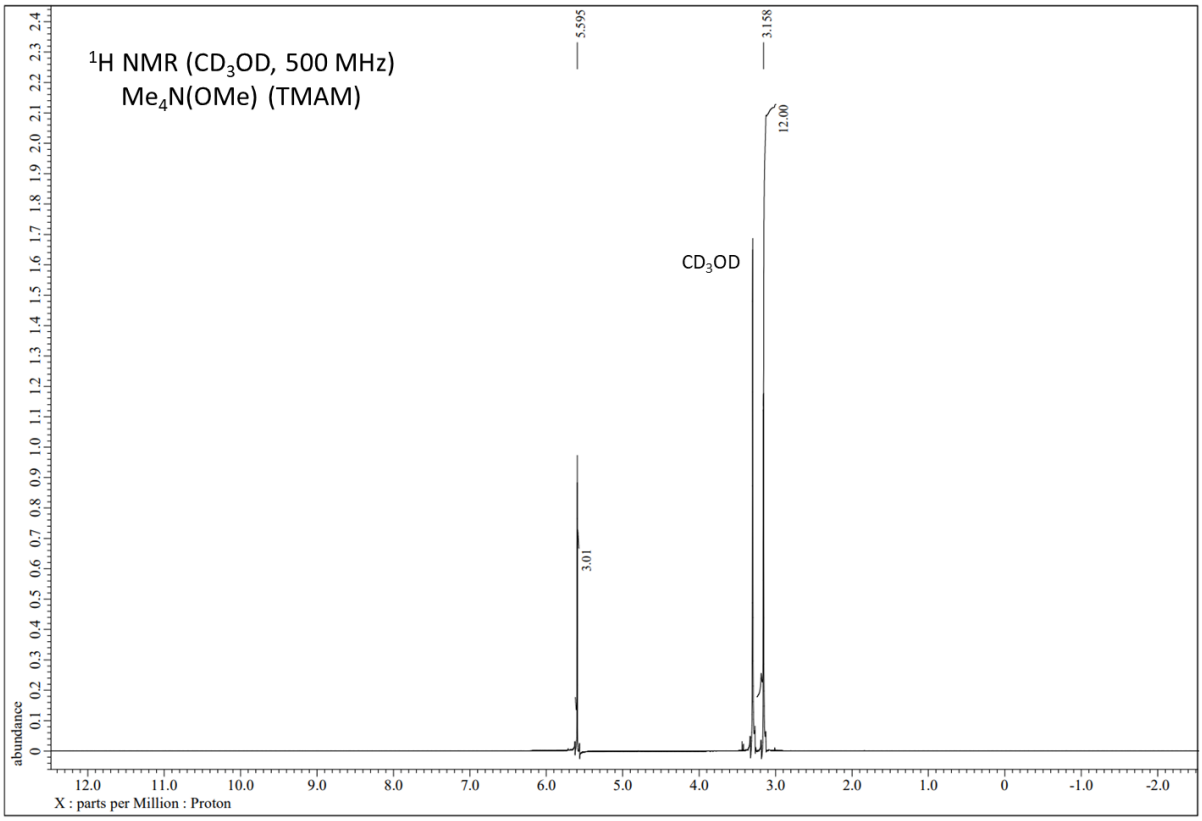

Figure S43. ^{1}H NMR Spectrum of Tetramethylammonium Methoxide (TMAM)

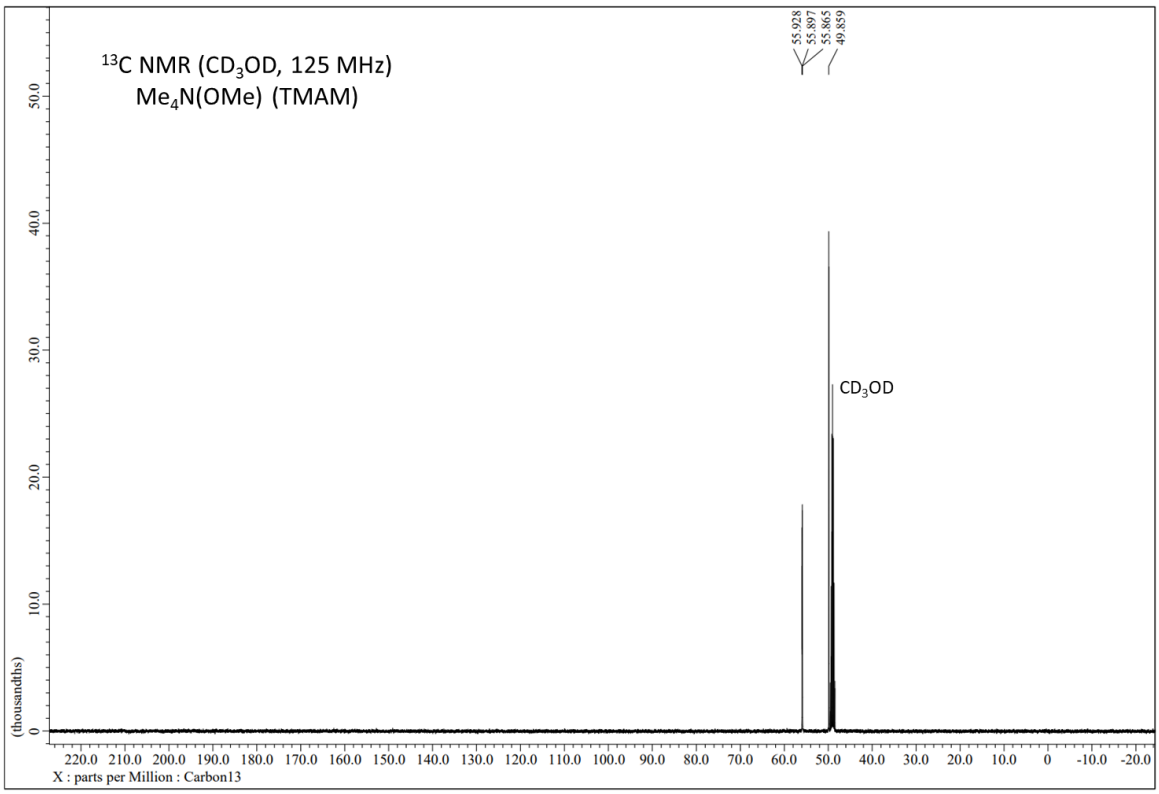

Figure S44. ^{13}C NMR Spectrum of Tetramethylammonium Methoxide (TMAM)

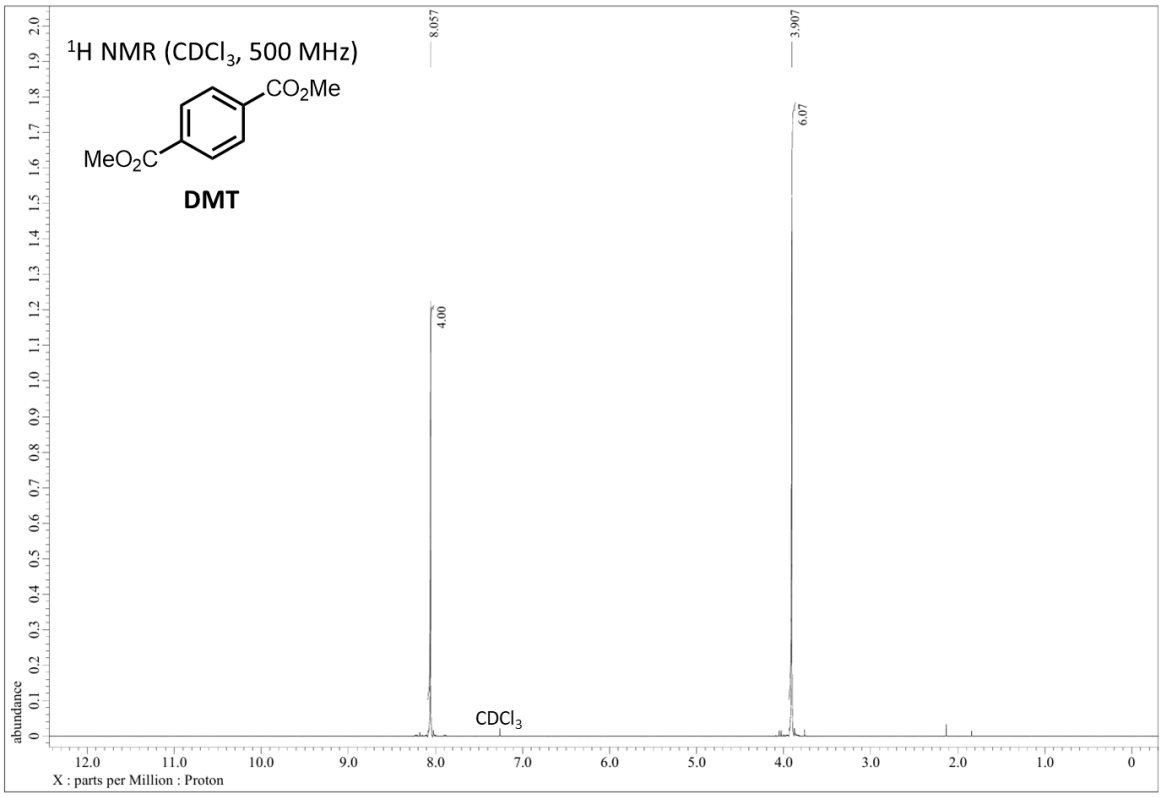

Figure S45. ^{1}H NMR Spectrum of Dimethyl Terephthalate (DMT)

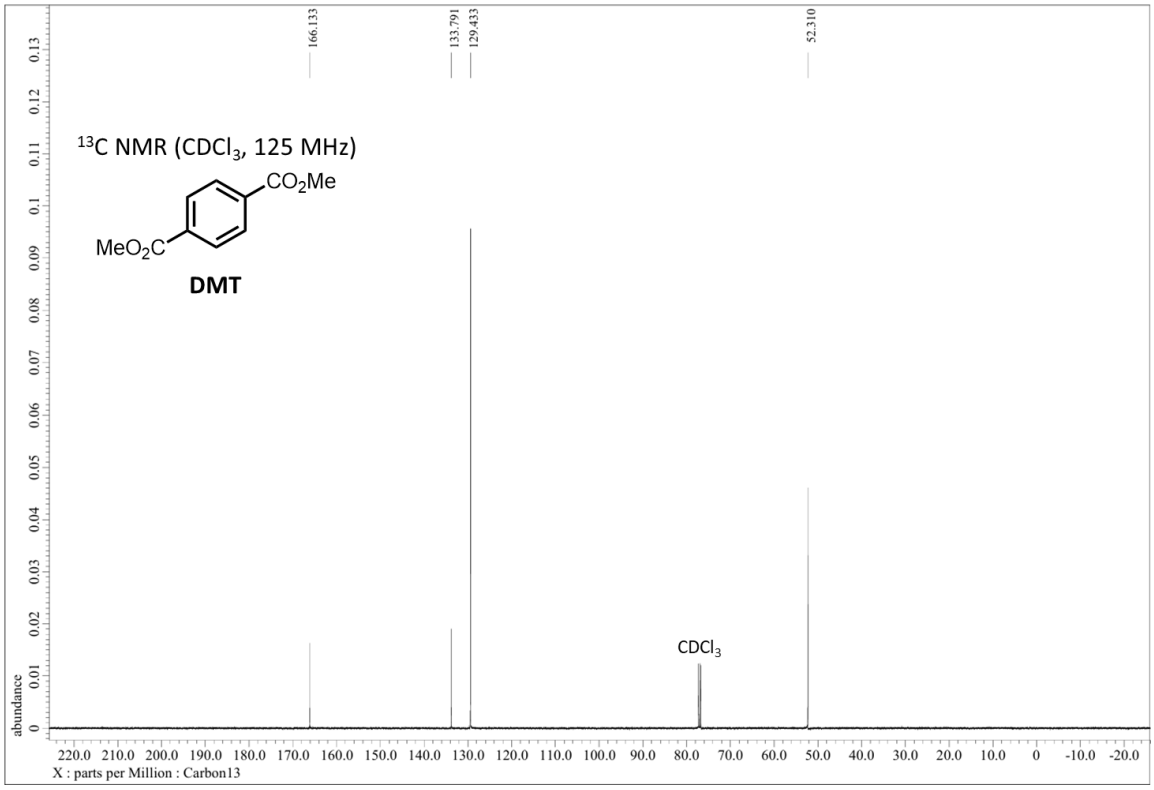

Figure S46. ^{13}C NMR Spectrum of Dimethyl Terephthalate (DMT)

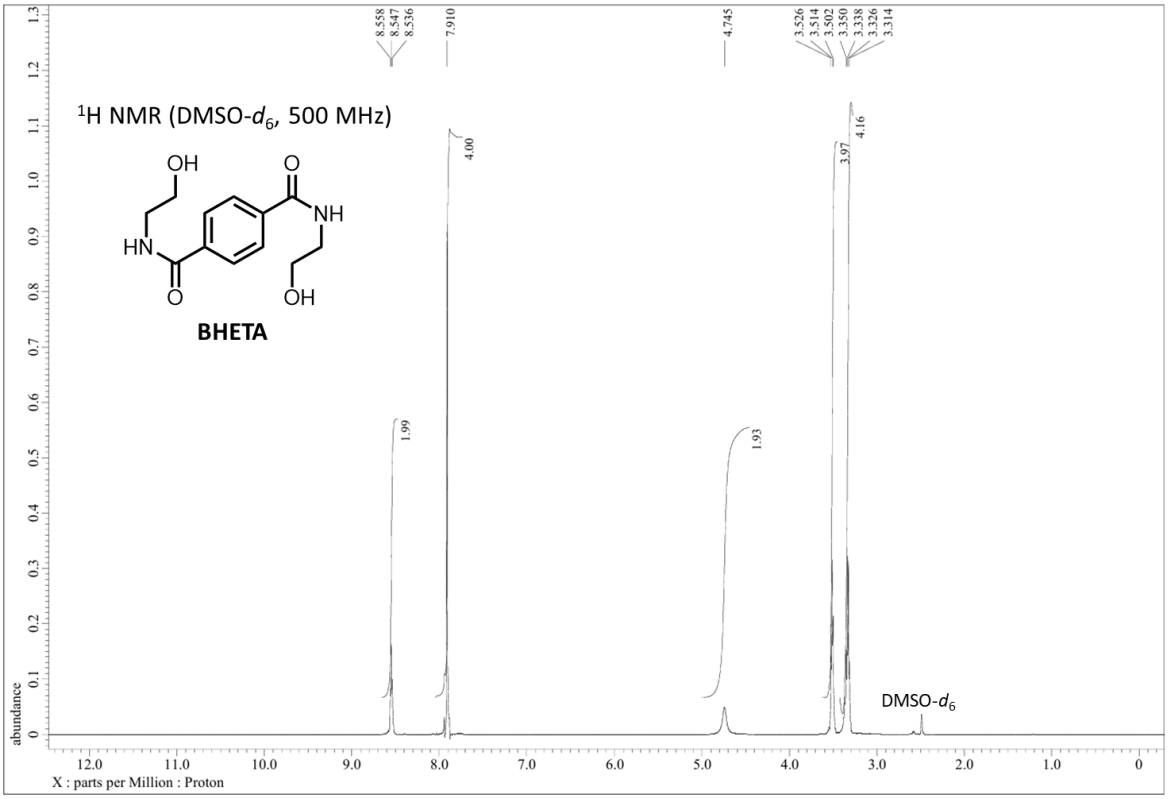

Figure S47. ^{1}H NMR Spectrum of *N*,*N'*-Bis(2-hydroxyethyl) Terephthalamide (BHETA)

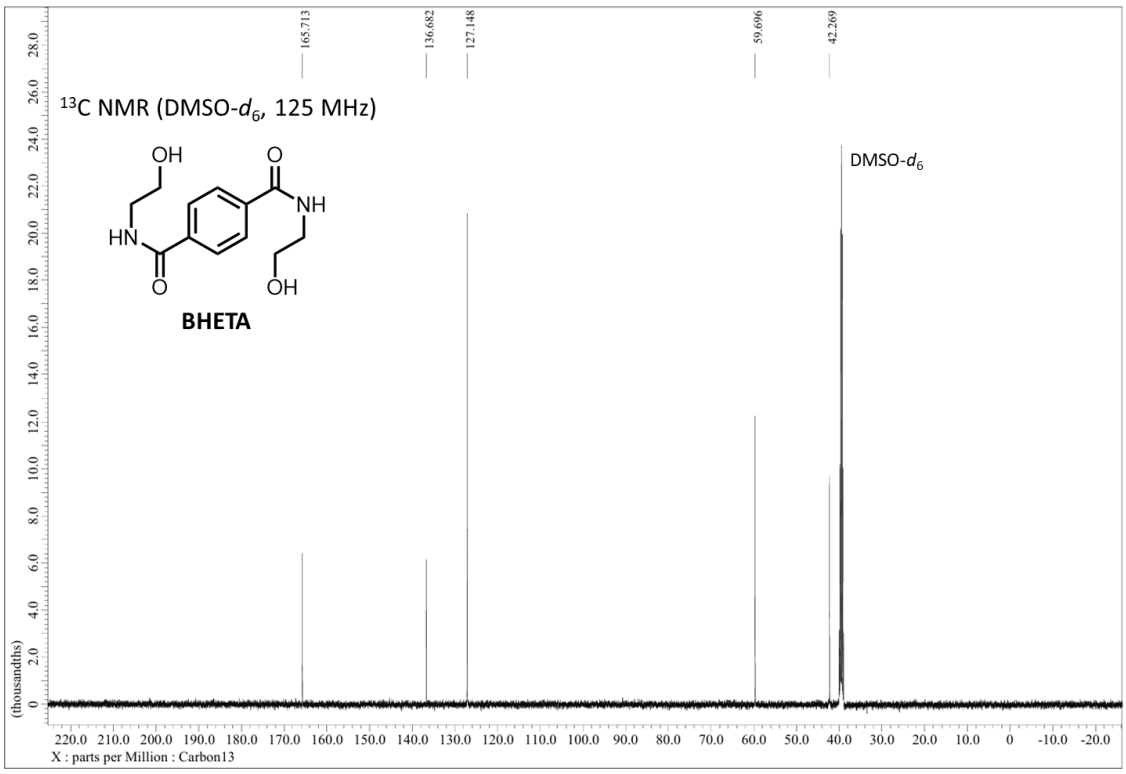

Figure S48. ^{13}C NMR Spectrum of *N*,*N'*-Bis(2-hydroxyethyl) Terephthalamide (BHETA)

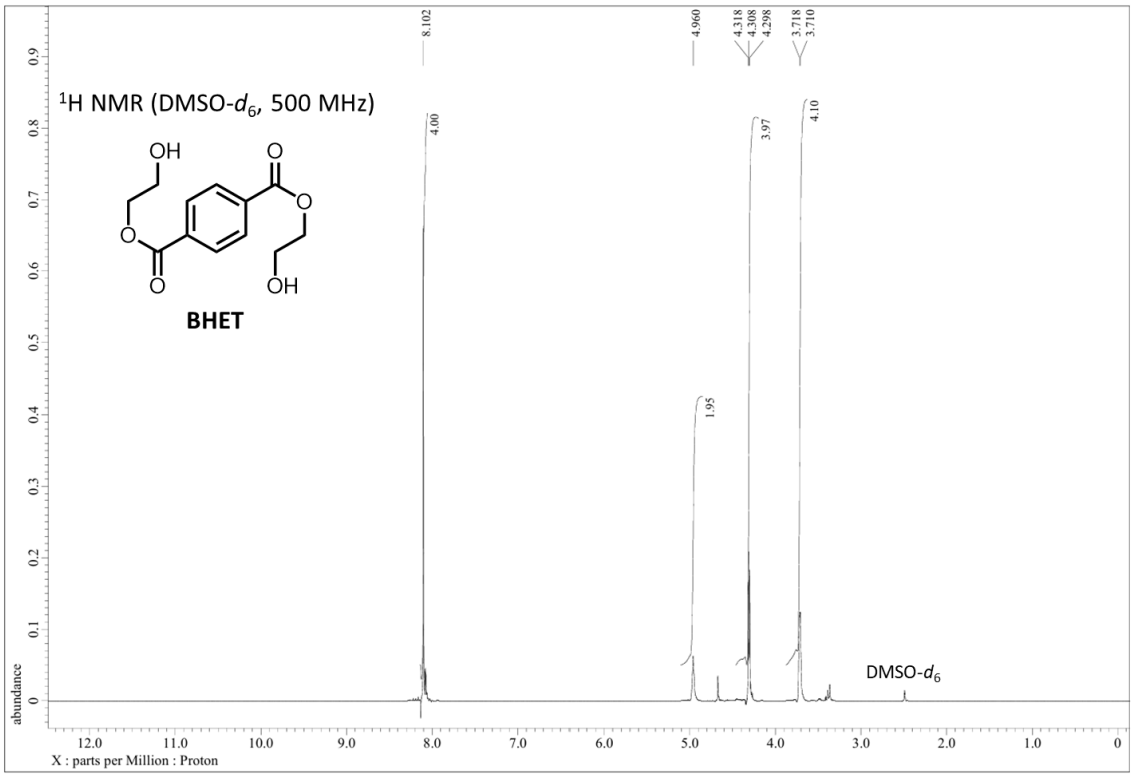

Figure S49. ^{1}H NMR Spectrum of Bis(2-hydroxyethyl) Terephthalate (BHET)

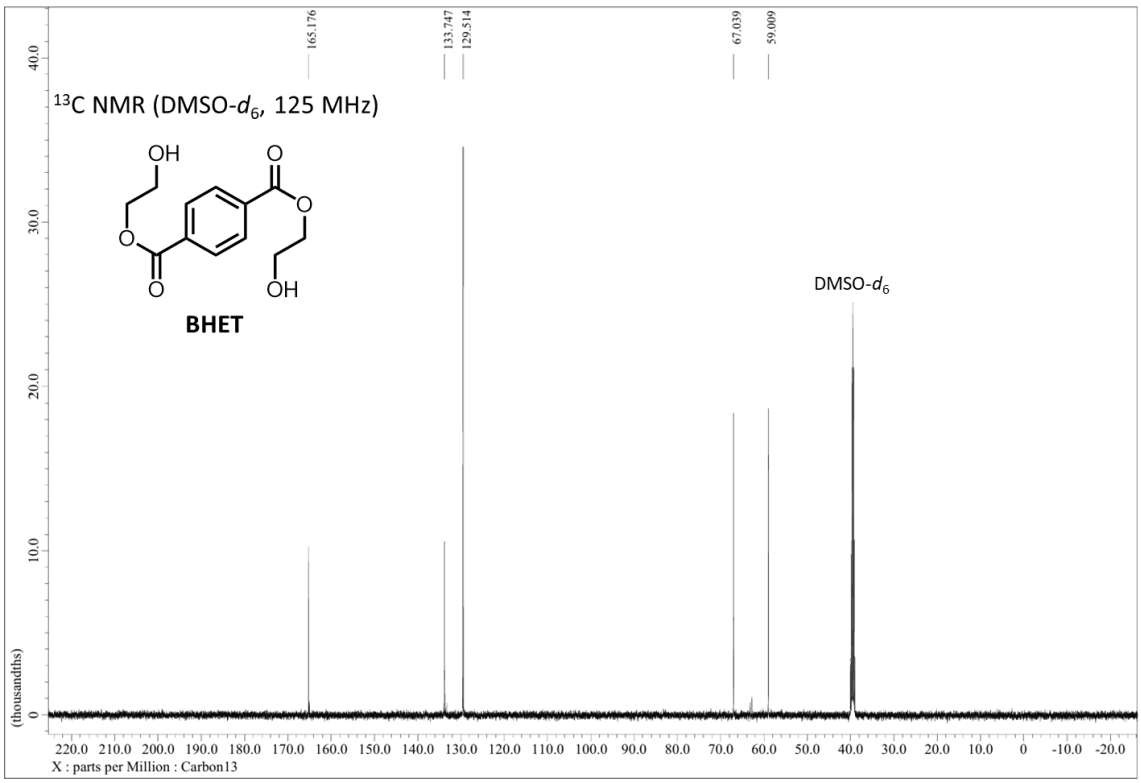

Figure S50. ^{13}C NMR Spectrum of Bis(2-hydroxyethyl) Terephthalate (BHET)

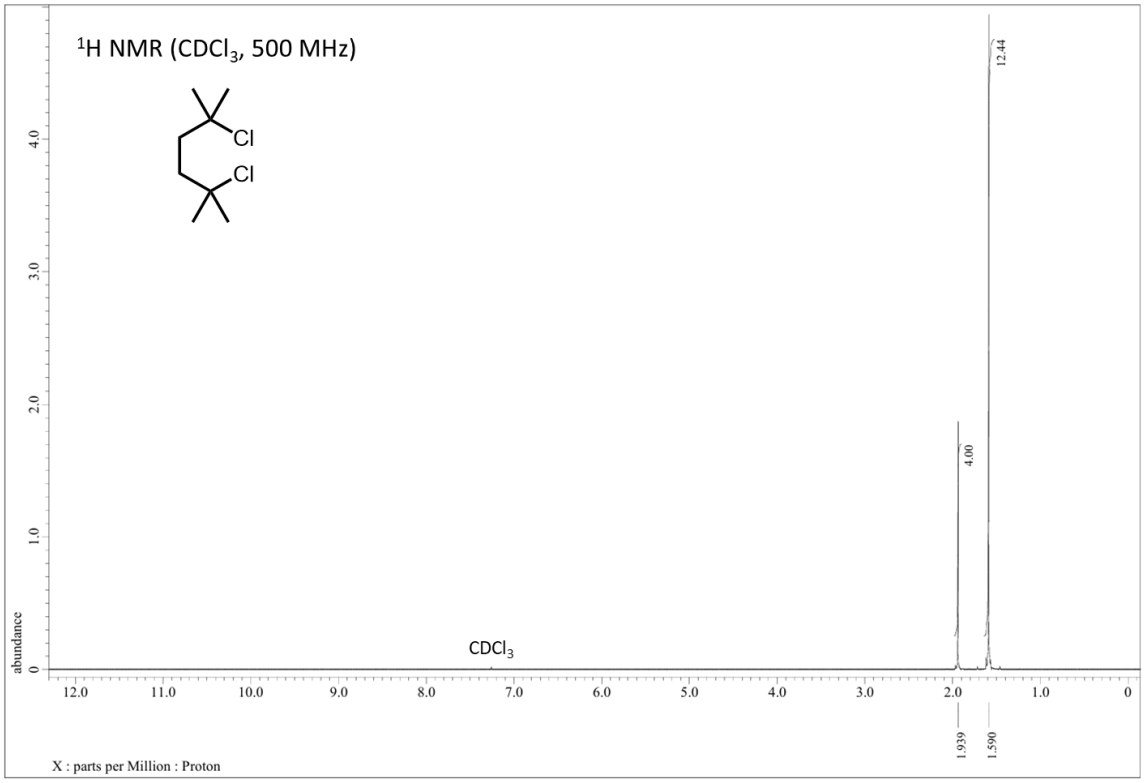

Figure S51. ^{1}H NMR Spectrum of 2,5-Dichloro-2,5-dimethylhexane

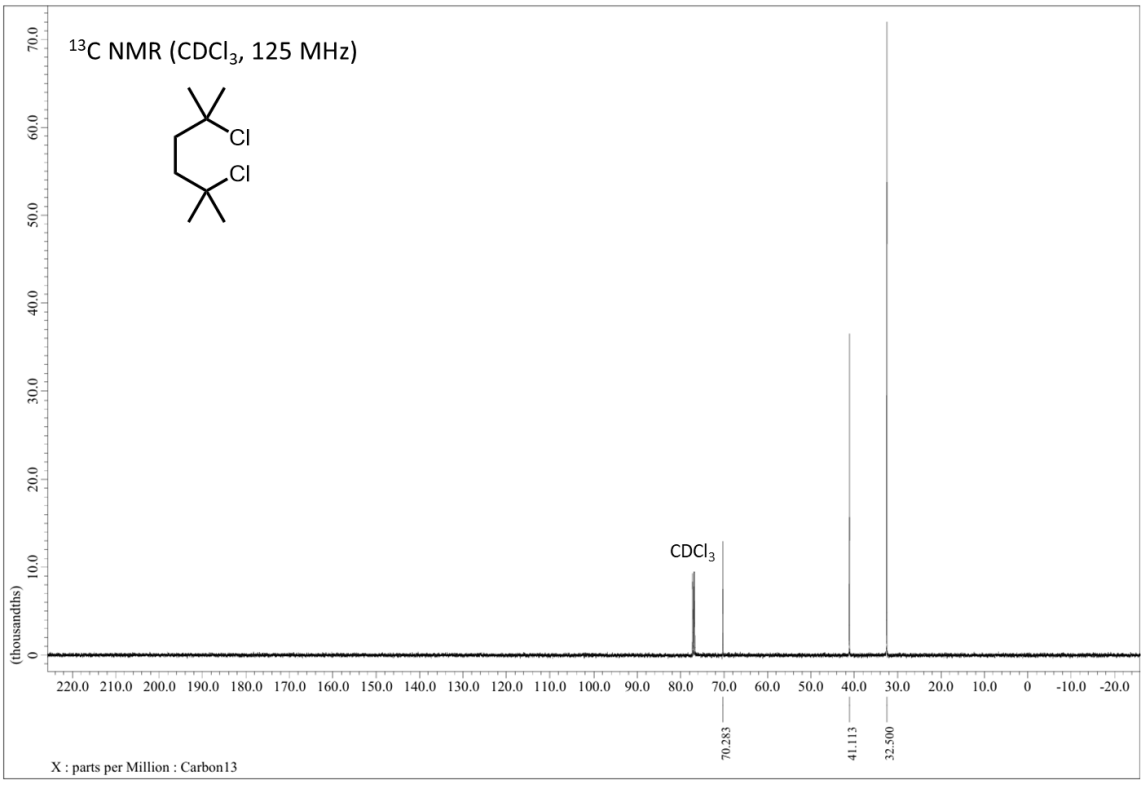

Figure S52. ^{13}C NMR Spectrum of 2,5-Dichloro-2,5-dimethylhexane

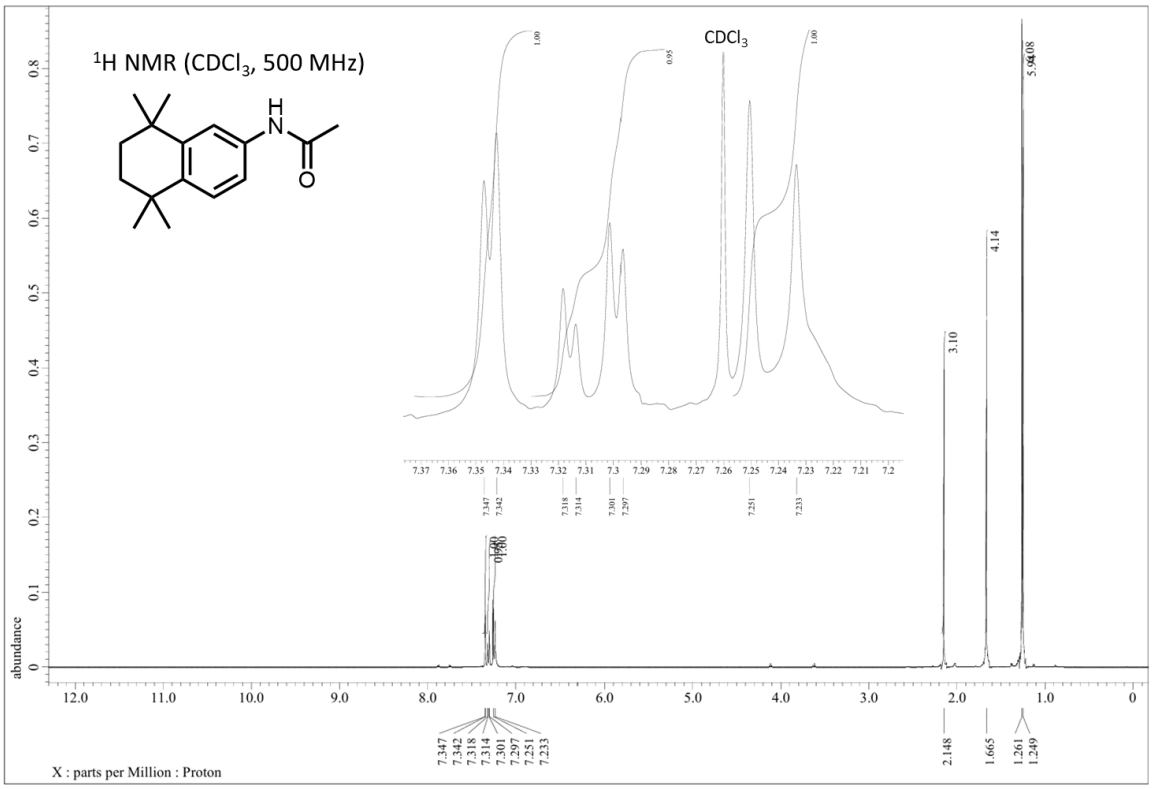

Figure S53. ^{1}H NMR Spectrum of 1,2,3,4-Tetrahydro-1,1,4,4-tetramethyl-6-acetaminonaphthalene

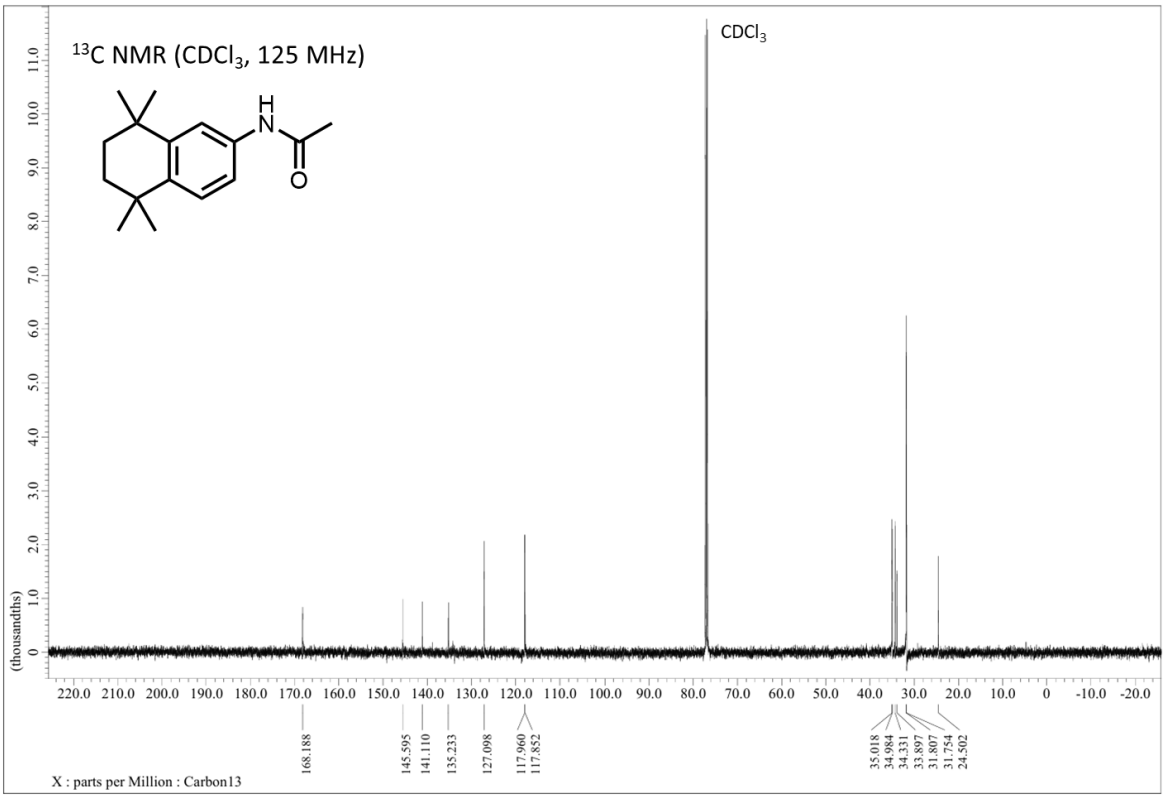

Figure S54. ^{13}C NMR Spectrum of 1,2,3,4-Tetrahydro-1,1,4,4-tetramethyl-6-acetaminonaphthalene

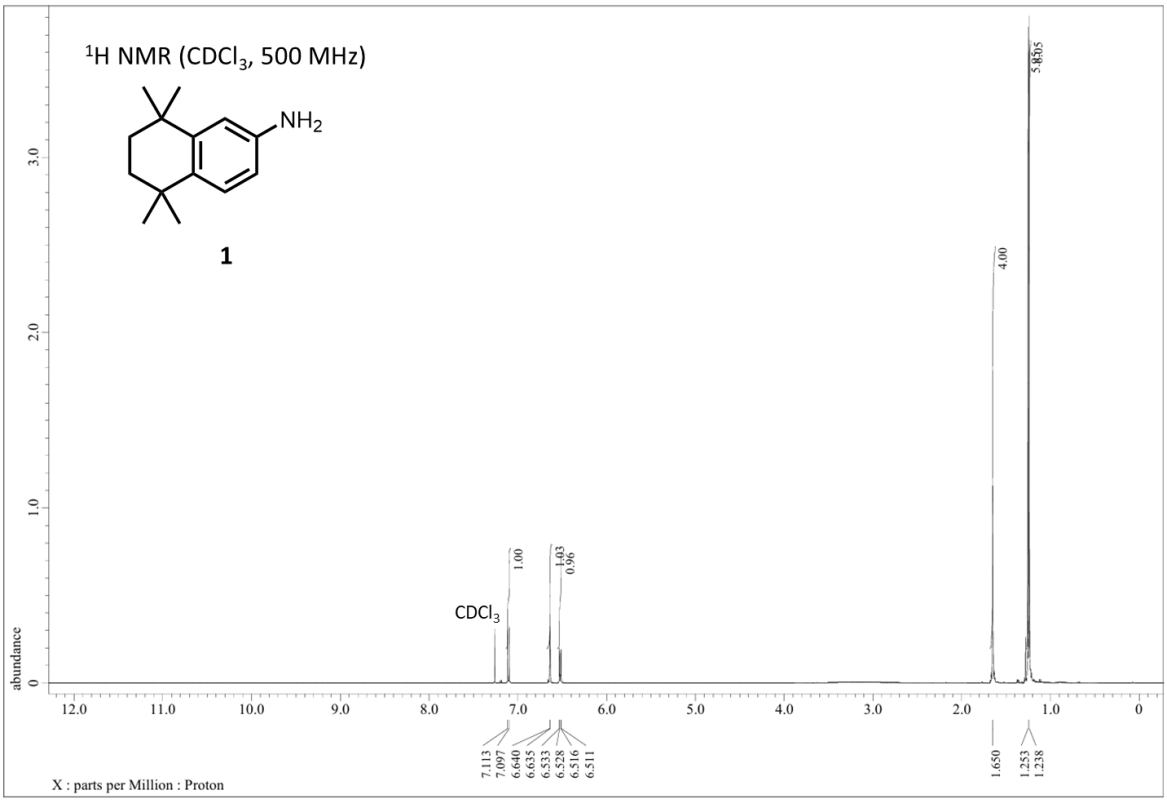

Figure S55. ^{1}H Spectrum of 5,6,7,8-Tetrahydro-5,5,8,8-tetramethyl-2-naphthalenamine (**1**)

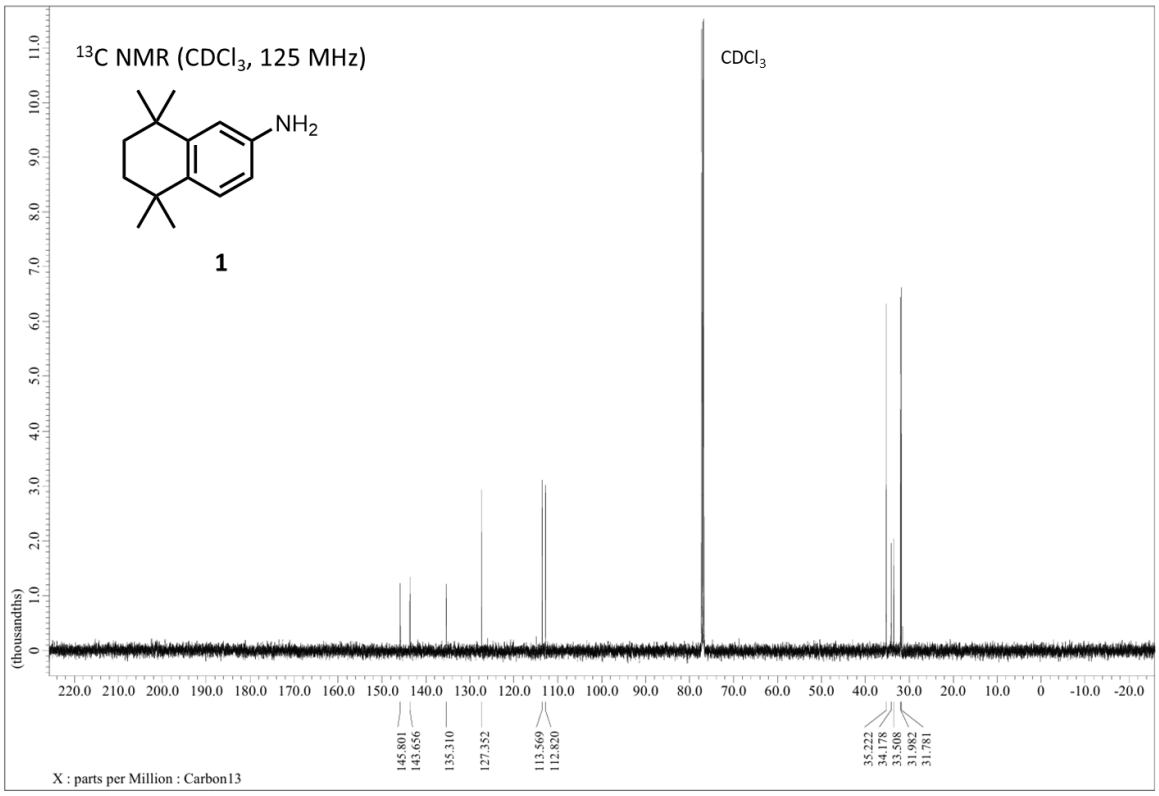

Figure S56. ^{13}C NMR Spectrum of 5,6,7,8-Tetrahydro-5,5,8,8-tetramethyl-2-naphthalenamine (**1**)

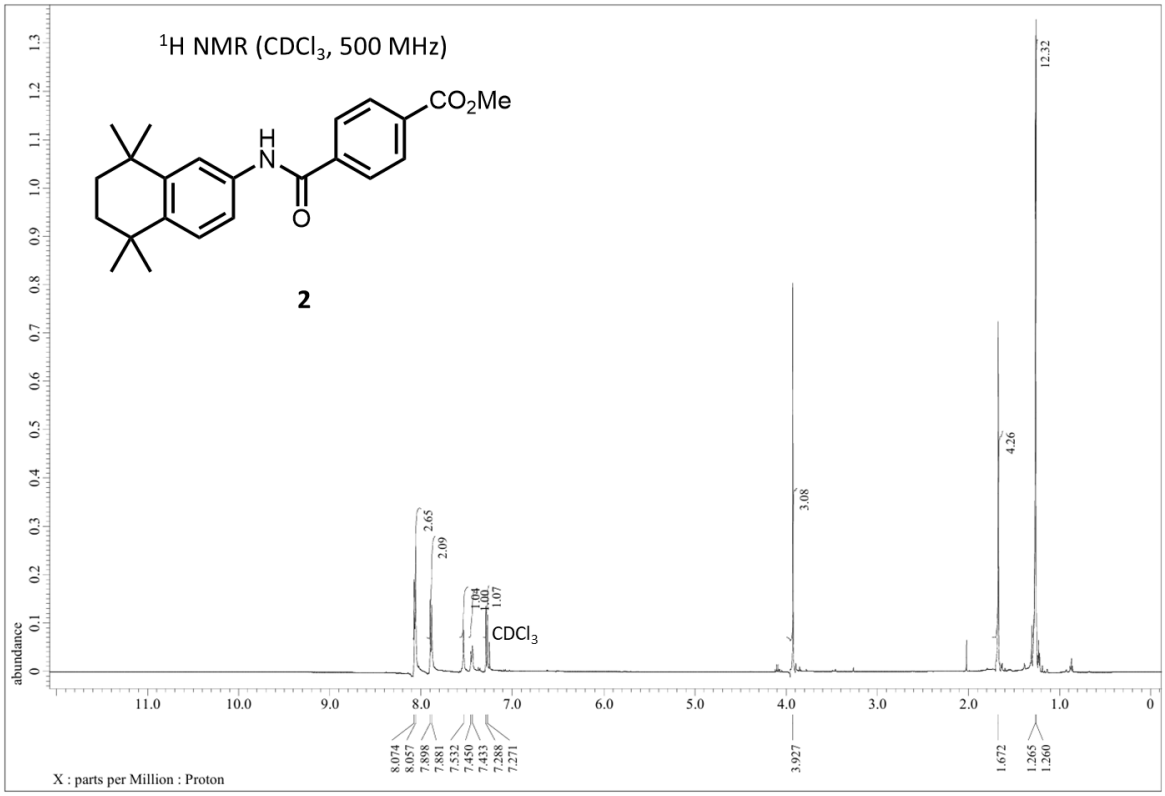

Figure S57. ^{1}H NMR Spectrum of methyl 4-[(5,6,7,8-tetrahydro-5,5,8,8-tetramethyl-2-naphthalenyl)caramoyl]benzoate (**2**)

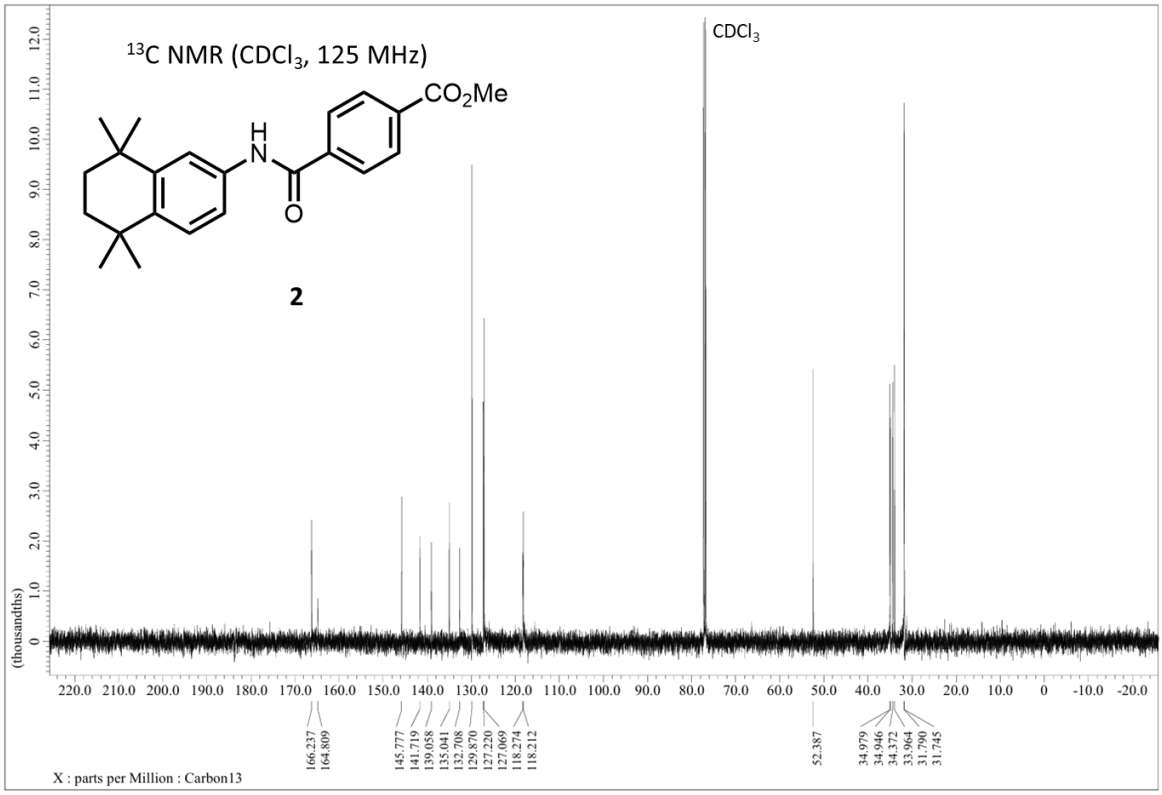

Figure S58. ^{13}C NMR Spectrum of methyl 4-[(5,6,7,8-tetrahydro-5,5,8,8-tetramethyl-2-naphthalenyl)caramoyl]benzoate (**2**)

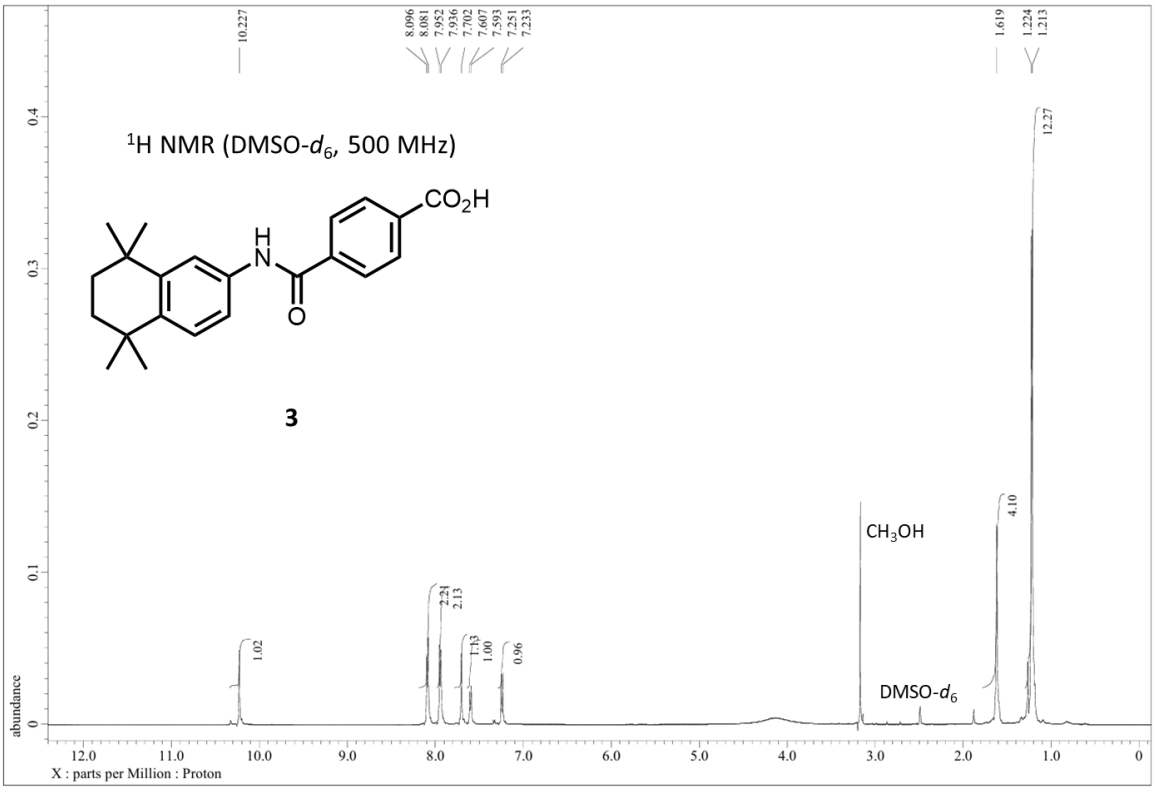

Figure S59. ^{1}H NMR Spectrum of Tamibarotene (**3**)

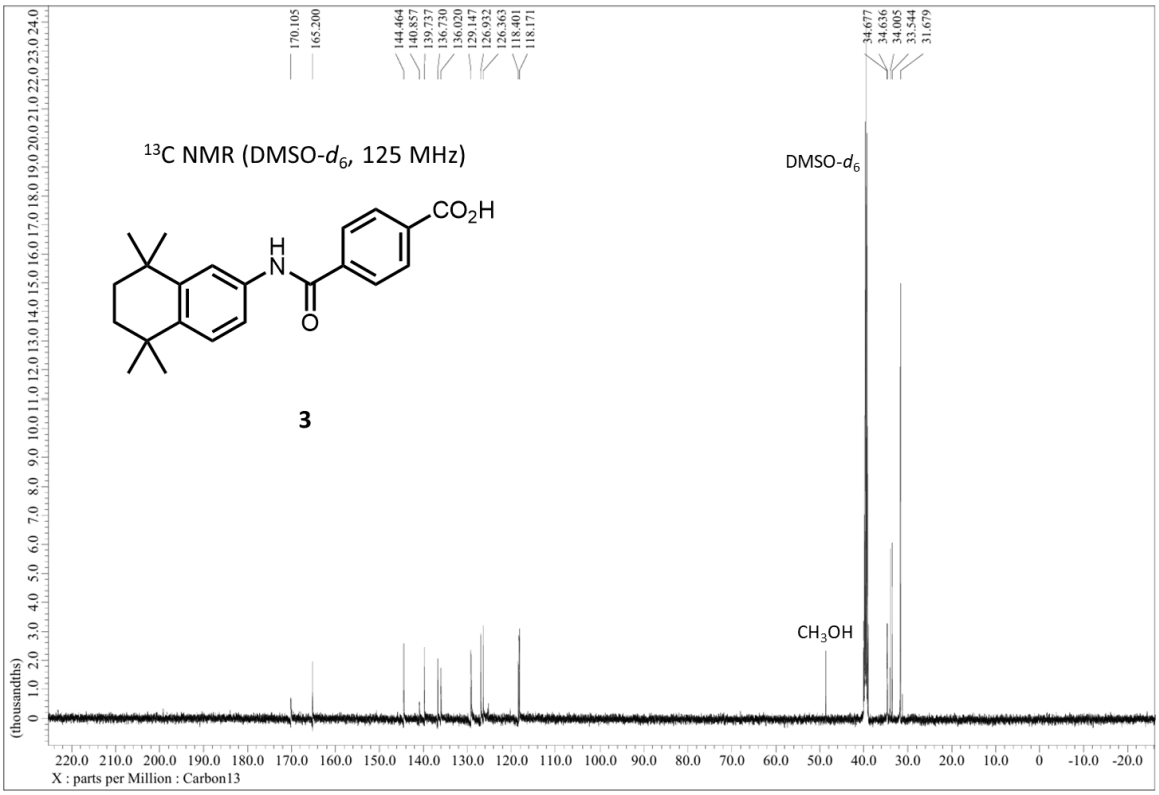

Figure S60. ^{13}C NMR Spectrum of Tamibarotene (**3**)

SI-14. References

(1) Usachev, S.; Gridnev, A. *Synth. Commun*. **2011**, 41, 3683.

(2) Hatano, M.; Tabata, Y.; Yoshida, Y.; Toh, K.; Yamashita, K.; Ogura, Y.; Ishihara, K. *Green Chem*. **2018**, *20*, 1193.

(3) Yue, Q. F.; Wang, C. X.; Zhang, L. N.; Ni, Y.; Jin, Y. X. *Polym. Degrad. Stab*. **2011**, *96*, 399.

(4) Jiang, X.; Zhang, J.; Zhao, D.; Li, Y. *Chem. Commun*. **2019**, *55*, 2797.

(5) Fukushima, K.; Lecuyer, J. M.; Wei, D. S.; Horn, H. W.; Jones, G. O.; Al-Megren, H. A.; Alabdulrahman, A. M.; Alsewailem, F. D.; McNeil, M. A.; Rice, J. E.; Hedrick, J. L. *Polym. Chem*. **2013**, *4*, 1610.

(6) Liu, Y.; Yao, X.; Yao, H.; Zhou, Q.; Xin, J.; Lu, X.; Zhang, S. *Green Chem*. **2020**, *22*, 3122.

(7) Giraldo-Narcizo, S.; Guenani, N.; Sánchez-Pérez, A. M.; Guerrero, A. *ChemBioChem* **2023**, *24*, e202200503.

(8) Bai, C.; Spontak, R. J.; Koch, C. C.; Saw, C. K.; Balik, C. M. *Polymer* **2000**, *41*, 7147.

(9) Zaker, A.; Auclair, K. *ChemSusChem* **2024**, e202401506.

(10) Parravicini, L.; Leone, B.; Auriemma, F.; Guerra, G.; Petraccone, V.; Di Dino, G.; Bianchi, R.; Vosa, R. *J. Appl. Polym. Sci.* **1994**, *52*, 875.

(11) Asano, T.; Baltá Calleja, F. J.; Flores, A.; Tanigaki, M.; Mina, M. F.; Sawatari, C.; Itagaki, H.; Takahashi, H.; Hatta, I. *Polymer* **1999**, *40*, 6475.

(12) Misra, A.; Stein, R. S. *J. Polym. Sci. Polym. Phys. Ed*. **1979**, *17*, 235.

(13) Chen, X.; Hou, G.; Chen, Y.; Yang, K.; Dong, Y.; Zhou, H. *Polym. Test*. **2007**, *26*, 144.

(14) Luna, E.; Olazabal, I.; Roosen, M.; Müller, A.; Jehanno, C.; Ximenis, M.; de Meester, S.; Sardon, H. *Chem. Eng. J*. **2024**, *482*, 148861.

(15) Ali, B. T. I.; Widiastuti, N.; Kusumawati, Y.; Ivansyah, A. L.; Jaafar, J. *Mater. Res. Express* **2022**, *9*, 125302.

(16) Vasiliu Oprea, C.; Neguleanu, C.; Simionescu, C. *Eur. Polym. J.* **1970**, *6*, 181.

(17) Charles M. Hansen. Hansen Solubility Parameters: A User's Handbook, 2nd Edition; CRC Press: Boca Raton, 2007.

(18) Pulido, B. A.; Habboub, O. S.; Aristizabal, S. L.; Szekely, G.; Nunes, S. P. *ACS Appl. Polym. Mater*. **2019**, 1, 2379.

(19) The Official Site for Hansen Solubility Parameters and HSPiP software https://www.hansen-solubility.com/ (accessed Jan 31, 2025).

(20) Karim, S. S.; Farrukh, S.; Matsuura, T.; Ahsan, M.; Hussain, A.; Shakir, S.; Chuah, L. F.; Hasan, M.; Bokhari, A. *Chemosphere* **2022**, *307*, 136050.

(21) Abe, R.; Komine, N.; Nomura, K.; Hirano, M. *Chem. Commun*. **2022**, *58*, 8141.

(22) Lee, D. W.; Park, Y. M.; Lee, K. Y. *Catal. Surv. Asia* **2009**, 13, 63.

(23) Hatano, M.; Ishihara, K. *Chem. Commun*. **2013**, 49, 1983.

(24) Neverov, A. A.; McDonald, T.; Gibson, G.; Brown, R. S. *Can. J. Chem*. **2001**, *79*, 1704.

(25) Chu, M.; Liu, Y.; Lou, X.; Zhang, Q.; Chen, J. *ACS Catal*. **2022**, *12*, 4659.

(26) Thiounn, T.; Smith, R. C. *J. Polym. Sci*. **2020**, *58*, 1347.

(27) George, N.; Kurian, T. *Ind. Eng. Chem. Res.* **2014**, *53*, 14185.

(28) Luo, H.; Tyrrell, H.; Bai, J.; Muazu, R. I.; Long, X. *Green Chem*. **2024**, *26*, 11444.

(29) Sinha, V.; Patel, M. R.; Patel, J. V. *J. Polym. Environ*. **2010**, *18*, 8.

(30) Payne, J.; Jones, M. D. *ChemSusChem* **2021**, *14*, 4041.

(31) Wang, M.; Li, Y.; Zheng, L.; Hu, T.; Yan, M.; Wu, C. *Polym. Chem*. **2024**, 15, 585.

(32) Ghasemi, M. H.; Neekzad, N.; Ajdari, F. B.; Kowsari, E.; Ramakrishna, S. *Environ. Sci. Pollut. Res*. **2021**, *28*, 43074.

(33) Debruin, B. R.; Naujokas, A. A.; Gamble, W. J. US5432203, 1995.

(34) Gruschke, H.; Hammerschick, W.; Medem, H. US3403115, 1968.

(35) Pham, D. D.; Cho, J. *Green Chem*. **2021**, *23*, 511.

(36) Tollini, F.; Brivio, L.; Innocenti, P.; Sponchioni, M.; Moscatelli, D. *Chem. Eng. Sci*. **2022**, *260*, 117875.

(37) Tanaka, S.; Sato, J.; Nakajima, Y. *Green Chem*. **2021**, 23, 9412.

(38) Mckeown, P.; Kamran, M.; Davidson, M. G.; Jones, M. D.; Román-Ramírez, L. A.; Wood, J. *Green Chem*. **2020**, 22, 3721.

(39) Wang, H.; Li, Z.; Liu, Y.; Zhang, X.; Zhang, S. Degradation of Poly(Ethylene Terephthalate) Using Ionic Liquids. *Green Chem*. **2009**, *11*, 1568.

(40) Al-Sabagh, A. M.; Yehia, F. Z.; Eissa, A. M. M. F.; Moustafa, M. E.; Eshaq, G.; Rabie, A. R. M.; Elmetwally, A. E. *Ind. Eng. Chem. Res*. **2014**, *53*, 18443.

(41) Wang, Q.; Geng, Y.; Lu, X.; Zhang, S. *ACS Sustain. Chem. Eng*. **2015**, 3, 340.

(42) Ju, Z.; Xiao, W.; Lu, X.; Liu, X.; Yao, X.; Zhang, X.; Zhang, S. *RSC Adv*. **2018**, *8*, 8209.

(43) Shirakawa, S.; Liu, S.; Kaneko, S.; Kumatabara, Y.; Fukuda, A.; Omagari, Y.; Maruoka, K. *Angew. Chem. Int. Ed*. **2015**, *54*, 15767.

(44) von Hofmann, A. W. *Liebigs Ann*. **1851**, *78*, 253.

(45) Hedrick, J. L.; Kilickiran, P.; Nyce, G. W.; Waymouth, R. M. US 20040127720A1, 2004.

(46) El Mahdi, A.; Medimagh, R.; Fourdin, T. WO2023194442, 2023.

(47) Tanaka, S.; Koga, M.; Kuragano, T.; Ogawa, A.; Ogiwara, H.; Sato, K.; Nakajima, Y. *ACS Mater. Au* **2024**, *4*, 335.

(48) Essaddam, H. WO2017007965, 2017.

(49) Koh, H. J.; Han, K. L.; Lee, H. W.; Lee, I. *Bull. Korean Chem. Soc*. **2002**, *23*, 715.

(50) Odinokov, V. N.; Akhmetova, V. R.; Savchenko, R. G.; Bazunova, M. V.; Khalilov, L. M. *Russ. J. Org. Chem*. **2001**, *37*, 598.

(51) Lei, Z.; Chen, B.; Koo, Y. M.; Macfarlane, D. R. *Chem. Rev*. **2017**, *117*, 6633.

(52) Hallett, J. P.; Welton, T. *Chem. Rev*. **2011**, *111*, 3508.

(53) Creary, X.; Willis, E. D.; Gagnon, M.; Dame, N. *J. Am. Chem. Soc*. **2005**, *127*, 18114.

(54) Neale, A. R.; Schütter, C.; Wilde, P.; Goodrich, P.; Hardacre, C.; Passerini, S.; Balducci, A.; Jacquemin, J. *J. Chem. Eng. Data* **2017**, *62*, 376.

(55) Hawker, R. R.; Haines, R. S.; Harper, J. B. *Chem. Commun*. **2018**, *54*, 2296.

(56) Matthewman, E. L.; Kapila, B.; Grant, M. L.; Weber, C. C. *Chem. Commun*. **2022**, *58*, 13572.

(57) Dunn, M. H.; Konstandaras, N.; Cole, M. L.; Harper, J. B. *J. Org. Chem*. **2017**, *82*, 7324.

(58) Olmstead, N.; Margolin, Z.; Bordwell, F. G. *J. Org. Chem*. **1980**, *45*, 3295.

(59) Zhang, Y.; Tian, F.; Wu, Z.; Li, X.; Liu, X.; He, Y. *Mater. Today Commun*. **2022**, *32*, 104045.

(60) Chen, H.; Wan, K.; Zhang, Y.; Wang, Y. *ChemSusChem* **2021**, *14*, 4123.

(61) Kosloski-oh, S. C.; Wood, Z. A.; Manjarrez, Y.; Fieser, M. E.; Wood, Z. A. *Mater. Horizons* **2021**, *8*, 1084.

(62) Huang, J.; Yan, D.; Zhu, Q.; Cheng, X.; Tang, J.; Lu, X.; Xin, J. *Polym. Degrad. Stab*. **2023**, *208*, 110245.

(63) Liu, B.; Lu, X.; Ju, Z.; Sun, P.; Xin, J.; Yao, X.; Zhou, Q.; Zhang, S. *Ind. Eng. Chem. Res*. **2018**, *57*, 16239.

(64) Zheng, W.; Liu, C.; Wei, X.; Sun, W.; Zhao, L. *Chem. Eng. Sci*. **2023**, *267*, 118329.

(65) Lv, B.; Jiao, Y.; Deng, X.; Fan, W.; Xin, B. *Sep. Purif. Technol.* **2025**, *354*, 128935.

(66) Mulindwa, P.; Kasule, J. S.; Nantaba, F.; Wasswa, J.; Expósito, A. J. *Int. J. Sustain. Eng.* **2024**, *17*, 582.

(67) Zheng, H.; Chen, Q.; Chen, Z. *Water Emerg. Contam. Nanoplastics* **2024**, *3*, 11.

(68) Hamada, Y.; Yamada, I.; Uenaka, M.; Sakata, T. US005214202A, 1993.

(69) Bao, X.; Qiao, X.; Bao, C.; Liu, Y.; Zhao, X.; Lu, Y.; Chen, G. *Org. Process Res. Dev*. **2017**, *21*, 748.

(70) Kagechika, H.; Kawachi, E.; Hashimoto, Y.; Himi, T.; Shudo, K. *J. Med. Chem*. **1988**, *31*, 2182.

(71) Bordwell, F. G.; Algrim, D.; Vanier, N. R. *J. Org. Chem*. **1977**, *42*, 1817.

(72) Bordwell, F. G.; Algrim, D. J. *J. Am. Chem. Soc.* **1988**, *110*, 2964.

(73) Kim, B. R.; Lee, H. G.; Kang, S. B.; Sung, G. H.; Kim, J. J.; Park, J. K.; Lee, S. G.; Yoon, Y. J. *Synthesis* **2012**, *44*, 42.

(74) Bordwell, F. G.; Ji, G. Z. *J. Am. Chem. Soc*. **1991**, *113*, 8398.